ECOR
'links the ocean engineering world'

Engineering Committee
on
Oceanic Resources

Oceanic Engineering International

Volume 9, Number 1, 2005

NRC · CNRC
Institute for Ocean Technology

Memorial
University of Newfoundland

Ocean Engineering Research Centre
Faculty of Engineering and Applied Science

ISSN: 1025-7187

Oceanic Engineering International

Volume 9 Number 1 2005

CONTENTS

Papers

Roll damping: a review 1
M. R. Haddara

Design criteria for parametric rolling 11
K.J. Spyrou

Removal of irregular frequency effect in the computation of wave-body interactions 28
using the panel-free method
W. Qiu, H. Peng, and C.C. Hsiung

Application of artificial cavitation for reducing ship drag 35
K. I. Matveev

Scour due to waves and currents around piles in clay 42
M. Ram Babu, S. Narasimha Rao, and V. Sundar

Cover design by John Brooke, ECOR, and Gary McManus, Geography, Memorial University of Newfoundland

Oceanic Engineering International

The oceans and their resources have been described as the last great unexplored and unexploited part of the world, yet they have the potential for yielding benefits far exceeding the costs of the associated research, survey and development work. Ocean engineering, which covers the technological activities concerned with the exploration, exploitation and conservation of the marine environment, performs a vital role in these endeavours.

The Ocean Engineering Research Centre of the Memorial University of Newfoundland, Canada, the Engineering Committee on Oceanic Resources, and the Institute for Ocean Technology, National Research Council, jointly publish this journal, *Oceanic Engineering International*, as a vehicle to aid communication across the extremely broad interdisciplinary area of oceanic engineering.

Manuscripts are invited in the categories of full journal papers (about 15 printed pages); technical notes or short papers (less than 5 printed pages); and reviews.

Instructions for authors are available at http://www.engr.mun.ca/research/centres/OERC/publications

Oceanic Engineering International — Editorial Board

SUBSCRIPTION INFORMATION

A subscription to *Oceanic Engineering International* can be obtained by sending your order to the editorial office (c/o Ocean Engineering Research Centre, Memorial University of Newfoundland, St. John's, Newfoundland, Canada, A1B 3X5; FAX: 1-709-737-6184). The rates for subscriptions are: Can. $140.00 for libraries, institutions and companies and Can. $70.00 for individuals. (GST will be charged on the above amounts to subscribers from Canada).

ADVERTISING

Advertisements in the journal can be arranged by contacting the editorial office: Tel. 1-709-737-6172; Fax. 1-709-737-6184. Rates are available on request.

Subscription Information

To continue receiving *Oceanic Engineering International* we ask that you begin or renew either a library or a personal subscription. You can subscribe in three ways.

1. A library or institution subscription (please forward the form below to your Acquisitions Librarian).
2. An individual subscription to the journal (please see form below).
3. A corporate or individual membership in the Engineering Committee on Oceanic Resources (ECOR) by contacting:
   Giuseppe Gigantesco, ECOR Executive Secretary
   Royal Institution of Naval Architects
   10 Upper Belgrave Street
   London, UK SW1X 8BQ
   email: ggigantesco@rina.org.uk

I wish to subscribe to *Oceanic Engineering International.*

Name & Title: _____

Address: _____

Tel: _____ Fax: _____ Email: _____

The rates for subscriptions are:

For libraries, institutions, and companies - Canadian $140.00 ( )

For individuals - Canadian $70.00 ( )

Please invoice me ( )

Please charge my: VISA ( )

MASTERCARD ( )

Card Number _____ Expiry Date _____

Signature _____ Date _____

(GST will be charged on the above amounts to subscribers from Canada)

Send Payment To:

Attention: Lisa O'Brien
Oceanic Engineering International
Faculty of Engineering & Applied Science
Memorial University of Newfoundland
St. John's, NL, Canada, A1B 3X5

Oceanic Engineering International, Vol. 9, No. 1, 2005, pp. 1-10

Roll Damping: a Review

M. R. Haddara

Faculty of Engineering and Applied Science, Memorial University of Newfoundland, St. John's, NL, Canada, A1B 3X5

ABSTRACT

The paper presents a review of the literature on roll damping. The review has been limited mostly to publications that appeared during the last thirty years. The paper surveys briefly the theoretical methods for estimating roll damping for ships, as well as the methods used to identify the damping parameters from free roll decay tests and full-scale measurements at sea. No attempt has been made to evaluate these methods, however, general statements regarding their effectiveness are made. A brief discussion of the effect of the various ship's parameters on roll damping is presented.

1. INTRODUCTION

Perhaps rolling motion is the degree of freedom which enjoyed most attention by naval architects and mathematicians in the last fifty years. Yet, it is the least understood and the most difficult to determine. The problem of rolling motion is multi-faceted. Various challenges face the naval architect in the process of designing a new ship. Obtaining estimates of the roll damping parameters, and determining the effect of varying ship's parameters on the motion and the stability are some of these challenges.

The pioneering work by Froude in the nineteenth century on roll damping opened the door for naval architects to the study of the mechanics of roll damping. However, very little work was done during the following sixty or seventy years. Interest in roll damping, and roll stability started to grow in the nineteen sixties and continued in the following years. Presently, there is a body of knowledge on roll damping that warrants a review. This paper attempts to address this need.

2. THEORETICAL METHODS

Himeno [1981] reviewed the state of the art of roll damping estimation methods. The review is based in large on the work of Ikeda *et al.* [1978] who divided roll damping for a ship into seven components: four are caused by the naked hull and three are caused by the bilge keels. The four components that are caused by the naked hull are friction, eddy, lift, and wave. Bilge keels damping arises from the change in pressure distribution over the hull as a result of the presence of the bilge keels, from the normal force acting on the bilge keels, and from the wave damping caused by the bilge keels. These seven components can be reduced to five if we sum up the three components of bilge keels damping into one.

$$B_e = B_F + B_E + B_L + B_W + B_{BK} \qquad (1)$$

where B_e, is the ship's equivalent linear roll damping coefficient, and B_F, B_E, B_L, B_W, B_{BK}, are the contributions of the friction, eddy, lift, wave, and the bilge keels.

(a) Friction Damping

Friction damping is caused by the shear stress in the boundary layer on the hull surface as a result of the rolling motion. The effect of the wave is ignored. The skin friction laws for a flat plate are used to estimate the friction roll damping.

The following equation is used to account for the effect of forward speed on the frictional component of the equivalent linear damping coefficient [Himeno 1981]

$$B_F = B_{Fo}\ (1 + 4.1 \times \frac{U}{\omega\, L}) \qquad (2)$$

where B_F, B_{Fo}, ω, U, and L are the frictional damping coefficient at zero speed, the frictional damping coefficient at forward speed, the frequency of roll, the forward speed, and the ship's length, respectively.

This shows that the additional frictional damping component caused by forward speed is linearly dependent on forward speed and inversely proportional to the frequency. The percentage contribution of the frictional damping component to the total roll damping coefficient is usually small. However, because of the dependence of this component

on the reciprocal of the frequency, this may not be the case for ships with low roll frequency.

(b) Eddy Damping

This is a nonlinear component caused by the pressure variation on the naked hull caused by the vortices generated as a result of the flow separation. This component decreases with forward speed. The rate of decrease depends on the hull shape and the aspect ratio of the body. Himeno [1981] suggests that for speeds above $F_n > 0.2$ this component can be neglected.

(c) Lift Damping

For a ship rolling and moving with forward speed, the flow around the hull becomes asymmetrical and a lift force is generated. The lift damping component is represented by a linear function of forward speed and a quadratic function of the distance between the roll center and the center of gravity of the ship. However, its coefficient is independent of the frequency of the rolling motion. Thus, lift damping becomes predominant for ships having low natural roll frequencies and moving with high forward speeds [Himeno 1981].

(d) Wave Damping

Wave damping is a consequence of the waves created by the rolling motion of a ship. Himeno [1981] showed that there is a fairly good agreement between wave damping estimated from experiments and that calculated using the strip theory for the zero forward speed case. Theoretical predictions of wave roll damping for a ship moving with forward speed is a difficult problem.

(e) Bilge-Keel Damping

Bilge-keel damping is the increment of damping caused by the bilge keels. It includes the damping of the bilge keel as well as the increase in hull damping created by the change in the pressure distribution over the hull as a result of bilge keels installation. Himeno [1981] concluded that bilge-keel damping is a nonlinear function of the roll amplitude and frequency and that it is not sensitive to forward speed.

Ikeda's original method was developed for conventional hull form with block coefficient in the range of 0.56 to 0.85 and a Froude number of about 0.25. Thus, the method could not yield good predictions when applied to slender, high speed ships. The original method was modified by Ikeda and Katayama [1994] to deal specifically with the case of slender high speed ships. They conducted an experimental study using models of two high speed slender vessels. Each of the models had a skeg and a round bilge. One of the models had a bulbous bow. The main improvement over the original method is in the calculation of the bilge damping component. This improved the agreement between theory and experiment. However, there was still a disagreement between theory and experiment at high forward speed. Their study concluded that the wave component of roll damping for slender ships plays a prominent role at high speeds and that lift damping produced by bilge keels having large aspect ratios cannot be ignored. Further modifications were added to the original method later. These modifications are summarized in Ikeda [2004]. The improvements included a correction of the lift damping component of the bilge keel due to forward speed and allowing for the use of a nonlinear lift coefficient in estimating the hull lift damping component. A modified expression for the eddy damping component that can be applied to shallow draft barges was also added, Ikeda *et al.* [1993]. However, this modification proved to over-estimate the barge's damping coefficient for roll angles greater than 5 degrees.

Using a similar approach, Schmitke [1978] estimated an equivalent linear roll damping coefficient for a fast ship performing coupled sway, roll, and yaw motion in oblique waves. This coefficient consisted of the hull damping derived from strip theory, and the contributions due to appendages such as rudders and fins, in addition to viscous effects.

Brook [1989] evaluated the methods of Ikeda, Schmitke, and a method developed by BMT using full-scale and model free roll decay data. The BMT method is based on the work of Graham [1979] and extended to include experimental drag coefficients reported by Tanaka *et al.* [1980]. Brook concluded that no single theoretical method consistently gives accurate roll damping coefficients for all vessel types and conditions.

Standing [1991] used the BMTIMP program to investigate the viscous contribution to roll damping. The BMTIMP program is based on the theoretical discrete vortex method. He concluded that the discrete vortex method satisfactorily predicts the roll damping of rectangular barges with sharp corners and bilge keels [Standing 1991]. However, the method is not successful in predicting damping parameters for round-cornered barges.

Chakrabarti [2001] summarized the formulae developed by Ikeda *et al.* and used them to estimate the damping coefficients for a container ship and a derrick barge. He points out that the use of these formulae for 3-dimensional offshore structures and special hull forms may not be suitable.

Other theoretical approaches used in estimating viscous damping include the use of methods based on potential-flow. Faltinsen and Petersen [1982] developed a method to predict the flow and associated vortex shedding around bluff bodies at high Reynolds number. Brown and Patel [1985] developed a discrete vortex-shedding method for predicting roll damping at and around resonance. These two methods were based on a two dimensional approach. Umeda and Ikeda [1988] calculated the equivalent linear damping coefficient for a rolling ship using slender body theory with both a free surface and free vortex layers. The contribution of the bilge keels to roll damping was calculated using slender body theory for a solitary wing. However, comparison between calculated and experimental results for a fishing boat proved to be unsatisfactory. The discrepancy is attributed to the fact that the theory ignores the non-linearity of roll damping and the change of the model attitude with forward velocity.

Al-Hukail *et al.* [1994] developed two vortex based methods for predicting roll damping. The first method uses the slender body theory assuming a low Froude number and a rigid free surface; and the second is based on matching a local vortex shedding model to an outer irrotational flow field.

Recently, use has been made of the unsteady Navier-Stokes techniques in calculating roll damping. Korpus and Falzarano [1997] used a combined Reynolds-averaged Navier Stokes approach with a potential flow panel method to estimate a viscous flow correction to existing potential flow codes. They hypothesized that "the vertical contribution to roll moment can be isolated by subtracting the potential flow result from the pressure component obtained from RANS." The method developed does not include the effects of free surface or forward velocity.

Chen *et al.* [2001] used a Reynolds-Averaged Navier-Stokes numerical method in conjunction with a chimera domain decomposition approach to obtain time-domain simulations of large amplitude ship roll motions. Calculations were made for a 57.3 m motor ship and a 36.58 m pontoon barge. Free decay motion as well as wave excited responses were generated. The method provides the pressure distribution over the hull which can be integrated to give the roll exciting moment acting on the hull. One can also study the vorticity inception and propagation mechanism. However, such method has an extremely large appetite for computer time.

Methods based on the unsteady Navier-Stokes techniques are still in the development stage. Their results need to be validated using experimental data and their huge requirement of computer time should be reduced.

3. FLOW VISUALIZATION

The recent advances in computational fluid dynamics techniques and the desire to integrate these techniques in the ship design process coupled with the progress in flow field measurements techniques motivated researchers to use experimental techniques to study the flow around a ship's hull performing rolling motion. The objective of these studies is twofold: to better understand the flow phenomenon around the hull of a rolling ship, and to develop a tool to validate the results of CFD codes. Felli *et.al.* [2004] studied the flow around a ship model performing forced rolling motion. The velocity field was measured around eight transverse sections of the model using a 2D Laser Doppler Velocimeter (LDV). The roll angle was measured simultaneously. The velocity measurements were made for the bare and the fully appended hull. These measurements show the inception and evolution of the vortices and allow the researcher to draw conclusions regarding the importance of contribution of each component to roll damping. It was observed that vorticity shed by the rudder is more significant than that produced by the bilge keel. However, free decay tests results indicate that bilge keel damping is greater than the rudder damping. The authors attribute this to the difference in the length of the two lever arms. This may also be caused by the fact that bilge keels generate higher lift damping with forward speeds (the experiments were carried out for a model moving with forward speed at a Froude number of 0.28).

Bishop *et al.* [2004] used a particle-image velocimetry system to perform two-component velocity field measurements near the mid section of a ship model with and without bilge keels. These tests were aimed at investigating the flow field in the region around the bilge keels. They suggest that vortex shedding off the bilge keels during rolling may play a dominant role in causing the damping coefficient to increase with forward speed.

Irvine, *et al.* [2004] used a 2D Dantec particle image velocimetry to measure the velocity field around a rolling ship model. The model used is a geometrically similar model to the one used by Bishop *et al.* [2004]. Flow velocities were measured for the rolling model at seven different forward speeds, with and without bilge keels. The measurements show clearly the mechanics of the generation, propagation, and decay of the bilge keels vortices as the model rolls.

4. DAMPING FORM

Most roll motion studies in the literature use a second order ordinary nonlinear differential equation that is traceable to the work of Froude, (see The Papers of William Froude [1955]). Both the damping and the restoring moments are nonlinear with the damping moment represented by linear-plus-quadratic velocity dependent terms.

$$N(\dot{\phi}) = n_1 \dot{\phi} + n_2 \dot{\phi}\left|\dot{\phi}\right| \tag{3}$$

Haddara [1971] was the first to suggest a damping moment that consists of linear-plus-cubic velocity dependent terms. The use of a cubic term instead of a quadratic term with an absolute value sign makes the analysis more tractable.

$$N(\dot{\phi}) = n_3 \dot{\phi} + n_4 \dot{\phi}^3 \tag{4}$$

The linear-plus-cubic model was also used by Lewison [1976]. Dalzell [1978] analysed free rolling motion data obtained from a number of sallying experiments, some of these experiments were originally used by Froude to develop his linear-plus-quadratic model. The data analysed originates from a variety of ship models and actual ships with lengths that ranged from 1.5 to 167.6 metres. The initial angles in the sallying experiments ranged from 5.5 to 32 deg. The study concludes that the linear-plus-cubic model is both quantitatively and qualitatively reasonable within the range and scatter of available experimental data. Dalzell [1978] went on to suggest that since the linear-plus-cubic roll damping model fits the experimental data about as well (sometimes better than) the linear-plus-quadratic model, one might speculate that the cubic model can be considered an "equivalent approach" rather than an "approximation." This conclusion was also confirmed by Haddara and Bennett [1989] who conducted an experimental investigation of the roll damping models using two models: a 1:80 scale model of an OBO ship (the MV Arctic) and a 1:40 model of an ice breaker (the R-Class). A linear-plus-cubic velocity dependent damping model described the roll damping best.

In an experimental study conducted by Bass and Haddara [1989], Haddara and Bass [1990], and Bass and Haddara [1991] free roll decay curves were measured using models of

three small fishing vessels. The models were about 1.50 metre in length. Although the models had similar overall dimensions, they had quite different hull forms. One of the models had a hard chine while the second had a round bilge. The third had a round bilge with a moderate rise of floor. None of the models had bilge keels. The results of the study showed that the equivalent linear damping coefficient is a linear function of the roll amplitude. The results also showed that the linear-plus-quadratic damping form is the best form to fit the experimental data for a lightly damped model; while the linear-plus-linear angle dependent is the damping form to fit best the experimental data of a heavily damped model. Haddara and Bennett [1989] and Haddara and Zhang [1994] found that roll amplitude has its greatest effect on the damping at low forward speed. At low forward speeds, roll damping consists mainly of friction, wave, and eddy-making components. These three components are functions of the roll amplitude. At speeds near but greater than zero, the contribution of lift damping to the total damping coefficient is small. As the forward speed increases, lift contribution becomes predominant and roll damping becomes almost independent of the roll amplitude. This is more pronounced when the hull has lift generating appendages, e.g. bilge keels.

Taylan [2000] investigated the effect of the form of the nonlinear damping on the amplitude of rolling motion in regular beam seas. He used a generalized Duffing's method to solve the nonlinear differential equation of roll to calculate the roll amplitude for four different vessels: a tanker, a bulk-carrier, a RO-RO passenger ship, and a RO-RO cargo ship. He compared the roll amplitudes when three different forms for the damping moment were used. All three forms consist of a linear velocity dependent term plus a nonlinear term. Three different nonlinear damping terms were used, as follows.

$$\begin{aligned} B1(\dot{\phi}) &= B_L\,\dot{\phi} + B_N\,\dot{\phi}\dot{\phi} \\ B2(\phi,\dot{\phi}) &= B_L\,\dot{\phi} + B_N\,\phi^2\,\dot{\phi} \\ B3(\dot{\phi}) &= B_L\,\dot{\phi} + B_N\,\dot{\phi}^3 \end{aligned} \tag{5}$$

The results obtained show that the use of different roll damping moments produces different roll amplitudes for each of the ships when excited with the same moment. It is not clear how the different damping coefficients were obtained and whether the damping coefficients used in the three models are the same.

Haddara [1984] studied the effect of the form of the damping moment on the roll response using experimental roll data obtained from the literature. Four roll damping moment forms were investigated. These are

$$\begin{aligned} N(\phi,\dot{\phi}) &= 2\zeta_1\,\omega_n\,(\dot{\phi} + \varepsilon_1\dot{\phi}\,|\phi| + \varepsilon_2\,\dot{\phi}\,|\dot{\phi}|) \\ N(\phi,\dot{\phi}) &= 2\zeta_2\,\omega_n\,(\dot{\phi} + \varepsilon_3\,\dot{\phi}\,\phi^2 + \varepsilon_4\,\dot{\phi}^3) \\ N(\phi,\dot{\phi}) &= 2\zeta_3\,\omega_n\,(\dot{\phi} + \varepsilon_5\,\dot{\phi}\,|\phi| + \varepsilon_6\,\dot{\phi}^3) \\ N(\phi,\dot{\phi}) &= 2\zeta_4\,\omega_n\,(\dot{\phi} + \varepsilon_7\,\dot{\phi}\,\phi^2 + \varepsilon_8\,\dot{\phi}\,|\dot{\phi}|) \end{aligned} \tag{6}$$

The coefficients in the different models were determined using a least-squares fit of the different formulae to data describing sallying experiments collected from the literature by Dalzell [1978]. The study concluded that, within the range and scatter of the experimental data, all damping models produced comparable free and forced responses. The form of the damping moment has no effect on the response provided that the same excitation is used. The effect of the form outside the range of the experimental data was not considered. The works by Dalzell [1978], Mathisen and Price [1984], and Chun *et al.* [2001] confirm that both the linear-plus-quadratic and the linear-plus-cubic forms predict the same response.

5. FACTORS AFFECTING DAMPING

(a) Wave Steepness and Frequency

Contento *et al* [1996] conducted a number of roll decay and forced roll experiments using 1:50 scale model of a RO-RO vessel. They studied the effect of varying the incident wave steepness and the exciting frequency on the damping parameters. Linear and quadratic damping parameters were identified from the free-decay using a time domain fitting procedure first introduced by Haddara and Bennett [1989], namely the energy method. The authors developed an extension to the energy method to analyse the forced roll case. The results of the experimental study showed that both the linear and the quadratic damping parameters are sensitive to both the exciting frequency and the wave steepness. The effect is more pronounced for frequencies away from resonance.

Mathisen and Price [1984] found that damping coefficients obtained from forced rolling tests indicated a dependence on the frequency of oscillation.

(b) Natural Frequency

Haddara and Zhang [1994] found that the coefficient of equivalent linear damping is not sensitive to the natural frequency. See also Haddara and Leung [1994] and Cumming *et al.* [1990].

(c) Forward Speed

Watanabe [1977] used the linear thin ship theory to derive a formula for the roll damping moment acting on a ship moving with forward speed. The damping is formed mainly by wave making and the side force as a result of the asymmetric flow around the hull. As Froude number increased, it was noticed that the wave making damping increased and then decreased. The formula derived indicates that the roll damping moment increases with the increase in the draft/length ratio. The theoretical results agreed with experimental results obtained from a bare-hulled model with no bilge keels.

Haddara and Cumming [1992] investigated the effect of forward speed on the roll damping. Roll decay curves were obtained for a nine metre long destroyer model. This is a twin propeller model with a middle rudder. Tests were done for the model with and without bilge keels and having different GM values. The contribution from the rudder and propellers is

important for the case of a model without bilge keels. However, damping caused by bilge keels overshadows that generated by the rudder and propellers. The experimental results showed that damping is a nonlinear function of forward speed.

Haddara and Zhang [1994] conducted an experimental investigation of the effect of forward speed on roll damping. Over 700 roll decay curves were obtained using the same models used by Bass and Haddara (1989). The study used the roll decay curves to determine an equivalent linear damping coefficient. It was noticed that the equivalent linear damping coefficient for the model with the hard chine exhibited a decrease in value at about Froude number of about 0.075 from its value at zero forward speed. This phenomenon was observed by other investigators, e.g. Cox [1977] and Cumming *et al* [1990], and was attributed to a vortex cancellation mechanism caused by the bilge keels. The model used in this investigation did not have a bilge keel but had a hard chine which could be the source of the vortex cancellation mechanism in this case. It was also noticed that as the forward speed increases there is a rapid decrease of the eddy damping accompanied by a slow increase in the lift damping until a certain speed is reached. As the forward speed increases beyond this value, lift damping increases rapidly and this causes a steady increase in the total damping.

Haddara and Zhang [1994] observed that the model's sinkage increased with forward speed. This affected the value of the arm OG to be substituted in Ikeda's formula [Ikeda *et al.* 1978]. A formula for OG was determined in the following form.

$$OG = OG_0 - b \times F_r \qquad (7)$$

where OG is the distance between the center of roll and the center of gravity when the model moves with a forward velocity, OG_0 is the distance between the center of roll and the center of gravity at zero forward speed, F_r is Froude's number, and b is a constant. It was determined that b is a linear function of the model's Block Coefficient. For the three models used in the experiments the function b, can be expressed as

$$b = -0.8485\, C_B + 0.5032 \qquad (8)$$

This will also affect the wave component. Figure 1 shows a comparison between predictions obtained using Ikeda's original formula and the modified formula with the experimental results.

The lift force acting on a ship model heeled at a fixed angle and moving with a forward speed was measured using two small models, Haddara and Leung [1994]. The models used represent small fishing vessels, and have a waterline of about 1.5 metres each. One of the models had a hard chine and the other had a round bilge. These are two of the three models used by Haddara and Zhang [1994]. The round bilge model was tested with and without the rudder. The rudder contribution to the lift force is important, however, its significance decreases as the forward speed is increased. This is caused by the increase in the lift generated by the naked hull. The equivalent linear roll damping coefficient was found to be a nonlinear function of the forward speed. The same conclusion was arrived at by Haddara and Zhang [1994] using a different approach.

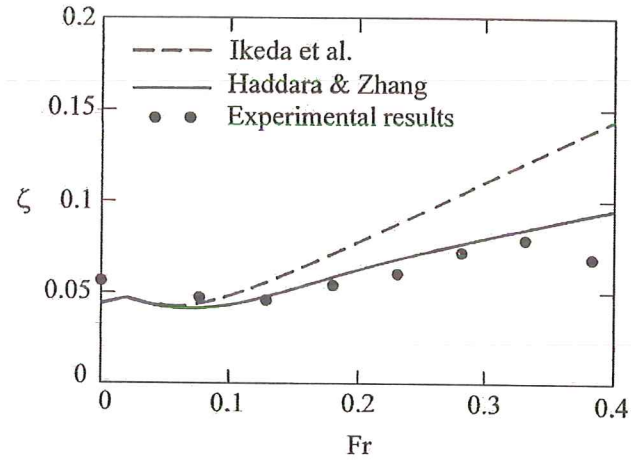

Figure 1. Predicted results using modified Ikeda's formula M363 GM – 5.33 cm.

(d) Surface Roughness

Martin *et al.* [1960] investigated the effect of roughness on roll damping by attaching plastic pins, 1/8 inch in diameter and 1/16 in high, to the bare hull of a 6.4 ft model. Damping was measured from steady state oscillatory response at the resonance frequency of the model. Motion data were obtained while the model was moving with forward speed as well as with the model rolling at zero forward speed. It was noticed that pins are effective in stimulating turbulence at zero forward speed and at high forward speed. There is a range of speeds for which pins are not effective. They concluded that turbulence stimulation is important for bare-hull models at zero forward speed.

Myrhaug [1981] studied the effect of fouling on the frictional damping by calculating the frictional resistance to forced harmonic roll oscillations of a circular cylinder. He concluded that the frictional damping is a function of the amplitude to roughness ratio but is independent of Reynolds number. Roughness is important for full-scale ships with accumulated fouling on their skins.

(e) The Position of the Roll Centre

Ikeda *et al.* [1982] carried out forced roll tests on four models representing small fishing vessels. They observed that lowering the position of the roll centre causes the roll damping to decrease.

The effect of the position of the roll centre was investigated by Bass and Haddara [1989] using models of three fishing vessels. The models were attached to a dynamometer to measure the angle of roll. The roll centre was changed by changing the vertical height of the point of attachment of the model to the dynamometer. It was shown that the equivalent non-dimensional linear roll damping coefficient increases as

distance between the roll centre and the centre of gravity increases. This conclusion was also arrived at independently by Chun *et al.* [2001] who investigated the roll damping characteristics of three models of a 3-ton class fishing vessel using free roll records in calm water and in head waves. Chun *et al.* [2001] used the energy method developed by Haddara and Bass [1990] to analyse the data.

Park *et al.* [2000] measured the roll damping of two dimensional models using forced roll tests. Their findings indicate that roll damping is sensitive to the position of the roll centre. Roll damping will increase or decrease with the change in the position of the roll centre depending on whether the roll centre is above or below the still water waterline.

Similar results were obtained using a freely floating series 60 block 60 model, Haddara [2001]. Figure 2 shows the equivalent linear damping coefficient as a function of the metacentric height, *GM*.

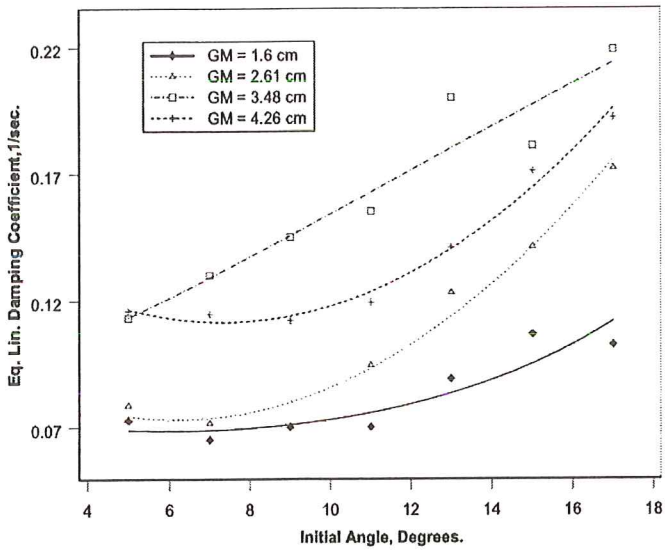

Figure 2. Equivalent linear damping coefficients zero-speed.

(f) Hull Form

Graham [1987] presented the results of a study to identify warship hull form characteristics which maximize roll damping. He concluded that the two main hull form characteristics, which influence the roll damping of warships at the cruise speed, are the separation of the appendages from the centre of gravity, and the form of the bilge.

6. IDENTIFICATION TECHNIQUES

Most roll damping parametric identification techniques use the measured amplitudes of the time history of rolling motion of a model or a ship to determine the damping coefficients. Recently, methods that use the complete time history have been developed. In the next sections, we briefly review the methods in both categories.

(a) Amplitude Based Methods

These methods are based on the utilisation of the amplitudes of the roll response to determine the values of the damping coefficients. Several methods have been used to determine roll damping coefficients using forced and transient roll time-histories. Spouge [1988] described and compared some of these methods using both simulation results and experimental data. A summary of these methods is given in the following two sections.

(*i*) *Forced Roll Response*

Quasi-linear methods: These methods use the steady forced roll response equation to determine an equivalent linear damping coefficient. The linear-plus-quadratic damping coefficients are then obtained from the equivalent linear damping coefficient using a method of least squares. Several runs are needed to determine the equivalent linear damping coefficient. These are obtained by applying a forcing moment with varying amplitude but with the same frequency.

Energy Method: This method is based on equating the energy lost to damping in each cycle to the work done by the exciting moment. The linear-plus-quadratic (or alternatively a linear-plus-cubic) damping coefficients are obtained using a least squares fit. Several runs are needed. These are obtained by either varying the frequency or the amplitude of the excitation, see Mathisen and Price [1984].

Perturbation Methods: Mathisen and Price [1984] developed a perturbation technique to estimate the damping coefficients in the linear-plus-quadratic and the linear-plus-cubic damping moments. The method was developed for ships with linear restoring moments.

(*ii*) *Free Decay Tests*

Quasi-linear Method: This is in effect an analysis to obtain an equivalent linear damping coefficient. A least squares curve fitting technique is used to extract the linear and nonlinear coefficients.

Froude Energy Method: This method equates the energy lost to damping in each half cycle to the work done by the restoring moment during the same period. This produces an expression for the slope of the roll decay curve as a function of the linear and nonlinear coefficients. The method was originally devised by Froude to obtain the coefficients in a linear-plus-quadratic damping model, and it was extended by Dalzell [1978] to the case of a linear-plus-cubic damping model.

Roberts Energy Method: Roberts [1985] treats the roll decrement as an energy loss function, which is equated to the roll damping. This method is sensitive to distortions in the roll decrement. This may be overcome by the use of cubic spline fairing technique, [Spouge 1988]. This requires a rather long free decay curve.

Averaging Technique: In the averaging technique developed by Kryloff and Bogoliuboff, see Flower and Sobti Aljaff [1980], one assumes that the free roll response is a sinusoidal function with a slowly-varying amplitude and phase.

Perturbation Method: Mathisen and Price [1984] developed a perturbation solution to the differential equation of the free

roll motion to obtain the coefficients in linear-plus-quadratic and linear-plus-cubic damping moments. The analysis assumes that the ship has a linear restoring moment.

Amplitude based methods normally require a long time-history record to obtain reliable values for the damping coefficients. In the examples given by Spouge [1988], the lowest number of peaks analysed is 12. This may not be possible for most models or ships especially when the damping is high.

(b) Complete Time-History Methods

(*i*) *The Energy Method*

Haddara and Bennett [1989] extended Froude's energy method by equating the energy dissipated to damping in one cycle to the work done by the restoring moment during the same time. The basic difference between the classical Froude's energy method and this method is that, this method uses the complete time history and not only the peaks of the response. This method is particularly suitable for the analysis of heavy damped rolling motion. Only one cycle is needed to produce reliable values for the damping coefficients.

(*ii*) *The Modified Energy Method*

Haddara and Wu [1993], and Zhang and Haddara [1993] combined the energy method with the Function Modulation Technique of Shinbrot [1954] to identify the roll damping parameters. This method can also be applied to the analysis of regular forced time-histories. The method produces remarkably good estimates.

(*iii*) *Neural Network Techniques*

Haddara and Hinchey [1995], Haddara [2001], and Haddara and Wishahy [2002] developed and used a feed-forward, back propagation neural network to identify the roll damping function of a ship.

(*iv*) *Fockker-Planck Approach*

Mahfouz and Haddara [2001] used the Fockker-Planck equation to derive differential equations describing the correlation functions and the variances of the roll angle and velocity. These equations were then used to determine the damping coefficients using an iterative technique.

Identification techniques which use the complete time history are particularly suitable for heavy damped models or ships. Usually, one or two roll cycles are sufficient to obtain reliable estimates for the damping parameters.

(c) Estimation of Damping Parameters from Measurements at Sea

(*i*) *Transfer Function Technique*

In these methods, the input and the output are measured and a transfer function is estimated. Kountzeris *et al.* [1989] used the linear wave diffraction theory to determine the roll exciting moment from wave-time history measurements. Their approach is based on constructing a linear transfer function and then using the state variable filter approach to estimate the parameters.

(*ii*) *Stochastic Averaging Approach*

Roberts *et al.* [1991; 1994] developed a technique to estimate all the parameters in the equations of motion describing the roll motion using roll amplitude measurements in random waves. Their method is based on the stochastic averaging technique. The method yielded accurate results when the damping level is low and when the restoring moment is linear. Long records are required to discriminate between linear and non-linear parameters.

(*iii*) *The Random Decrement Technique*

This technique was originally developed to identify damping parameters for linear structures [Cole 1968]. Haddara [1992] extended the technique to the nonlinear rolling motion of a ship. Using this technique, one can derive the differential equation that describes the free roll motion from the stationary random response. Haddara [1992] showed that the free roll decay response can be obtained by averaging the stationary time-history of a ship excited by random waves having a White noise spectrum. However, because of the narrow banded nature of the rolling motion, the White noise condition may be relaxed. It was also shown that the free roll decay time-history can be obtained from the autocorrelation function of the rolling motion by multiplying by a constant. Figure 3 shows a comparison of the free response and the random decrement obtained by averaging the stationary random response, [Haddara 2001].

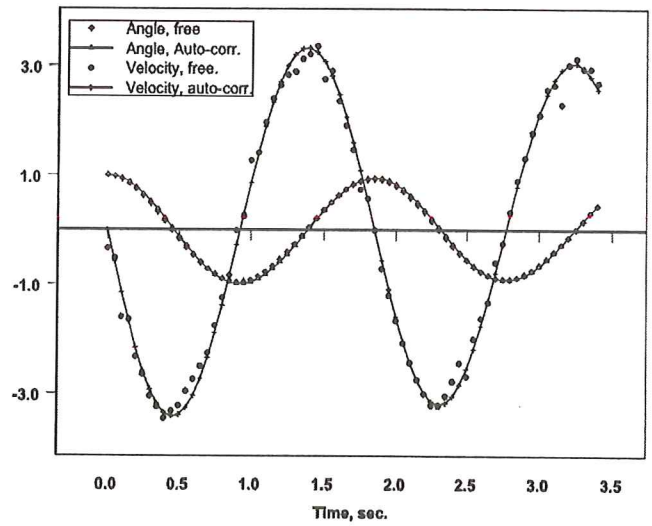

Figure 3. Free decay from free roll and from random response.

The random decrement technique is a powerful tool to obtain the free roll decay curve from the stationary random response of the ship. The only input needed is the roll motion of the ship, which can be easily measured at sea. Having obtained the free roll decay curve a parametric identification technique can be used to determine the instantaneous roll

characteristics the ship. Predictions of future roll response can then be easily made.

CONCLUSIONS

The last thirty years witnessed a growth in the studies of roll damping. These studies were aimed at understanding the physics of roll damping and tried to use this understanding to develop methods for estimating the damping moment acting on a rolling ship. In spite of the progress which these studies accomplished, roll damping estimates are still being made using one of two methods: analysis of experimental data using geometrically similar models; or use of empirical formulae, a method which finds its roots in Ikeda's method. The use of the results obtained using these two approaches are limited to the type of hulls used to produce the data. Any attempt to generalize the results to other hull forms may prove futile. We are still unable to find a universal method which yields reliable roll damping estimates for all hull forms.

Recent studies aiming at measuring the velocity field around the hull of a rolling ship model brings hope that soon we will be able to understand the physics of the flow produced by a rolling hull. In addition, one can use these results to validate algorithms obtained using computational fluid dynamics. The coupling of the flow visualization and computational fluid dynamics methods should prove beneficial for the development of a reliable method to estimate roll damping.

However, this approach will not solve the problem of the scale effect. To study the scale effect, one needs full scale results. The random decrement technique coupled with a reliable identification technique should prove useful in obtaining roll damping estimates for full scale ships. Roll damping estimates can then be obtained from measured roll responses without a need to measure wave spectrum and to calculate the resulting exciting moment acting on the ship. This will reduce the sources of error in the estimates.

REFERENCES

Al-Hukail, A., Bearman, M., Downie, M., Graham, J., and Zhao, Y. 1994 Numerical prediction of the effect of forward speed on roll damping. In *Proceedings of the 20th Symposium on Naval Hydrodynamics*, Santa Barbra, CA, USA, 118-127.

Bass, D.W. and Haddara, M.R. 1989 Roll damping for small fishing vessels. In *Proceedings of the 22nd American Towing Tank Conference*, St. John's, Canada, 443-449.

Bass, D.W. and Haddara, M.R. 1991 Roll and sway-roll damping for three small fishing vessels. *International shipbuilding progress*, **38**, 51-71.

Bishop, R., Atsavaprancee, P., Percival, S., Shan, J., and Engle, A. 2004 An investigation of viscous roll damping through the application of particle-image velocimetry. In *Proceedings of the 25th Symposium on Naval Hydrodynamics*, St. John's, NL, Canada, **2**, 233-241.

Brook 1989 Evaluation of theoretical methods for determining roll damping coefficients. *The Royal Institution of Naval Architects, Spring Meetings, Paper No. 4.*

Brown, D.T., and Patel, M.H. 1985 A theory for vortex shedding from the keels of marine vehicles. *Journal of engineering mathematics,* **19**, 265-295.

Chakrabarti, S. 2001 Empirical calculation of roll damping for ships and barges. *Ocean engineering, technical note, 28*, 915-932.

Chen, Hamn-Ching, and Liu, T., Huang, E.T. 2001 Time-domain simulation of large amplitude ship roll motions by Chimera RANS method. In *Proceedings of the Eleventh International Offshore and Polar Engineering Conference*, Stavanger, Norway, 299-306.

Chun, H.H., Chun, S.H., and Kim, S.Y. 2001 Roll damping characteristics of a small fishing vessel with a central wing. *Ocean engineering*, **28**, 1601-1619.

Cole, H. A. 1968 On the line analysis of random vibrations. In *Proceedings of the AIAA/ASME 9th Structures, Structural Dynamics, and Materials Conference, Paper no. 68-288,* Palm Spring, California.

Contento, G., Francescutto, A., and Piciullo, M. 1996 On the effectiveness of constant coefficients roll motion equation. *Ocean engineering*, **23**, 597-618.

Cox, G. G. And Lloyd, A. R. 1977 Hydrodynamic design basis for navy ship roll stabilization. *Transactions of the Society of Naval Architects and Marine Engineers*, **85**, 51-93.

Cumming, D., Haddara, M.R., and Graham, R. 1990 Experimental investigation of roll damping characteristics of a destroyer model. *National Research Council Canada, Institute for marine Dynamics, Report LR - 1990 –03.*

Dalzell, J.F. 1978 A note on the form of ship roll damping. *Journal of Ship Research*, **22**, 178-185.

Faltinsen, O. and Petersen, B. 1982 Vortex shedding around two-dimensional bodies at high Reynolds number. In *Proceedings of the 14th Symposium on Naval Hydrodynamics*, Ann Arbor, MI, USA, 1171-1213.

Felli, M., Di Felice, F., and Lugni, C. 2004 Experimental study of the flow field around a rolling ship model. In *Proceedings of the 25th Symposium on Naval Hydrodynamics*, St. John's, NL, Canada, **2**, 221-232.

Flower, J.O. and Sobti Aljaff, W.A.K. 1980 Kriloff-Bogoliuboff's solution to decaying non-linear oscillations in marine systems. *International shipbuilding progress*, **27** (313).

Graham, J.M.R. 1979 Force on cylindrical bodies in oscillatory flow at Keulegan-Carpenter numbers. In *Mechanics of wave induced forces on cylinders*, (T.L. Shaw, ed.)

Graham, Ross 1987 The effects of hull form variations on the roll damping of war ships. *Naval engineers journal*, **99**, 55-61.

Haddara, M.R. 1971 On the stability of ship motion in regular oblique waves. *International shipbuilding progress*,

18 (207), 416-434.

Haddara, M.R. 1984 A note on the effect of damping moment form on rolling response. *International Shipbuilding Progress*, **31** (363), 285-290.

Haddara, M.R. and Bennett, P. 1989 A study of the angle dependence of roll damping moment. *Ocean engineering*, **16**, 411-427.

Haddara, M.R. and Bass, D.W. 1990 On the form of roll damping moment for small fishing vessels. *Ocean engineering*, **17** (6), 525-539.

Haddara, M.R. 1992 On the random decrement for nonlinear rolling motion In *Proceedings of the 11th Offshore Mechanics and Arctic Engineering Conference, Safety and Reliability* **II**, American Society of Mechanical Engineers, 321-324.

Haddara, M.R. and Cumming, D. 1992 Experimental investigation into the physics of roll damping of a long slender hull form. *International shipbuilding progress*, **39**, 323-343.

Haddara, M.R. and Wu, X. 1993 Parameter identification of nonlinear rolling motion in random seas. *International shipbuilding progress*, **40** (423), 247-260.

Haddara, M.R. and Leung, S.K. 1994 Experimental investigation of the lift component of roll damping. *Ocean engineering*, **21**, 115-127.

Haddara, M.R. and Zhang, S. 1994 Effect of forward speed on the roll damping of three small fishing vessels. *Journal of the Offshore Mechanics and Arctic Engineering*, **116**, 102-108.

Haddara, M.R. and Hinchey, M. 1995 On the use of neural network techniques in the analysis of free roll decay curves. *International shipbuilding progress*, **42** (430), 166-178.

Haddara, M. R. 2001 On the roll damping characteristics of a series 60 block 60 model. *Oceanic engineering international*, **5** (1), 54-60.

Haddara, M.R. and Wishahy, M. 2002 An investigation of roll characteristics of two full scale ships at sea. *Ocean Engineering*, **29**, 651-666.

Himeno, Y. 1981 Prediction of ship roll damping - state of the art. *Report No. 239, Department of Naval Architecture and Marine Engineering,* The University of Michigan, Ann Arbor, Michigan, U.S.A.

Ikeda, Y., Himeno, Y., and Tanaka, N. 1978 A prediction method for ship roll damping. *Report of the Dept. Of Naval Architecture,* University of Osaka Prefecture, No. 405.

Ikeda, Y., Tanaka, N., and Himeno, Y. 1982 Effect of hull form and appendage on roll motion of small fishing vessel. In *Proceedings of the Second International Conference on Stability of Ships and Ocean Vehicles*, Tokyo, 129-141.

Ikeda, Y., Fujiwara, T., and Katayama, T. 1993 Roll damping of a sharp-cornered barge and roll control by a new type stabilizer. In *Proceedings of the 3rd International Society of Offshore and Polar Engineers Coneference*, Singapore **3**, 634-639.

Ikeda, Y. and Katayama, T. 1994 Roll motion characteristics of high speed slender vessels. In *Proceedings Fifth International Conference on Stability of Ships and Ocean Vehicles*, Melbourne, Florida, **1**.

Ikeda, Y. 2004 Prediction methods of roll damping of ships and their application to determine optimum stabilization devices. *Marine technology*, **41**, (2), 89-93.

Irvine, M., Longo, J., and Stern, F. 2004 Towing-tank tests for surface combatant for free roll decay and coupled pitch and heave motions. In *Proceedings of the 25th Symposium on Naval Hydrodynamics*, St. John's, NL, Canada, **2**, 242-260.

Kountzeris, A., Roberts, J.B., and Gawthrop, P.J. 1989 Estimation of ship roll parameters from motion in irregular seas. *Transactions of the Royal Institution of Naval Architects.*

Korpus, R.A. and Falzarano, J.M. 1997 Prediction of viscous ship roll damping by unsteady Navier-Stokes techniques. *Journal of offshore mechanics and arctic engineering*, **119**, 108-113.

Lewison, G.R.G. 1976 Optimum design of passive roll stabilizer tanks. *The naval architect*, The Institution of Naval Architects.

Mahfouz, A. B. and Haddara, M.R. 2001 Estimation of ship rolling parameters using measured response at sea. *Oceanic engineering international*, **5** (1), 42-53.

Martin, M., McLeod, C, and Landweber, L. 1960 Effect of roughness on ship-model rolling. Schiffstechnick Bd. 7, Heft 36, 67-70.

Mathisen, J.B. and Price, W.G. 1984 Estimation of ship roll damping coefficients. *Transactions of the Royal Institution of Naval Architects*, 295-307.

Myrhaug, D. 1981 A note on the effect of roughness on frictional roll damping, *International shipbuilding progress*, **28** (322), 128-135.

Park, In-kyu; Shin, Hyun-Soo; Kim, Jong-Wook; and Cho, Jin-Wook. 2000 Effect of the roll centre position on the roll damping of FPSO. In *Proceedings of the Tenth International Offshore and Polar Engineering Conference*, Seattle, USA, 308-311.

Robert, J.B. 1985 Estimation of non-linear ship roll damping from free-decay data. *Journal of ship research,* **29** (2), 127-138.

Roberts, J.B., Dunne, J.F., and Debonos, A. 1991 Estimation of ship roll parameters in random waves. In *Proceedings of the Tenth International Conference on Offshore Mechanics and Arctic Engineering*, **II**, 97-106.

Roberts, J.B., Dunne, J.F., and Debonos, A. 1994 Stochastic estimation methods for non-linear ship roll motion. *Probabilistic engineering mechanics*, **9**, 83-93.

Schmitke, R.T. 1978 Ship sway, roll, and yaw motions in oblique seas. *Transactions of the Society of Naval Architects and Marine Engineers*, **86**, 26-46.

Shinbrot, M. 1954 On the analysis of linear and nonlinear dynamical systems from transient response data. *NACA TN 3288.*

Spouge, J.R. 1988 Non-linear analysis of large-amplitude rolling experiments. *International shipbuilding progress*, **35** (403), 271-320.

Standing, R.G. 1991 Prediction of viscous roll damping and response of transportation barges in waves. In *Proceedings of the First International Offshore and Polar Engineering Conference*, Edinburgh, U.K., 409-419.

Tanaka, N. *et al* 1980 Experimental study on hydrodynamics viscous force acting on oscillatory bluff body. *Kansai Society Naval Architects of Japan*, **179**.

Taylan, M. 2000 The effect of nonlinear damping and restoring in ship rolling. *Ocean engineering*, **27**, 921-932.

The papers of William Froude 1955 London: The Institution of Naval Architects.

Umeda, N. and Ikeda, Y. 1988 Application of slender body theory to rolling motion of a moving ship with bilge keels. *Journal of the Society of Naval Architects of Japan*, **163**, 181-193.

Watanabe, Iwao 1977 The effect of the forward velocity on the roll damping moment. *Papers of the Ship Research Institute, No.51.*

Zhang, Y. and Haddara, M.R. 1993 Parametric identification of nonlinear roll motion using roll response. *International shipbuilding progress*, **40** (424), 299-310.

Oceanic Engineering International, Vol. 9, No. 1, 2005, pp. 11-27

Design Criteria for Parametric Rolling

K.J. Spyrou

School of Naval Architecture and Marine Engineering, National Technical University of Athens, 9 Iroon Polytechniou, Zographou, Athens 157 73, Greece. Tel: +30 210 7721418, Fax: +30 210 7721408

email: k.spyrou@central.ntua.gr

ABSTRACT

Parametric rolling is a phenomenon of instability of a ship's upright state that can be realised in a longitudinal seaway and often leads to an oscillatory roll motion with moderate or large amplitude. In recent years it has been brought to the centre of attention following an accident and a discussion has been opened about the possibility of the adoption of relevant design criteria. Among ship parameters, roll damping has been singled out as the key factor governing the propensity toward this behaviour. This paper presents a review of the state of the art covering the various facets of parametric rolling for a deterministic, as well as for a probabilistic, environment. Furthermore, some new ideas about the development of practical design criteria are presented, based on the interfacing of deterministic transient responses with the probabilistic characteristics of wave groups.

1. INTRODUCTION

The problem of parametric rolling behaviour of ships in waves has attracted considerable interest recently following the accident of a C11-class containership, which has been described as the most costly containership casualty in history [France *et al.* 2003]. Attention was focussed on the propensity of large post–Panamax containerships for parametric rolling in "head-seas", the condition where the accident was reported to have occurred. However, parametric rolling has been traditionally linked with ship operation in following-seas where for several ship types it is easier, given a relatively low metacentric height, to satisfy one of the key conditions of parametric rolling; that is, the period of the waves as encountered by the ship to be near to one half of the natural roll period. IMO's [1995] "guidance to the master" (which notably refers to following-seas only) contains a recommendation for detecting the onset of parametric rolling during operation: ship masters are advised to determine the wave period through observation, transform it to encounter period on the basis of a suitable diagram that takes into account speed and heading, and then compare it to the one half of the natural roll period (as well as to the natural period itself, for the avoidance of "synchronous" rolling). Susceptibility to parametric rolling also depends, however, on the degree of variation of roll restoring moment between wave crests and troughs. The required amplitude of variation is determined principally by roll damping, by the wave "groupness" of the seaway, and by the run length of the encountered wave groups. Roll damping may be singled out as the key design parameter, determining the extremity of the environment where parametric rolling could be realised.

Whilst well-known as a phenomenon for at least half a century [Grim 1952; Kerwin 1995; Arndt & Roden 1958; Pauling & Rosenbersg 1959], no specific design requirements referring to parametric rolling have yet found their way into the IMO stability regulations. A possible explanation is that, while it is often the cause of intensive rolling, it is rarely documented to lurk behind a specific capsize accident. Yet, the market is becoming gradually conscious of the fact that even 'non capsizal' instabilities could be responsible for tremendous effects in terms of loss or damage of property and business interruption. Furthermore, the large number of containers lost overboard every year, according to a source between 2,000 and 10,000, represents a serious hazard for smaller vessels [Roenbeck 2003]. It is indicative of current interest that articles about parametric rolling appear often in the daily maritime press (e.g. Gray [2001]; Tinslay [2003]). A classification society has recently taken the lead, publishing a technical guide for the parametric rolling of containerships [ABS 2004].

A review of recent literature leads to the conclusion that, by-and-large, the dynamics of parametric rolling are nowadays well understood [Blocki 1980; Spyrou 2000 & 2004; Neves 2002; Bulian *et al* 2003; Umeda *et al* 2003; Shin *et al.* 2004].

Design aids, ranging between simple analytical formulae and complex numerical simulation codes, can be used for ruling out, or at least for containing, the probability of displaying parametric rolling. Unfortunately, as the process of ship design continues to be primarily regulations-led, this wealth of knowledge seems to be little utilised by the designers. As a matter of fact, some ships like modern post Panamax containerships and probably some of the new large passenger ships, especially those characterised by a heavily flared bow and flat stern with wide transom, may be sailing without having examined their tendency to display parametric rolling in a longitudinal seaway. Dedicated experiments like those of Dalinga *et al.* [1998] centred on a typical cruise ship and those reported by France *et al.* [2003] for the C11 containership seem to substantiate the concern.

In the present paper the intention is to demonstrate what current theories could offer in terms of prediction of parametric rolling. Deeper issues, such as the effect of nonlinearities, new phenomena due to coupled motions (especially the effect of heave/pitch in head seas and the interference of surging in following seas) and, last but not least, parametric rolling in a probabilistic context are also reviewed. As a resonance phenomenon by nature, parametric rolling calls, in the first instance, for a "deterministic" treatment where the effect of the environment is assumed as basically periodic. But of course, none could disregard that the seaway is stochastic. A meaningful interfacing of the deterministic and probabilistic facets of the problem is very desirable as it is can help to set the right level of stringency for the design requirements that accrue from the application of the various theories. Yet the issue is still scientifically unsettled. A methodology that promises to bring these two together within a single assessment procedure is also outlined in the paper.

2. BASIC "DETERMINISTIC" ANALYSIS

Parametric rolling is a resonance phenomenon manifested by the sudden oscillatory growth of roll which develops despite the absence of wave excitation in the direction transverse to the ship. It is broadly perceived to occur if the ratio of natural roll frequency, ω_0, to the encounter frequency, ω_e, satisfies the following resonance condition

$$2\frac{\omega_0}{\omega_e} \cong \pm n, \quad n = 1,2,3,... \tag{1}$$

The above condition defines, in fact, the vertices of the instability regions of Mathieu's equation. Basic facts about the instability regions of Mathieu systems, as well as their mathematical description, can be found in standard mechanics textbooks like Nayfeh & Mook [1979] and Hayashi [1985]. Given that $\omega_e = k(c\text{-}U)$, with $k = 2\pi/\lambda$, $c = \sqrt{gk}$, where k is wave number, c is wave celerity and λ is wave length, it is possible to convert equation (1) to an expression of Froude number. For positive frequencies of encounter this yields the following useful expression

$$Fn = \left(\frac{1}{\sqrt{2\pi}} \sqrt{\frac{\lambda}{L}} - \frac{2}{nT_0'} \frac{\lambda}{L} \right) \tag{2}$$

where L is the ship length and $T_0' = T_0\sqrt{g/L}$ is the non-dimensional natural roll period. With all other factors assumed unaffected, if the ship were sailing in an oblique sea the Froude number should be divided by $\cos\psi$ (with $\psi = 0$ corresponding to a following sea). This happens when the waves overtake the ship and also in all 'head sea' scenarios. A plot of equation (2) for a containership is shown in figure 1. The case $n = 1$ is the most likely to be realized and, in general, it dominates the attention in the literature.

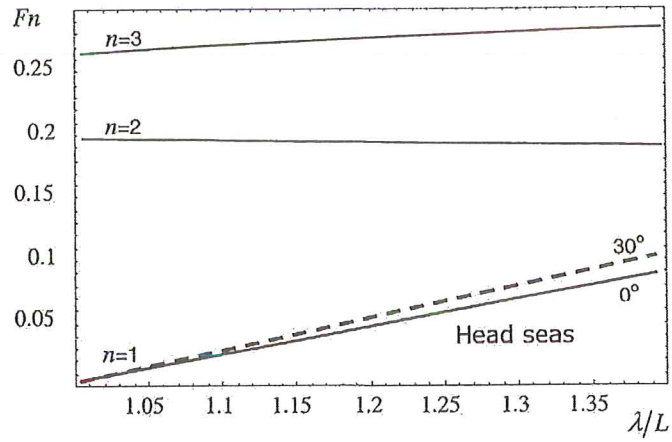

Figure 1. Froude numbers that could give rise to exact resonance for a containership. (L_{BP} = 262.0 m and T_0 = 25.7 s).

If the ship is prone to large variations of metacentric height (GM) from crest to trough, then encounter frequencies that depart from the exact resonance condition $\omega_e = \pm(2/n)\omega_0$ could still be eligible for producing growth of roll. As a matter of fact, it suffices to satisfy equation (1) or (2) only in an approximate sense. We shall scale the amplitude of GM variation against the average GM of the ship on the wave. In order to simplify the analysis the latter could be assumed, in the first instance, to be approximately equal to still water GM. Of course, strictly speaking there is no need for having the still water GM to coincide with the GM at the middle of the wave's up-slope or down-slope and, if a detailed calculation of the critical GM fluctuation is underway, the average GM on the considered wave should be used for the scaling (which means of course that the scale will vary with wave length and steepness). Taking things further, there also isn't any need for having a harmonic fluctuation of GM from crest to trough even if the wave were assumed to be perfectly harmonic. Strictly speaking this effect should be periodic and an analysis in Fourier series is likely to show several multiple frequencies in the fluctuation of GM. As a matter of fact, a so-called Hill's equation would be perhaps more representative. Whilst a direct attack on the problem in this spirit is nowadays possible, in the present context it would not help us to acquire the basic understanding about the phenomenon. Under the

assumptions of 'small' and harmonically varying h ($= \frac{\delta GM}{GM} = \frac{GM_{trough} - GM_{crest}}{2GM}$), a well-known result from perturbation analysis for the boundary line of the first (principal) resonance is (see for example Hayashi [1985])

$$h_{1+} = 2\left(1 - \frac{1}{a}\right) \quad h_{1-} = 2\left(\frac{1}{a} - 1\right) \tag{3}$$

where the first equation refers to $a \geq 1$ and the second to $a < 1$. The independent parameter a is defined as $a = 4\omega_0^2/\omega_e^2$. To grasp the order of magnitude, an ω_e higher than the frequency of exact principal resonance ($= 2\omega_0$) by 10%, would entail, according to equation (3), $h = 0.42$. On the other hand, for an ω_e 10% lower than $2\omega_0$ the required h becomes 0.3471.

3. RATE OF GROWTH OF ROLL IN THE FIRST REGION OF INSTABILITY

For a "Mathieu system" the unstable motion that corresponds to the first region of instability should build up according to the following approximate general solution [Hayashi 1985]

$$\varphi(t) \approx c_1 e^{\mu\omega_0 t} \sin(\omega_0 t - \sigma) + c_2 e^{-\mu\omega_0 t} \sin(\omega_0 t + \sigma) \tag{4}$$

where μ, σ, are functions of a, h and they are determined from the relationships (only first-order terms are kept)

$$\cos 2\sigma \approx \frac{2(a-1)}{ah} \quad \left(-\frac{\pi}{2} \leq \sigma \leq 0\right), \qquad \mu \approx -\frac{\sqrt{a^2h^2 - 4(a-1)^2}}{4} \tag{5}$$

At $a = 1$ the coefficient μ obtains its maximum value $\mu_{max} = -h/4$ where $\sigma = -\pi/4$. We can then determine the corresponding growth per roll cycle

$$\frac{\varphi(T_0)}{\varphi(0)} = \frac{\frac{\sqrt{2}}{2}\left(c_1 e^{\frac{\pi h}{2}} - c_2 e^{-\frac{\pi h}{2}}\right)}{\frac{\sqrt{2}}{2}(c_1 - c_2)} \tag{6}$$

After substitution of the initial conditions $\varphi(0) = \varphi_0$ and $\dot{\varphi}(0) = 0$ in equation (6), it can be shown that $c_1 = -c_2 = \varphi_0\sqrt{2}/2$. Then equation (6) yields (see also figure 2)

$$\frac{\varphi(T_0)}{\varphi_0} = \frac{e^{\frac{\pi h}{2}} + e^{-\frac{\pi h}{2}}}{2} \approx 1 + \frac{\pi^2 h^2}{8} \tag{7}$$

In general, after p roll cycles the growth is

$$\frac{\varphi(pT_0)}{\varphi_0} = \frac{e^{\frac{p\pi h}{2}} + e^{-\frac{p\pi h}{2}}}{2} \tag{8}$$

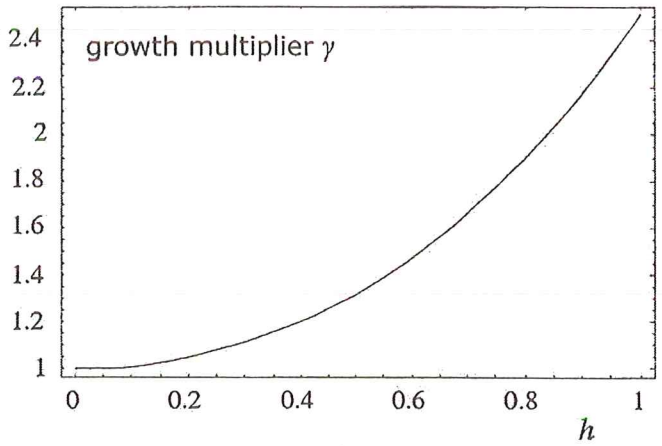

Figure 2. Growth of roll in the first region, for a single roll cycle, as function of the parametric amplitude h (no damping).

4. THE EFFECT OF DAMPING

Let us consider now a roll model based on Mathieu's equation with damping,

$$\ddot{\varphi} + 2k\dot{\varphi} + \omega_0^2\left[1 - h\cos(\omega_e t)\right]\varphi = 0 \tag{9}$$

k is half the dimensional damping divided by the roll moment of inertia including the added moment. The above can be transformed into an equivalent Mathieu equation (with no "explicit" damping term) by introducing the change of variable $\varphi = we^{-kt}$

$$\ddot{w} + \left(\omega_0^2 - k^2\right)\left(1 - \frac{\omega_0^2}{\omega_0^2 - k^2} h\cos\omega_e t\right) w = 0 \tag{10}$$

The effect of damping on the growth of amplitude is easily perceived. The combination of equations (8) and (10) yields the amplitude after one roll cycle

$$\varphi(T_0) = w(T_0)e^{-\frac{2\pi k}{\omega_0}} \approx \underbrace{\frac{e^{\frac{\pi h}{2}} + e^{-\frac{\pi h}{2}}}{2}}_{\gamma} \underbrace{e^{-\frac{2\pi k}{\omega_0}}}_{\gamma_d} w_0 = \frac{e^{\frac{\pi}{2}\left(h - \frac{4k}{\omega_0}\right)} + e^{-\frac{\pi}{2}\left(h + \frac{4k}{\omega_0}\right)}}{2} \varphi_0 \tag{11}$$

From the exponential term $e^{\frac{\pi}{2}\left(h-\frac{4k}{\omega_0}\right)}$ we extract the well-known condition of stability (i.e. no growth)

$$h_{crit} = \frac{4k}{\omega_0} \tag{12}$$

It is observed that the 'apparent' damping of the system is intensified at low frequencies.

Damping shifts the first region of instability (and in fact also all subsequent regions) upwards; i.e. it incurs a stabilising effect on the upright state, rendering it insensitive to small or moderate amplitude fluctuations of restoring and thus, loosely speaking, to waves of small or moderate height, even if these arrive with the right tuning. As a matter of fact, proper selection of damping can lead to negligible probability of encountering critical wave groups (in terms of the combination of the amount of height exceeded and frequency tuning). This provides the key instrument for eliminating parametric rolling through design.

The boundary line of the region of principal resonance obtained, e.g. with the method of harmonic balance, is

$$h_{crit} = 2\sqrt{\frac{(a-1)^2}{a^2} + \frac{4k^2}{a\omega_0^2}} \tag{13}$$

If we set $a = 1$ we come to an alternative derivation of the stability criterion equation (12). Strictly speaking, there should be a slight shift of the vertex, from $a = 1$ to $1+2k^2/\omega_0^2$ if damping up to second order were kept; then the lowest point of the boundary curve should also be slightly modified, to $4k\sqrt{\omega_0^2+3k^2}\,/\left(\omega_0^2+2k^2\right)$.

The growth inside this region may be determined, to first approximation, from equation (4). The exponent μ indicates how deeply we lie inside the instability region; while the phase σ (ranging from 0 to $-\pi/2$) indicates the distance from the sides of the boundary ($\sigma = 0$ at the right boundary and $\sigma = -\pi/2$ at the left boundary).

In general, the growth of amplitude after p roll cycles at exact resonance ($a = 1$) is

$$\varphi\left(pT_0\right) \approx e^{-\frac{2p\pi k}{\omega_0}}\left(\frac{e^{\frac{p\pi h}{2}}+e^{-\frac{p\pi h}{2}}}{2}\right)\varphi_0 \tag{14a}$$

For the first one or two cycles the growth is first order for k (i.e. k influences growth) but second order for h

$$\varphi\left(pT_0\right) \approx \left(1-\frac{2\pi\, pk}{\omega_0}+\frac{2\pi^2 p^2 k^2}{\omega_0^2}\right)\left(1+\frac{\pi^2 p^2 h^2}{8}\right)\varphi_0 \tag{14b}$$

A q-fold increase in roll amplitude from some initial angle of disturbance should entail, according to equations (14a) and (14b), p roll cycles

$$\ln q \approx -\frac{2p\pi k}{\omega_0} + \ln\left(\frac{e^{\frac{p\pi h}{2}}+e^{-\frac{p\pi h}{2}}}{2}\right) \tag{15}$$

Given that, after a few roll cycles the dominant exponential term of (15) is the one with positive sign, the above may be written further, approximately, as

$$\ln q \approx -\frac{2p\pi k}{\omega_0} + \frac{p\pi h}{2} - \ln 2 = \frac{p\pi}{2}\left(h-\frac{4k}{\omega_0}\right) - 0.693 \tag{16}$$

It follows that for a q-fold increase of amplitude the necessary number of cycles p should be

$$h - \frac{4k}{\omega_0} = \frac{0.693 + \ln q}{1.571\, p} \tag{17}$$

The time t_m required for this should be p times the natural period T_0

$$t_q = pT_0 \tag{18}$$

To demonstrate the usefulness of formula (17), let us think in terms of the following tentative criterion: a 10-fold increase of roll amplitude should never come about in less than 4 roll cycles for a wave with $\lambda/L = 1.0$, $H/\lambda = 1/20$. At principal resonance 4 roll cycles mean 8 critical wave encounters (it is possible to link this with the probability of encounter of a dangerous wave group with these dominant characteristics). The above translate into the following relationship for the parameters h, k

$$h - \frac{4k}{\omega_0} \le \frac{0.693 + \ln 10}{1.57 \times 4} \approx \frac{3}{6.282} = 0.477 \tag{19}$$

Criterion (17) targets transient response. Compared to equation (12), which is a criterion of asymptotic stability, it is superior in the sense that it does not suffer from the unrealistic assumption of the encounter of a critical wave group with infinite run length. The condition of asymptotic stability is recovered from equation (17) if we set $p \to \infty$ at the right hand side of (17). The transient response criterion (17) should probably be supplemented by a time requirement based on equation (18). For example, the 4 roll cycles would take $25.7 \times 4 = 102.8$ s. For very low natural frequencies, i.e. following seas, the required time becomes excessive. This leaves time for reaction (i.e. change of speed or heading) as soon as the beginning of the phenomenon is realised.

5. THE HIGHER REGIONS OF INSTABILITY

Among all parametric resonances, the principal one requires the lowest amplitude h (in general the required amplitude h is

proportional to $k^{1/n}$ where n is the order of the resonance). Although a criterion like equation (12) is stringent, it informs about the minimal h required for reaching the region of principal resonance (n = 2). In some cases the ship's natural frequency is such that the scenario of principal resonance turns improbable, whereas the second resonance falls within the attainable speed range.

The perturbation analysis result for the boundary of the region of fundamental resonance is [Hayashi 1985]

$$h_{2+} = 4\sqrt{\frac{3}{5}}\frac{\sqrt{a-4}}{a}$$
$$h_{2-} = 4\sqrt{3}\frac{\sqrt{4-a}}{a} \qquad (20)$$

The third or higher instability regions require long encounter periods [$\omega_e = (2/n)\omega_0 < \omega_0$ since $n = 3, 4 \ldots$], i.e. following seas and speeds quite near to wave celerity. However, these resonances have extremely low probability of occurrence, primarily due to the stabilising effect of damping.

There are several general formulae for predicting, approximately, the critical h for any resonance region, with damping taken into account. Two of these are Taylor & Narendra [1969]

$$h = \pi\frac{k}{\omega_0}\sqrt{a} \qquad (21)$$

and Gunderson, Rigas & Van Vleck [1974]

$$h = \left(1 - \frac{k^2}{\omega_0^2}\right)\tanh\left(\pi\frac{k}{\omega_0}\sqrt{a}\right) \qquad (22)$$

Equation (22) is free from the assumption of small damping that usually limits the applicability of perturbation methods.

Perhaps the most accurate expression for the minimal h is from Turyn [1993]

$$h = \frac{8}{n^2}\sqrt[n]{\frac{k\,n!}{2\omega_0}} \qquad (23)$$

The above is calculated at a = 1 for n = 1 while for n $n \geq 2$ it should be calculated at

$$a = n^2 + \frac{8}{n^2-1}\sqrt[2/n]{\frac{k(n!)^2}{2\omega_0}} + \frac{k^2 n^2}{\omega_0^2} \qquad (24)$$

It turns out that the required h (which is, practically, the representative of wave steepness through the "filter" of the hull) increases quickly from n = 1 to n = 2. Take for example a ship with $\zeta = k/\omega_0 = 0.06$. At principal resonance the threshold is $h = 4\zeta = 24\%$ while at the fundamental it becomes, according to Turyn's formula, about 45.2%. Later resonances require even higher h although the rate of increase is lowered. The combination of requirements for high speed [see equation (2) and figure 1] and extreme restoring fluctuation (which calls for unrealistic wave dimensions), render the resonances above n=2 of almost negligible probability.

6. STOCHASTICALLY VARYING METACENTRIC HEIGHT: REVIEW OF STABILITY CRITERIA

For a section of the Market the occurrence of parametric rolling in a realistic sea is rather unfounded (see for example Ractliffe [2002]). Nonetheless, since the 70s and the 80s the problem has been recognised as important in naval architecture and a theoretical basis for the analysis of probabilistic parametric rolling has been developed [Price 1974; Vinje 1975; Skomedal 1982; Muhuri 1980; Roberts 1982; Dunwoody 1989]. Conceptually, all these approaches represent adaptations of theories from the field of stochastic differential equations (see for example Caughey & Dienes [1962]; Kozin [1969]; Arnold [1973]; Ariaratnam & Tam [1979]; Roberts & Spanos [1986]; Ibrahim [1986]). In the literature of mechanics it is more common to come across investigations of systems excited parametrically by white noise. However, in a parametric rolling investigation, the shape of the spectrum, and especially the "narrow-band" characteristic that creates a higher probability of encounter of wave groups, should not be neglected. As is well known, even for a linear stochastic system one could think of different definitions of stability. We may think in terms of convergence in probability, convergence in the mean and "almost sure" convergence. Hence a variety of criteria are found in the literature. Two concepts seem to be the most popular: The so called "almost sure" or "sample function" stability which implies that, as time tends to infinity, all samples, except for a set of measure zero, tend to the stationary solution; and the stability of moments. These criteria can take into account the damping and some characteristic of the spectrum of the fluctuating metacentric height.

For systems whose evolution is a diffusion Markov process the method of stochastic Lyapounov functions is one of the possible ways for deriving a criterion of almost sure asymptotic stability (see for example Gray [1967]). Assuming Gaussian fluctuation of GM with zero mean, Vinje [1975] derived the following simple ship stability criterion of parametric rolling based on a Lyapounov function $V(\varphi)$ that, as time goes to infinity, tends to 0 with probability 1.

$$\sigma < \frac{\sqrt{2\pi}\,k}{\omega_0} \qquad (25)$$

For a harmonic process with amplitude h, the standard deviation is $\sigma = \frac{\sqrt{2}}{2}h$ and the above should become

$h < \frac{2\sqrt{\pi}\,k}{\omega_0}$ which falls midway between $\frac{4k}{\omega_0}$ of equation (12) and Taylor & Narendra's $\frac{\pi k}{\omega_0}$ from equation (21), i.e. the criterion may be too stringent.

By using the extreme properties of quadratic forms, Infante [1968] has shown that for a typical parametric system

$$\frac{d\mathbf{x}}{dt} = \left[\mathbf{A} + \mathbf{F}(t)\right]\mathbf{x} \tag{26}$$

a sample time evolution can be expressed as

$$\|\mathbf{x}(t)\| < \|\mathbf{x}(0)\|\, e^{\left[\frac{1}{t}\int_0^t \lambda(\tau)d\tau\right]t} \tag{27}$$

where, $\lambda(\tau)$ is the maximum eigenvalue of the matrix $\left\{\left[\mathbf{A}+\mathbf{F}(t)\right]^T\mathbf{B} + \mathbf{B}\left[\mathbf{A}+\mathbf{F}(t)\right]\right\}\mathbf{B}^{-1}$. The constant matrix B is symmetric positive definite and determines the norm of the process x which is expressed as $\sqrt{\mathbf{x}^T\,\mathbf{B}\,\mathbf{x}}$. Assuming that $\mathbf{F}(t)$ is ergodic, then

$$\lim\frac{1}{t}\int_0^t \lambda(\tau)d\tau = \mathrm{E}\left[\lambda(\tau)\right] \quad \text{with probability 1.0} \tag{28}$$

It accrues that it suffices to request the expectation $\mathrm{E}\left[\lambda(\tau)\right] < 0$. The derived condition is a sharper one compared to equation (25)

$$\sigma < \frac{2k}{\omega_0} \tag{29}$$

"Almost sure" stability depends on the exponential growth rate of the response of the random system. This is critically influenced by the sign of the maximum Lyapounov exponent which may be regarded as the stochastic analogue of the real part of the largest eigenvalue of a linearised system under deterministic excitation.

$$\lambda = \lim\frac{1}{t}\ln\|\mathbf{x}(t;\mathbf{x}_0)\| \tag{30}$$

Here, by $\|\ \|$ is meant the norm of the stochastic process $\mathbf{x}$. A j-dimensional system should have j Lyapounov exponents at most. If the largest one is less than 0, then "almost surely" $\mathbf{x}(t;\mathbf{x_0})$ should tend to 0 as time goes to infinity. The maximum Lyapounov exponent may be obtained from the so-called "Fustenberg-Khasminski" formula [Namachchivaya & Ramakrishnan, 2003]

$$\lambda = -\varepsilon^2\, 2k\left[-\frac{1}{2} + \frac{\pi\,\omega_0^2}{8k}S_h(2\omega_0)\right] \tag{31}$$

and the following definitions apply.

$$S_h(2\omega_0) = 2\times\frac{1}{2\pi}\int_0^\infty R_{hh}(\tau)\cos(2\omega_0\tau)\,d\tau, \qquad R_{hh}(\tau) = E\left[h_t\, h_{t+\tau}\right] \tag{32}$$

To ensure that λ is negative, the condition is

$$k > \frac{\pi\omega_0^2}{4}S_h(2\omega_0) \tag{33}$$

The largest Lyapounov exponent does not provide information about the rate of convergence or about the stability of moments. This could be obtained from the moment Lyapounov exponent [Nolan & Namachchivaya 1999] that, however, leads to criteria of higher stringency. To determine the p-th moment stability we solve for the p-th moment of the amplitude response and compute the moment Lyapounov exponent defined as

$$\lambda^{(p)}(\varphi_0) = \lim\frac{1}{t}\ln \mathrm{E}\|\varphi(t;\varphi_0)\|^p \tag{34}$$

where $\mathbf{E}$ denotes the expectation. As previously, if $\lambda^{(p)}(\varphi_0) < 0$ then $\mathrm{E}\|\varphi(t;\varphi_0)\|^p \to 0$ as time tends to infinity (condition of p-th moment stability). For our parametric system the above condition produces the following moment stability criterion

$$\lambda^{(p)} = \varepsilon^2\, 2p\,k\left[-\frac{1}{2} + \frac{p+2}{16}\frac{\pi\,\omega_0^2}{k}S(2\omega_0)\right] \tag{35}$$

The condition ensuring negative $\lambda^{(p)}$ is

$$k > \frac{p+2}{8}\pi\omega_0^2\, S_h(2\omega_0) \tag{36}$$

Roberts [1982] applied to roll stability the method of stochastic averaging of Stratonovitch (see Roberts & Spanos [1986] for a review) in order to circumvent the problem of dealing with non-white noise parametric excitation. He proposed that, since the joint process of roll amplitude and phase (A,ϑ) converges weakly (as the damping goes to zero) to a two-dimensional Markov process, (A,ϑ) is governed by the so-called 'Ito equations' (see, for example, Ito [1951]) from which a Fokker-Planck-Kolmogorov (FPK) equation is derived for the transition probability density of the joint process. Especially in the amplitude Ito equation the phase is not present and thus $A(t)$ can be treated as a one-dimensional Markov process whose transition probability density should depend only on $A(t)$. The assumption of the stationary nature of $A(t)$ means that the time derivative of the transition probability function should be zero. This simplifies the calculations resulting in the criterion of Ariaratnam and Tam [1979] for sample function stability, which involves the natural frequency, the damping and the spectral density of the fluctuating GM process at twice the natural frequency

$$k > \frac{\pi \omega_0^2 S_h(2\omega_0)}{4} \tag{37}$$

The above criterion, which is useful for linear stability (i.e. only for the upright state), is identical with criterion (29) based on the largest Lyapounov exponent. But, as noted also by Bulian *et al.* [2003], it is not useful for telling the characteristics of the ensuing nonlinear response because in the expression of roll amplitude the nonlinear stiffness term does not partake in the averaging process. Skomedal [1982] carried out a comparison against model test data of Roberts' predictions of the variance of roll amplitude and found that the predicted roll variance is overestimated.

Stability of sample functions is perhaps what interests us most. The criteria for the stability of moments are more severe in terms of the required minimal damping; by 50% (in terms of minimal k) for the first moment and by 100% for the second.

Dunwoody [1989] proposed a sample function stability criterion on the basis of the observation (already apparent from our investigations in previous sections) that the fluctuations of GM produce an effect that works like a reduction of roll damping. By requesting that the damping ratio is greater than the expectation of this effective damping due to GM's fluctuation, a criterion of stability can be deduced which is identical with equation (12). Assuming that the amplitude h is Rayleigh distributed, its expectation is

$$E[h] = \sqrt{\frac{\pi}{2}}\,\sigma_h < \frac{4k}{\omega_0} \tag{38}$$

7. A UNIFYING APPROACH BASED ON WAVE GROUPS

It is well known that higher waves tend to arise in groups. As the nearly regular characteristics of waves in a group are essential for giving rise to resonant motions like parametric rolling, there is a meaningful link between the probabilistic nature of ocean waves and the deterministic analysis of the earlier sections of this paper. The probability of occurrence of parametric rolling could be assumed to be equal to the probability of encountering a wave group with a suitable run length and exceeding the threshold wave height determined from the deterministic analysis, given that the frequency falls in the critical range. This viewpoint is indeed fundamentally different form the conventional one of linear seakeeping analysis where the wave field is approached as the superposition of regular waves with arbitrary phase and energy. Instead, here the extreme wave field is approached as a sequence of wave groups [Spyrou 2004].

Attention to wave groups is not completely new. Assuming no correlation between successive wave heights and without setting any requirement about the period, Blocki [1980] determined the probability of encounter of a dangerous wave group by using a Rayleigh probability density function for the amplitude, whose integration from a critical level ρ to infinity should produce the probability of exceeding ρ. The probability of encountering a succession of j waves (i.e. a group) having this property should be calculated from the well known formula (e.g. Goda [1976])

$$P(A_j) = P^{j-1}(1-p) \tag{39}$$

Takaishi *et al.* [2000] targeted the probability of encountering a "high run" of waves and developed an operational guidance for shipmasters. His approach was based on Longuet-Higgins' [1984] statistical properties of wave groups. The key point was the observation that, in following/quartering seas, there is a range of speeds where all the energy of the wave field is concentrated within a very narrow range of encounter wave frequencies due to the Doppler effect. In other words, the encounter spectrum becomes very narrow, which increases the probability of encounter of a "high run". The well-known relation between the encountered wave spectrum $S(\omega_e, \mu)$ and the "true" wave spectrum is

$$S(\omega_e, \mu) = \frac{S(\omega)}{\left|1 - \frac{2\omega U \cos\mu}{g}\right|}, \quad \omega_e = \omega - \frac{\omega^2 U}{g}\cos\mu \tag{40}$$

where μ is the encounter angle and U is ship speed. As a resonance mechanism, parametric rolling entails the encountered wave frequency to be in some approximate relationship with the natural roll frequency. If, at the encounter frequencies of energy concentration, this approximate relationship holds true, then a very dangerous setup for parametric rolling is in place. However, from a design point of view the anticipated speed U in a storm is quite uncertain and some probability distribution $P(U)$ should be assumed instead of a discrete value.

An improved approach concerning the same problem could incorporate theoretical or parametric models for the joint distributions of wave parameters because wave height and period, successive wave heights, as well as successive wave periods of extreme waves are generally correlated. Unfortunately, the desirable multivariate distributions are not yet available in the literature. For practicality, one has to make certain assumptions about the correlation of key parameters in a wave group and opt to use available bivariate distributions. Bivariate probability density functions of height and period of ocean waves have been proposed by a number of investigators, (see for example Longuet-Higgins [1975], Cavanié *et al.* [1976], Longuet-Higgins [1983]). The last one of Longuet-Higgins is shown below as described by Demirbilek & Linwood Vincent [2002]

$$p(H,T) = \frac{\pi f(\nu)}{4}\left(\frac{H_*}{T_*}\right)^2 e^{-\frac{\pi H_*^2}{4}\left(1+\frac{1-\frac{\sqrt{1+\nu^2}}{T_*}}{\nu^2}\right)} \tag{41}$$

where

$$H_* = \frac{H}{\overline{H}} \tag{42}$$

$$T_* = \frac{T}{\overline{T}_z}, \tag{43}$$

$$f(\nu) \approx \frac{2\left(1+\nu^2\right)}{\nu + \sqrt{1+\nu^2}} \tag{44}$$

$$\nu = \sqrt{\frac{m_0 m_2 - m_1^2}{m_1^2}} \tag{45}$$

As usual m_0, m_1, m_2, are respectively zeroth, first and second moment of the (encountered) wave spectrum, $\overline{H}$ is the mean wave height; and $\overline{T}_z$ is the mean zero- upcrossing period that is calculated from the spectral moments, $\overline{T}_z = 2\pi\sqrt{m_0/m_2}$. It is to be noted that the spectral width parameter ν, and subsequently the distribution, depends only on the first three moments.

The probability of encounter of a wave with height above the critical one H_c and with ω_e near to $2\omega_0$ (say ±20%), should be calculated from the double integral

$$P\left[H > H_c,\ 0.8T_c < T_e < 1.2T_c\right] = \int_{H_c}^{\infty}\int_{0.8T_c}^{1.2T_c} p(H,T_e)\,dT_e\,dH \tag{46}$$

Thereafter, the probability of encountering a wave group with these characteristics and, in addition, a run length j, should be given by again applying equation (39). Even this approach, however, takes into account neither the correlation between successive wave periods nor the correlation between successive wave heights.

Distributions of successive wave periods have been employed by Myrhaug *et al.* [2000] for developing a probabilistic assessment of beam-sea rolling. Although ideally this correlation should be inside a probabilistic assessment of parametric rolling, it is less important compared to the correlation of successive wave heights because, due to the interference of speed, the critical wave period is relatively uncertain at the design stage. On the other hand, parametric instability becomes possible only if a certain wave height is exceeded. As a matter of fact, if a choice has to be made, the correlation of wave heights should be higher priority.

The degree of correlation between successive wave heights depends on the sharpness of the spectral peak. For the effect of the spectral bandwidth on the distribution of wave height see, for example, Kimura [1980], Tayfun [1983] and Longuet-Higgins [1984]. Stansell *et al.* [2002] found that, as bandwidth increases, there is a rather slight reduction in the mean run and group length, up to a bandwidth $\nu = 0.6$ beyond which they become rather insensitive. To obtain a sense of magnitude we note that $\nu = 0.425$ for a Pierson Moskowitz and $\nu = 0.389$ for a JONSWAP spectrum).

According to Tayfun, the sharpness of the spectral peak reflects the variability of height between successive waves and is best represented by the correlation coefficient of the wave envelope R_{HH} which could be calculated as

$$R_{HH} = \frac{E(\kappa) - \left(1-\kappa^2\right)\frac{K(\kappa)}{2} - \frac{\pi}{4}}{1-\frac{\pi}{4}} \approx \frac{\pi}{16-4\pi}\left(\kappa^2 + \frac{\kappa^4}{16} + \frac{\kappa^6}{64}\right) \tag{47}$$

$E(\ )$, $K(\ )$ are complete elliptic integrals of the first and second kind, respectively. The correlation parameter κ could be calculated as follows (see Stansell *et al.* [2002] for an extensive discussion on alternative methods).

$$\kappa\left(\overline{T}_z\right) = \frac{1}{m_0}\sqrt{A^2 + B^2}, \tag{48}$$

$$A = \int_0^{\infty} S(f)\cos 2\pi f\,\overline{T}_z\,df, \tag{49}$$

$$B = \int_0^{\infty} S(f)\sin 2\pi f\,\overline{T}_z\,df \tag{50}$$

where $f = \omega_e/2\pi$ (Hz) and $S(\ )$ is the encounter spectrum. Goda [1976] has found that, for swells, the correlation coefficient R_{HH} is about 0.6 while for wind waves it is only about 0.2.

Assuming that successive wave heights follow a Rayleigh distribution, Kimura [1980] derived the following bivariate probability density function $p(H_1, H_2)$ for consecutive wave heights

$$p_{HH}(H_1, H_2) = \frac{4H_1H_2}{\left(1-\kappa^2\right)H_{rms}^4} e^{-\frac{\left(H_1^2+H_2^2\right)}{\left(1-\kappa^2\right)H_{rms}^2}} I_0\left(-\frac{2\kappa H_1 H_2}{\left(1-\kappa^2\right)H_{rms}^2}\right) \tag{51}$$

where H_{rms} is the root mean square wave height and I_0 is the modified Bessel function of zeroth order. The probability of having two consecutive wave heights above the critical height H_c will then be

$$P\left(H_{i+1} \geq H_c \middle| H_i \geq H_c\right) = \frac{\int_0^{H_c}\int_0^{H_c} p_{HH}(H_1,H_2)dH_1\,dH_2}{\int_0^{H_c} p_H(H)dH} \tag{52}$$

where $p_H(H)$ is the marginal probability density which is Rayleigh type

$$p_H(H) = \frac{2H}{H_{rms}^2} e^{-\frac{H^2}{H_{rms}^2}} \tag{53}$$

The assumption of a Markov chain for successive wave heights means that the probability of occurrence of a group with length j and heights above H_c can be calculated again on the basis of equation (39) where this time, however, $P = P\left(H_{i+1} \geq H_c \middle| H_i \geq H_c\right)$. To overcome the neglect of wave period, the above could be multiplied by a susceptibility factor indicating whether the speed range of the ship produces

encounter frequencies that overlap with the frequencies of principal resonance.

8. RESPONSE FEATURES DUE TO GEOMETRICAL NONLINEARITIES

We shall revert now to the deterministic case, in order to consider behaviour away from the vicinity of the upright state. As is well known, there is no reason for the parametric growth of roll to persist up to infinity and thus lead by necessity to capsize. The detuning due to the nonlinear character of the *GZ* curve combined with the increased dissipation due to the mild nonlinearity of damping, creates the prospect of realising bounded rolling with moderate amplitude. In effect, for a typical parametric growth with nonlinear restoring the boundary curves of stability discussed earlier represent loci of sub-critical and supercritical bifurcations creating, respectively, unstable and stable oscillatory behaviour (see for example Skalak & Yarymovych [1960], Soliman & Thompson [1992]). At a supercritical bifurcation the new type of stable behaviour emerges smoothly while at a sub-critical the new type comes about with a jump.

A truly interesting observation is that the instability boundary curves determined earlier for the upright state do not entirely contain the domain where parametric oscillations are realisable. At first sight, in an idealised environment of a periodic seaway that is free from other external disturbances, the system should find no reason to leave the upright state as long as the combination of frequency ratio and parametric amplitude corresponds to some point in the region of stability. Nonetheless, the emerging stable roll oscillations need not be confined inside the "tongues" of the linear system and stable oscillations also exist well outside these regions [Scalak & Yarymovich 1961; Thompson & Soliman 1993; Francescutto & Dessi 2001]. Should the stable upright condition be sufficiently disturbed, this oscillatory behaviour can be incurred in an abrupt way. A well-focused experimental effort is required for establishing this theoretical prediction.

To take these points further, let us consider a Mathieu-type roll equation with a nonlinear term

$$\ddot{\varphi} + 2k\dot{\varphi} + \omega_0^2\left[1 - h\cos(\omega_e t)\right]\varphi - c_3\omega_0^2\varphi^3 = 0 \qquad (54)$$

The constant c_3 could be negative, in which case we are practically confined to studying the oscillations corresponding to the initial part of the $GZ(\varphi)$ curve which may be of "hardening spring" type; or it could be positive in which case we may be referring generically to the whole $GZ(\varphi)$ curve up to the angle of vanishing stability. In the last case, the vanishing angle is linked to c_3 with the relationship $\varphi_v = 1/\sqrt{c_3}$. There is no strict justification for assuming c_3 to be non-time-dependent. If the oscillations were of reasonably small amplitude, the product of the 3rd power of the scaled roll angle times the amplitude (assumed as small by necessity) of the fluctuating part of nonlinear stiffness might be considered negligible. Hence a representation like equation (49) could be taken as the basic generic model.

With the definitions

$$\tau = \omega_e t\,, \qquad a = 4\frac{\omega_0^2}{\omega_e^2} \qquad (55)$$

the above can be written further as

$$\frac{d^2\varphi}{d\tau^2} + \frac{2k\sqrt{a}}{\omega_0}\frac{d\varphi}{d\tau} + a\left(1 - h\cos 2\tau\right)\varphi - ac_3\varphi^3 = 0 \qquad (56)$$

If we confine ourselves to symmetric-type responses (it sounds strange that non-symmetric responses could exist; but this is well-known for several parametrically-excited mechanical systems), we may write the solution of the above as a Fourier series with odd terms only as

$$\varphi = \sum_{\nu=1}^{\infty}\left[A_\nu(\tau)\sin\nu\tau + B_\nu(\tau)\cos\nu\tau\right], \quad \nu = 1,3,5,\ldots \qquad (57)$$

In general, the first term ($\nu = 1$) in the series suffices for the level of accuracy sought by the present analysis. Substitution of the approximate solution $\varphi = A_1(\tau)\sin\tau + B_1(\tau)\cos\tau$ into (57) and assuming that the sine and cosine amplitudes $A_1(\tau)$, $B_1(\tau)$, respectively vary slowly in time, yields the following two equations.

$$\begin{aligned}\dot{B}_1(\tau) = &\left(-1 + a + \frac{ah}{2}\right)A_1(\tau)\\ &-\frac{3}{4}ac_3A_1(\tau)\left[A_1^2(\tau) + B_1^2(\tau)\right]\\ &-\frac{2k\sqrt{a}}{\omega_0}B_1(\tau)\end{aligned} \qquad (58)$$

$$\begin{aligned}\dot{A}_1(\tau) = &-\frac{2k\sqrt{a}}{\omega_0}A_1(\tau)\\ &+\frac{3}{4}ac_3B_1(\tau)\left[A_1^2(\tau) + B_1^2(\tau)\right]\\ &-\left(-1 + a - \frac{ah}{2}\right)B_1(\tau)\end{aligned} \qquad (59)$$

At steady state there is no change of amplitude and hence we should request

$$\left(-1 + a + \frac{ah}{2}\right)A_1 - \frac{3}{4}ac_3A_1\left(A_1^2 + B_1^2\right) - \frac{2k\sqrt{a}}{\omega_0}B_1 = 0 \qquad (60)$$

$$\frac{2k\sqrt{a}}{\omega_0}A_1 - \frac{3}{4}ac_3B_1\left(A_1^2 + B_1^2\right) + \left(-1 + a - \frac{ah}{2}\right)B_1 = 0 \qquad (61)$$

By expressing A_1,B_1 in terms of the steady roll amplitude $A = \sqrt{A_1^2 + B_1^2}$ and phase ϑ, i.e. $A_1 = A\sin\vartheta$, $B_1 = A\cos\vartheta$, and

following some further algebraic manipulation we arrive at the following set

$$\sin 2\vartheta = \frac{4k}{h\omega_0\sqrt{a}} \tag{62a}$$

$$\cos 2\vartheta = \frac{2}{h}\left(1-\frac{1}{a}-\frac{3}{4}c_3A^2\right) \tag{62b}$$

The right hand side of (62a) is always positive; hence $0 \le \vartheta \le \pi/2$. The right hand side of the lower expression may be positive or negative, depending on the sign of the coefficient of the nonlinear term c_3 and on whether we lie to the left or to the right of $a = 1$.

The combination of the above produces the following explicit formula for the amplitude.

$$A^2 = \frac{4}{3c_3}\left[\left(1-\frac{1}{a}\right) \mp \sqrt{\frac{h^2}{4}-\frac{4k^2}{a\omega_0^2}}\right] \tag{63}$$

Setting $A \to 0$ we find the curve whereon the oscillations are created. It comes as no surprise that this curve is independent of the nonlinear coefficient n and it coincides with the boundary of linear stability. Also, the term inside the square root, as well as the whole expression of A^2, should be non-negative. For, say, an initially hardening restoring ($c_3 < 0$) these yield

$$h \ge \frac{4k}{\omega_0\sqrt{a}} \quad \text{and} \quad a \le 1 \tag{64}$$

Essentially, equations (64) define a locus of "saddle-node" bifurcations where the response curve is "folded". The unstable periodic orbits that emerged at the left boundary of the region of instability go through a U-turn and they are rendered stable. Equation (64) determines the true boundary of periodic response. For a certain level of h, the region with oscillations is wider than the one predicted from linear analysis. The stability boundary of the principal resonance is in fact a bifurcation locus as shown in figure 3. For hardening restoring the right part ($a>1$) is of super-critical type and the left part ($a>1$) of sub-critical type. These properties are reversed when the restoring is softening.

For $c_3 < 0$ ("hardening GZ") the amplitudes are

$$a \ge 1: \quad A_{a=1+} = \sqrt{-\frac{4}{3c_3}}\sqrt{\left(\frac{1}{a}-1\right)+\sqrt{\frac{h^2}{4}-\frac{4k^2}{a\omega_0^2}}} \tag{65a}$$

$$a < 1: \quad A_{a=1-} = \sqrt{-\frac{4}{3c_3}}\sqrt{\left(\frac{1}{a}-1\right)\pm\sqrt{\frac{h^2}{4}-\frac{4k^2}{a\omega_0^2}}} \tag{65b}$$

Figure. 4 is a bifurcation diagram, i.e. it shows the change of steady-state roll response as a control parameter, in this case h, is varied. Even without carrying out a formal stability analysis, to an experienced eye the stability of the emerging steady roll oscillations is quite obvious. On the right boundary (higher a) of the instability region a supercritical bifurcation takes place, whereas the boundary at $a<1$ gives birth to a sub-critical one (see also figure 3).

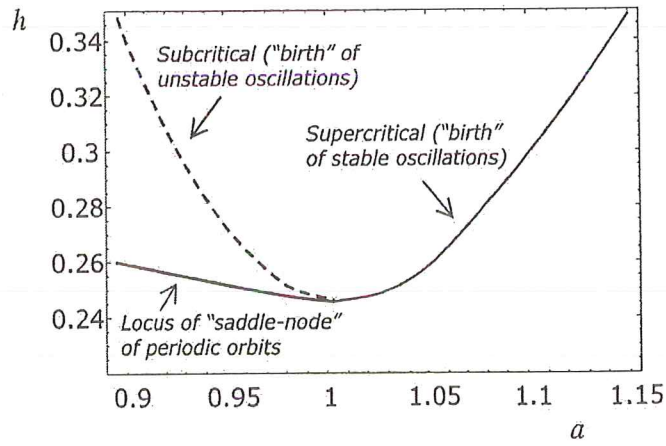

Figure 3. Boundary of parametric roll: $k = 0.015s^1$, $\omega_0 = 0.2448s^{-1}$ (hardening restoring).

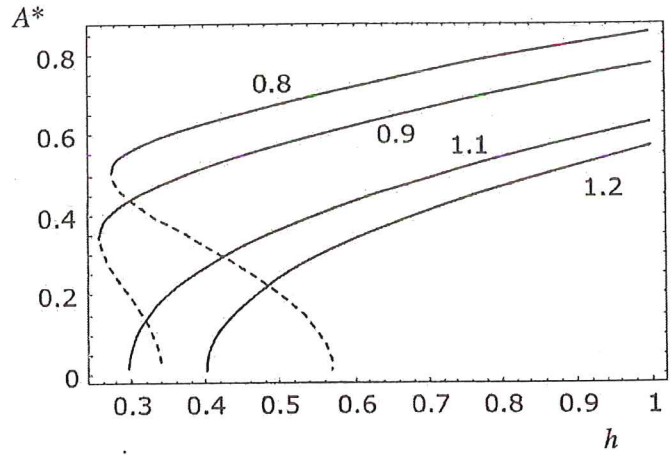

Figure 4. Amplitude of response for hardening restoring ($A^* = \sqrt{\frac{3c_3}{4}}A = 0.866\frac{A}{\varphi_v}$).

The domain of oscillatory behaviour can easily be found with some manipulation of equation (51)

$$h = \sqrt{4\left[\frac{3c_3}{4}A^2-\left(1-\frac{1}{a}\right)\right]^2+\frac{16k^2}{\omega_0^2 a}} \tag{66}$$

The combinations of (h,a) that give rise to oscillations of predefined A^* is shown in figure 5. It is easily proven that the descending part of each iso-A^* curve corresponds to stable rolling and the ascending to unstable rolling. The boundary of stable rolling is reconfirmed (thick continuous line). As we have multiple coexisting stable responses, the initial conditions

and the availability of sufficiently strong external disturbances determine whether the ship can stay upright, or should adopt the one (desired) or the other (undesired and possibly dangerous) way of behaviour.

In figure 6 is shown the variation of the roll amplitude A for $c_3 = 2.35$ as a function of the linear damping and the amplitude of parametric forcing. As deduced from expression (63), the amplitude A goes with the square root of both the parametric forcing and the damping. For small (yet realistic for many operating ships) damping, the effect on the response amplitude is relatively small. This is perhaps counterintuitive, given that damping is the most critical parameter for the onset of parametric rolling in the first place. Whilst the same applies for h, the latter should be quite high (well above $4k/\omega_0$) since the occurrence of parametric rolling is taken here as a fact. A, say, 10% increase of h incurs a considerably larger quantitative effect on the amplitude than a 10% reduction of damping. Another influential parameter that is linked to ship geometry is the coefficient c_3 of cubic stiffness: on the basis of (63), c_3 is inversely proportional to A^2 (see also figure 7).

For $c_3 > 0$ (softening GZ) the amplitudes are

$$a \geq 1: \qquad A_{a=1+} = \sqrt{\frac{4}{3c_3}} \sqrt{\left(1-\frac{1}{a}\right) \mp \sqrt{\frac{h^2}{4} - \frac{4k^2}{a\omega_0^2}}} \qquad (67a)$$

It is noted above that there are two solutions corresponding to the stable and unstable part. Their maximum values (for "large" a) are

$$A_{a=1+} = \sqrt{\frac{4}{3c_3}} \sqrt{1 \mp \frac{h}{2}} \qquad (67b)$$

However it should not be disregarded that the formula was derived for the vicinity of principal resonance and also that if the roll amplitude becomes large a more accurate representation of restoring is entailed.

$$a < 1: \qquad A_{a=1-} = \sqrt{\frac{4}{3c_3}} \sqrt{\left(1-\frac{1}{a}\right) + \sqrt{\frac{h^2}{4} - \frac{4k^2}{a\omega_0^2}}} \qquad (67c)$$

In figure 8 is shown the change of roll amplitude as the parametric forcing h is raised, for frequency ratios surrounding $a = 1$. Contours of iso-h on the plane of roll amplitude against a are shown in figure 9.

The bifurcation diagram of figure 8 suggests that, for a less than 1.0, the oscillations are stable as they emerge from a supercritical bifurcation. To the contrary, for a above 1.0 the oscillations are the result of a subcritical bifurcation, hence they are initially unstable (dashed line). However, these unstable oscillations later revert to stable at saddle-node bifurcation points. It is noted that the vanishing angle is approached quicker for the higher a (which for a given ship could be interpreted as a lower frequency of encounter) and at $a = 1.2$ the required h is more than 1.0. It should be recalled that the critical h for parametric rolling of the discussed containership is $4k/\omega_0 = 0.245$; i.e. the distance is substantial.

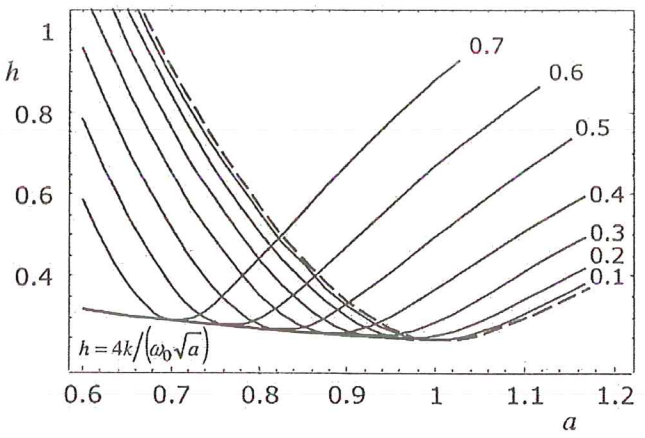

Figure 5. Iso-A curves (from 0.1 to 0.7 rad) for $k = 0.015 s^{-1}$, $c_3 = 2.35$ (hardening), $\omega_0 = .2448 s^{-1}$.

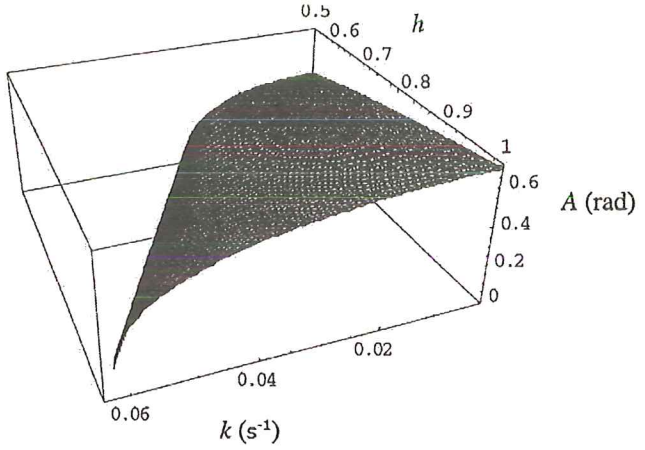

Figure 6. Steady response as function of k, h.

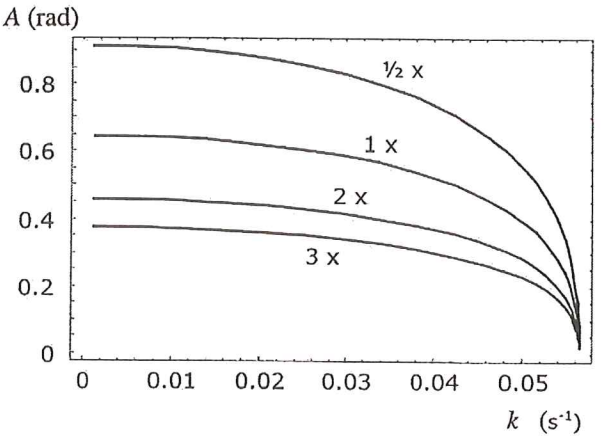

Figure 7. Effect of damping on the amplitude of periodic response with parameter the coefficient of nonlinear stiffness ("hardening").

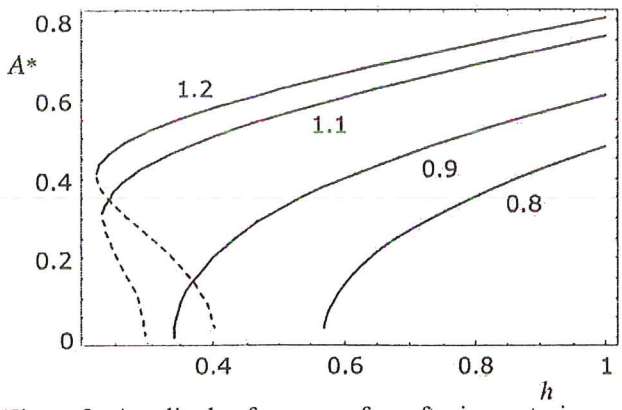

Figure 8. Amplitude of response for softening restoring, $k = 0.015\ s^{-1}$.

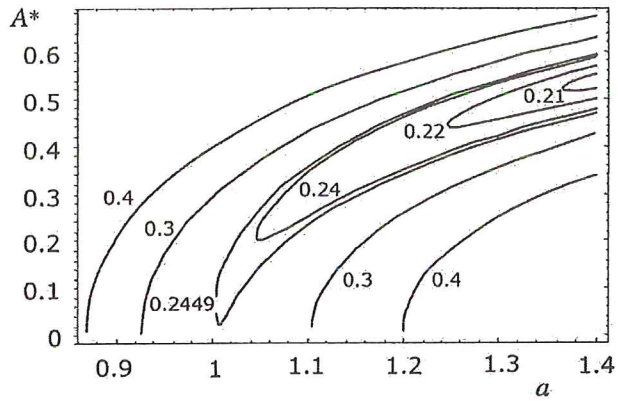

Figure 9. Contours of iso-h.

(a) Transient Behaviour

From the equations of amplitude given earlier and those of phase given below, we observe that the amplitude is changed indirectly through the variation of the phase

$$\frac{d}{d\tau}A^2(\tau) = A^2(\tau)\left(a\,h\,\sin 2\vartheta(\tau) - \frac{4k\sqrt{a}}{\omega_0}\right) \qquad (68a)$$

$$\frac{d\vartheta(\tau)}{d\tau} = \frac{h}{2}\cos 2\vartheta(\tau) - 1 + \frac{1}{a} + \frac{3}{4}c_3 A^2(\tau) \qquad (68b)$$

An approximate expression for transient roll on the basis of the perturbation method of Krylov-Bogoliubov can be found in Blocki [1980].

(b) Effect of the Fifth Order Term (Iinitially Hardening, then Softening)

Consider again the roll equation with a fifth-order polynomial for restoring which can better take into account the detail of the *GZ* curve up to larger inclinations.

$$\frac{d^2\varphi}{d\tau^2} + \frac{2k\sqrt{a}}{\omega_0}\frac{d\varphi}{d\tau} + a(1 - h\cos 2\tau)\varphi - c_3\,a\varphi^3 - c_5\,a\varphi^5 = 0 \qquad (69)$$

The pair of equations that in this case have to be simultaneously zero become

$$\sin 2\vartheta = \frac{4k}{h\omega_0\sqrt{a}} \qquad (70)$$

$$\cos 2\vartheta = \frac{2}{h}\left(1 - \frac{1}{a} - \frac{3}{4}c_3 A^2 - \underline{\underline{\frac{5}{8}c_5 A^4}}\right) \qquad (71)$$

We notice that only the lower one has been modified (by the underlined term). As expected, the boundary of parametric rolling remains unchanged and thus the criterion $h = 4k/\omega_0\sqrt{a}$ does not depend on the order of the restoring polynomial. The amplitude A is obtained from the quadratic equation

$$\frac{5}{8}c_5 A^4 + \frac{3}{4}c_3 A^2 - \left(1 - \frac{1}{a}\right) \pm \sqrt{\frac{h^2}{4} - \frac{4k^2}{\omega_0^2 a}} = 0 \qquad (72)$$

and the explicit expression of A is

$$A^2 = -\frac{3}{5}\frac{c_3}{c_5} \pm \sqrt{\left(\frac{3}{5}\frac{c_3}{c_5}\right)^2 - \frac{8}{c_5}\left(-1 + \frac{1}{a} \pm \sqrt{\frac{h^2}{4} - \frac{4k^2}{\omega_0^2 a}}\right)} \qquad (73)$$

We select a *GZ* curve (see figure 10) very close to that of the post-panamax containership discussed by France *et al.* [2001]. The selected values for the coefficients c_3 and c_5 are, respectively, -0.14 and 0.25. The amplitudes, as functions of the parametric term h, for the frequency ratios examined earlier, are shown in figure 11. Several changes of stability are taking place on each one of these curves. An interesting feature of this diagram is that it shows the behaviour at large angles where the fifth order term of the restoring function becomes influential. Contrasting figure 11 with figure 4 is enlightening in this respect.

A supplementary criterion based on steady amplitude may be introduced: for a steep wave, say with $\lambda/L = 1.0$, $H/\lambda = 1/20$, the max roll amplitude should not exceed, say, 15 deg (the same angle is proposed also in the ABS guide of parametric roll). From equation (73) is obtained the combination of restoring and damping characteristics that guarantee this limiting angle is not exceeded

(c) Nonlinear Damping

By including a cubic damping term $\delta\dot{\varphi}^3$ the equation of amplitude (67a) is modified directly; however that of phase is not.

$$\frac{d}{d\tau}A^2(\tau) = A^2(\tau)\left(a\,h\,\sin 2\vartheta(\tau) - \frac{4k\sqrt{a}}{\omega_0} - \frac{3\omega_0\delta}{2\sqrt{a}}\right) \qquad (74a)$$

$$\frac{d\vartheta(\tau)}{d\tau} = \frac{h}{2}\cos 2\vartheta(\tau) - 1 + \frac{1}{a} + \frac{3}{4}c_3 A^2(\tau) \qquad (74b)$$

Thereafter the steady amplitude should become

$$A^2 = \frac{4}{3c_3}\left[\left(1-\frac{1}{a}\right) \mp \sqrt{\frac{h^2}{4} - \left(\frac{2k}{\omega_0\sqrt{a}} + \frac{3}{4}\frac{\omega_0\,\delta}{a^{3/2}}\right)^2}\right] \qquad (75)$$

The nonlinear damping coefficient is much smaller than the coefficient of the linear. Quantitative assessment of the various contributions to the amplitude A suggests that the effect of nonlinear damping to the reduction of A is much lower than that of the linear.

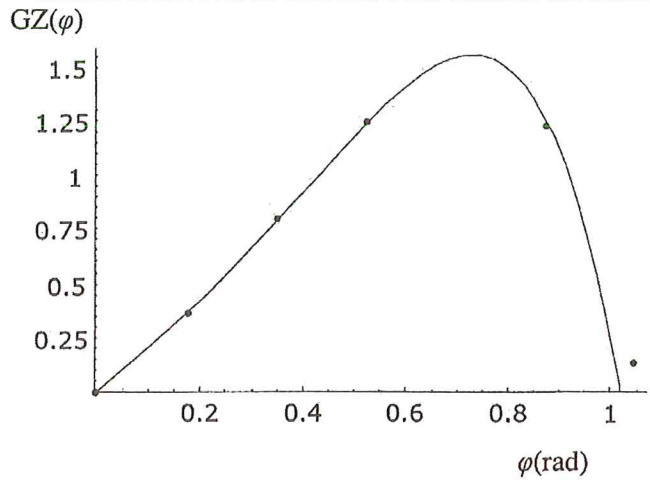

Figure 10. The exact (dots) and the polynomial fit (line) of the GZ curve.

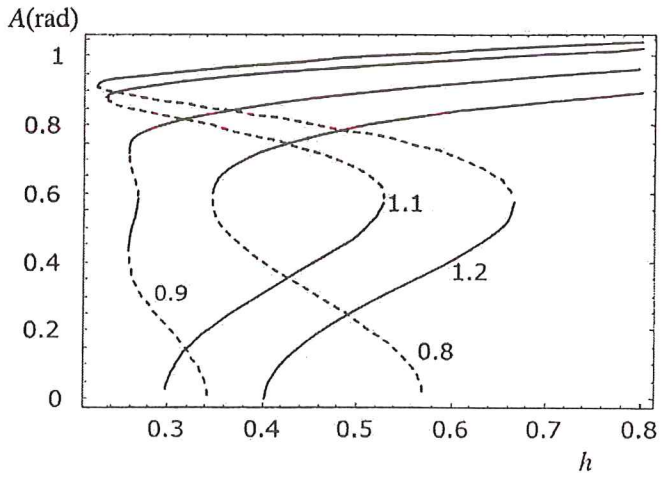

Figure 11. Amplitude of roll oscillation for 5th order restoring, assuming time dependence only in the linear term. The parameter is a.

(d) Capsize due to Parametric Rolling

Could there be an imminent danger of capsize if a ship is caught in parametric rolling? At a theoretical level this could be assessed by identifying the h level where loss of integrity of the basins of attraction of the emerging oscillatory roll responses is initiated. Relevant formulae are found, for example, in Kan [1992], Esparza & Falzarano [1993] and Nayfeh & Balachandran [1995] based on Melnikov's method. However, as the required h for loss of integrity is in general quite high (and notably, it is reduced at very low encounter frequencies), it seems that the danger of capsize is not high, unless the ship suffers from a short stability range combined with very significant GZ variations even in moderately steep waves.

9. COUPLING WITH PITCH AND HEAVE MOTIONS

In head waves, when the wave length becomes comparable to ship length, vertical ship motions often reach their maximum. Hence added resistance and loss of speed should be expected. The added resistance in regular head waves may be predicted by the well-known strip-theory formula of Gerritsma & Beukelman [1972]

$$R_W = \frac{k}{2\omega_e}\int_L \left[B_{33}(x) + U\frac{dA_{33}(x)}{dx}\right] w_{amp}^2(x)\,dx \qquad (76)$$

$A_{33}(x), B_{33}(x)$ are added mass and damping of a transverse section located at x along the ship, U is the ship's speed and $w_{amp}(x)$ is the amplitude of vertical velocity of the section relative to the wave. A coupled model of surge, heave and pitch should provide the mean speed for the specific ship-wave encounter scenario. Furthermore, pitch and heave should modify the instantaneous waterline as well as the location of the centre of buoyancy, resulting in an extra modulation of roll restoring with the pitch angle $\vartheta(t)$ and heave displacement $z(t)$. Therefore, if we intended to stretch out the conventional analysis of parametric rolling for application to a head sea scenario, the actual speed and restoring modulation should be determined in advance. However, a 4-degree coupled model of surge, heave, pitch and roll is the best option for a head sea scenario, not least because it can cope with a possible transfer of energy between the vertical modes and roll. A single roll model is limited in its capability to incorporate such a full dynamic effect.

If first order analysis is performed (where heave, pitch and wave slope are first order quantities), one could superimpose the GZ fluctuation due to pitch and heave to the semi-static one. The parametric driver of roll motion from concurrent heave and pitch could arise even in still water. Froude had observed this. Nearly 50 years ago, Paulling & Rosengerg [1959] showed that a prescribed harmonic heave or pitch motion (which in a different context could be assumed to be the response to direct wave excitation) acts like parametric

excitation for roll. This should affect the predicted critical roll damping quantitatively but there should be no qualitative change concerning the character of the instability and the encounter frequency where it might occur because, in this semi-coupled scenario, pitch and heave are unaffected by the simultaneous rolling. However, the two other motions through second-order stiffness terms influence roll. More specifically, for small excursions from the upright condition the restoring function could be expressed as the following superposition

$$\begin{aligned} &\rho g \nabla_0 GM_0 (1 + h\cos\omega_e t)\varphi \\ &+\rho g \frac{\partial[\nabla(\zeta,\vartheta) GM(\zeta,\vartheta)]}{\partial\zeta}\zeta\varphi \\ &+\rho g \frac{\partial[\nabla(\zeta,\vartheta) GM(\zeta,\vartheta)]}{\partial\vartheta}\vartheta\varphi \end{aligned} \qquad (77)$$

The subscript 0 refers to the "still" waterline. The origin of our "right-handed" body-fixed axes is placed at the ship's centre of gravity with the x-axis pointing along the ship, y transversely and z vertically (positive downwards). We define heave displacement as $\zeta = z_{w0} - z_w$ where z_w is the vertical distance of the (instantaneous) waterline from the origin (therefore positive ζ corresponds to extra immersion). Also, let the positive pitch angle ϑ be by the stern. A key step is to determine how the two partial derivatives are influenced by hull geometry. Summarizing the investigation of Paulling & Rosenberg [1959], these derivatives are expressed as follows. The derivative with respect to heave is

$$-2\rho g \int_{x_s}^{x_b} y_{w0}^2(x) \left.\frac{\partial y}{\partial z}\right|_{z=z_{w0}(x)} dx + \rho g\, z_{w0}\, A_{wo} \qquad (78)$$

and the one with respect to pitch is

$$2\rho g \int_{x_s}^{x_b} x\, y_{w0}^2(x) \left.\frac{\partial y}{\partial z}\right|_{z=z_{w0}(x)} dx - \rho g\, z_{w0}\, A_{w0}\, x_F \qquad (79)$$

In the above, A_{w0} is the still waterline and x_F is the longitudinal coordinate of the centre of flotation. Also, x_s, x_b are longitudinal coordinates of the furthest points at the stern and bow respectively. It is immediately noticed that flare, as represented by the derivative $\partial y/\partial z$ is very important. Furthermore, deck submergence in steep waves as well as a wide transom should enhance the fluctuation of restoring incurred by the heave and pitch motions.

Several semi-coupled or fully coupled models of heave, pitch and roll, for longitudinal waves, have been investigated in the past (see, for example, Blocki [1980], Hua [1992], Oh, Nayfeh & Mook [1992], Neves [2002]). In principle, the mathematical model should account for direct excitations in heave and pitch and for the parametric one in roll. Inspection of stability of this system leads to taking its linear variational vector equation, which is essentially a set of three 2nd-order o.d.e. s with time-dependence in the coefficients of damping and restoring. For these it is known that additional instabilities (and thus "resonances" of the original system) arise for ω_e near to sub-multiples of the sum and difference of the natural frequencies of the participating modes (see, for example, Hsu [1963]; [1965], Neves [2002]), provided that "sufficient" parametric amplitudes are present. In our case, given that the natural frequencies of heave and pitch are usually higher than that of roll, the eligible ω_e should be in the vicinity of $\frac{\omega_0^r + \omega_0^p}{j}, \frac{\omega_0^r + \omega_0^h}{j}, \frac{\omega_0^p - \omega_0^r}{j}, \frac{\omega_0^h - \omega_0^r}{j}$ where $j = 1,2,3,...$

Assuming that the pitch and heave natural frequencies are considerably larger than (e.g. double) the roll natural frequency, taking $j = 1$ should create resonances near the fundamental one (resulting from the two subtractions) and two lower than the principal (with reference to the frequency axis $a = \omega_0^2/\omega_e^2$). Those near the fundamental should not be relevant for a head-sea scenario. But the others, which correspond to a high frequency of encounter, may not be ruled out. With a similar thinking, it is highly unlikely that the $j > 1$ resonances can be realised. Neves [2004] suggested recently that the linear roll variational equation is, after substitution of the linear heave and pitch responses, a Hill- type equation rather than a Mathieu one as customarily believed.

10. EFFECT OF SURGING IN FOLLOWING SEAS

Very often parametric instability is examined assuming that, despite the wave passage, the forward motion of the ship is unaffected. This assumption could be off the truth when a ship is sailing in steep following waves with a nominal speed that falls in the region of the so-called large amplitude surging motion. This speed region has been identified by IMO to be approximately between $(1.4 - 1.8)\sqrt{L}$ (in knots). The characteristic of this behaviour is the large and asymmetric fluctuation of surge velocity. For an observer moving with the wave celerity, the ship should appear to be overtaken by the wave quickly when its middle is near a trough, but very slowly when it lies near a crest (in absolute terms the speed of the ship will be highest around the crests and lowest near the troughs). As a matter of fact, the assumption that a ship transits from all positions of the incident wave with the same speed should be, in this case, inappropriate. The solution is to adopt a "position-dependent" representation of the fluctuating restoring, instead of the ordinary time-dependent one. But such a substitution of the time-dependent restoring by a position-dependent one means that the equation of surge motion should be considered simultaneously; i.e. a coupled model is pertinent [Spyrou 2000]

(Roll)

$$\ddot{\varphi} + 2k\dot{\varphi} + \omega_0^2 \left[1 - h\cos(kx)\right]\varphi - n\omega_0^2 \varphi^3 = 0 \qquad (80)$$

(Surge)

$$(m - X_{\dot{u}})\dot{U} = T(x,U;n;Ak,\lambda) - R(x,U;Ak,\lambda) - X_w(x;Ak,\lambda) \quad (79)$$

where $m, -X_{\dot{u}}$ stand respectively for ship mass and surge added mass, the functions T, R represent the propeller thrust and ship resistance, respectively, X_w is surge wave force and Ak is wave slope. Given that $\dot{x} = U - c$ where c is the wave celerity, we essentially have a system of two o.d.e.s with respect to φ, x that can be easily solved in the time domain.

The coupling with surge should alter the layout of the instability regions. Indicatively, in figure 12 the theoretical instability regions are compared with and without surge coupling, taking as a basis a fishing vessel that had been known to show tendency for large amplitude surging. This vessel was not prone to principal parametric resonance but it seemed theoretically possible to display higher parametric resonances in a very extreme environment. The effect incurred upon the resonance regions is quite obvious. Further investigations with other ships should reveal the full potential of this effect.

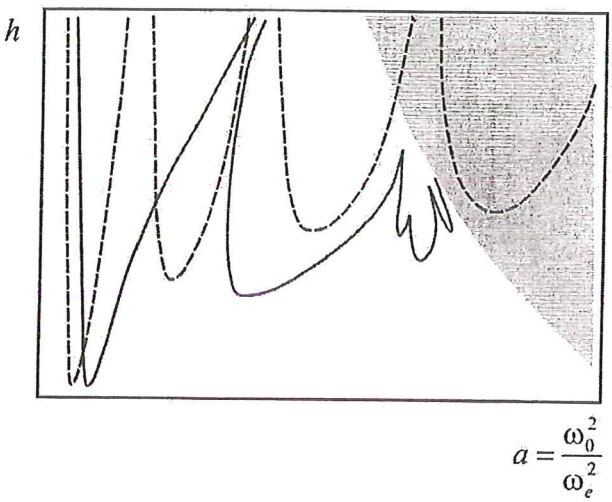

Figure 12. Layout of parametric instability regions with (continuous line) and without (dashed) surge coupling, for a fishing vessel. The grey area corresponds to surf-riding (a possibility only for the coupled model). Note that the principal resonance did not exist for this vessel, i.e. the first shown resonance for each scenario corresponds to the fundamental one. The higher resonances required excessively large h.

11. CONCLUDING REMARKS

According to the review of the field and the new findings presented above, it appears that there is currently sufficient understanding for developing scientifically sound as well as practical design criteria for parametric rolling. ABS's [2004] criteria move into this direction, yet their neglect of the probabilistic character of the seaway, might lead to requirements that are expensive and tough to meet at the design stage. As has been proposed here, a criterion that combines an assessment of transient roll response with the "groupness" characteristic of extreme waves should be more practical compared to a classical criterion deduced from the condition of asymptotic stability of the upright state of the ship, since the latter presupposes a finely tuned critical wave group with infinite run length. Another advantage of the probabilistic viewpoint is that it could be easily integrated within a risk assessment methodology; because the probability of parametric rolling becomes equal to the probability of encounter of a critical wave group. This could be obtained from current theoretical or parametric models of probability distributions of wave parameters. Knowledge of the critical wave group leads directly to the definition of the least roll damping and the tolerable restoring fluctuation.

Coupled motions should receive more attention. At the moment, their quantitative effect on the classical prediction formulae for parametric rolling, which are derived from single degree-of-freedom models, is still uncertain although the available theoretical basis is quite complete. Complex numerical codes could prove useful in this direction, provided that a "black-box" approach is not followed; i.e. the scope, limitations and assumptions of these codes concerning parametric rolling phenomena should be comprehended before deriving conclusions.

Lately, a discussion has been initiated about the effectiveness of standard seakeeping methods in ascertaining, from model experiments or numerical simulations, that a ship is safe from parametric rolling [Belenky *et al.* 2003]. In particular, the assumption of ergodicity of parametric rolling has been questioned and subsequently, the validity of deriving conclusions from single temporal averages of roll response (especially as these are usually of limited time, e.g 30 mins at full scale). It appears that a different approach to this problem that could cope with both the nonlinearity that is responsible for the observed finite roll oscillations and the fact that the wave "groupness" (i.e. time localized non-stationary features of the wave field) is the essential instigator of the phenomenon.

REFERENCES

ABS 2004 *Guide for the parametric roll for the design of container carriers*. Houston, USA.

Ariaratnam, S.T. & Tam, D.S.F. 1979 Random vibration and stability of a linear parametrically excited oscillator. *Zeitschrift für Angewandte Mathematic und Mechanic*, **59**, 79-84.

Arndt, B. & Roden, S. 1958 Stabilität bei vor- und achterlichen Seegang. *Schiffstechnik*, **5** (29), 192-199.

Arnold, L. 1973 *Stochastic differential equations - theory and applications*. New York: Wiley.

Belenky, V., Weems, K.M. & Paulling, J.R. 2003 Probabilistic analysis of roll parametric resonance in head seas. In *Proceedings of 6th International Conference on the Stability of Ships and Ocean Vehicles*, Escuela Tecnica Superior de Ingenerios Navales, Madrid, September 14-19.

Blocki, W. 1980 Ship safety in connection with parametric resonance of the roll. *International Shipbuilding Progress*, **27**, 36-53.

Bulian, G., Francescutto, A. & Lugni, C. 2003 On the nonlinear modeling of parametric rolling in regular and irregular waves. In *Proceedings of 8th International Conference, Stability of Ships and Ocean Vehicles*, Madrid, 305-324.

Caughey, T.K. & Dienes, J.K. 1962 The behaviour of linear systems with random parametric excitation. *Journal of Mathematical Physics*, 41, 300-310.

Cavanié, A., Arhan, M. & Ezrtaty, R. 1976 A statistical relationship between individual heights and periods of storm waves. In *Proceedings of Conference on Behaviour of Offshore Structures*, Trondheim, 354-360.

Dallinga, P.R., Blok, J.J. & Luth, H.R. 1998 Excessive rolling of cruise ships in head and following waves. In *Proceedings of International Conference on Ship Motions and Manoeuvrability*, London, February 18-19, **14**.

Demirbilek, Z. & Linwood Vincent, C. 2002 *Coastal engineering manual – part II, chapter 1: water wave mechanics*. U.S. Army Corps of Engineers.

Esparza, I. & Falzarano J.M. 1993 Nonlinear rolling motion of a statically biased ship under the effect of external and parametric excitations. In *Proceedings of Symposium on Dynamics and Vibration of Time-Varying Systems, OE*, ASME, **56**, , 111-122.

France, W.N., Levadou, M., Michel, R.K., Moore, C., Paulling, J.R., & Treakle, T.W. 2003 An investigation of head-sea parametric rolling and its influence on container lashing systems. *Marine Technology*, **40** (1), 1-19.

Francescutto, A. &. Dessi, D. 2001 Some remarks on the excitation threshold of parametric rolling in nonlinear modeling. In *Proceedings of 5th International Workshop on Stability and Operational Safety of Ships*, 4.9.1 - 4.9.8.

Gerritsma, J. & Beukelman, W. 1972 Analysis of the resistance increase in waves of a fast cargo ship. *International Shipbuilding Progress*, **19** (217), 285-293.

Goda, Y. 1976 On wave groups. In *Proceedings of BOSS'76*, **1**, 115-128.

Gray, A.H. 1967 Frequency-dependent almost sure stability conditions for a parametrically excited random vibrational system. *Journal of Applied Mechanics*, **34**, 1017-1019.

Gray, M. 2001 Rolling case for more research. *Lloyd's List (Section: Insight and Opinion)*. February 18, London.

Grim, O. 1952 Rollschwingungen, Stabilität und Sicherheit im Seegang. *Schiffstechnik*, **1** (1), 10-21.

Gunderson, H., Rigas, H. & Van Vleck, F.S. 1974 A technique for determining stability regions for the damped Mathieu equation. *SIAM Journal of Applied Mathematics*, **26** (2), 345-349.

Hayashi, C. 1985 Nonlinear oscillations in physical systems. Princeton, New Jersey: Princeton University Press, (ISBN 0-691-08383-5).

Hsu, C.S. 1963 On the parametric excitation of a dynamic system having multiple degrees of freedom. *Journal of Applied Mechanics*, 30, *Transactions ASME*, 85, *Series E*, 367-372.

Hsu, C.S. 1965 Further results on parametric excitation of a dynamic system. *Journal of Applied Mechanics*, 32, *Transactions of ASME*, 87, *Series E*, 373-377.

Hua, J. 1992 A study on the parametrically excited roll motion of a RoRo ship on following and heading waves. *International Shipbuilding Progress*, **39** (420), 345-366.

Ibrahim, R.A. 1985 Parametric random vibration. *Engineering Dynamics Series, No. 4*, Chichester: Wiley, (ISBN 0471908304).

IMO 1995 Guidance to the master for avoiding dangerous situations in following seas. *MSC/Circ. 707*, London.

Infante, E.F. 1968 On the stability of some linear nonautonomous random systems. *Journal of Applied Mechanics*, **35** (1), 7-12.

Ito, K. 1951 On stochastic differential equations. *Memoirs of the American Mathematical Society*, **4**, 1-51.

Kan, M. 1992 Chaotic capsizing. *Osaka Meeting on Seakeeping Performance, the 20th ITTC Seakeeping Committee*, September 10-11, 155-180.

Kerwin, J.E. 1955 Notes on rolling in longitudinal waves. *International Shipbuilding Progress*, **2** (16) 597-614.

Kimura, A. 1980 Statistical properties of random wave groups. In *Proceeding of 17th Coastal Engineering Conference*, **2**, 2955-2973.

Kozin, F. 1969 A survey of stability of stochastic systems. *Automatica*, **5**, 95-112.

Longuet-Higgins, M.S. 1975 On the joint distribution of the periods and amplitudes of sea waves. *Journal of Geophysical Research*, **80**, 6778-6789.

Longuet-Higgins, M.S. 1983 On the joint distribution of wave period and amplitudes in a random wave field. In *Proceedings of the Royal Society*, London, Series A, **310**, 219-250.

Longuet-Higgins, M.S. 1984 Statistical properties of wave groups in a random sea state. In *Proceedings of the Royal Society, Series A*, London, **389**, 241-258.

Muhuri, P.K. 1980 A study of the stability of the rolling motion of a ship in an irregular seaway. *International Shipbuilding Progress*, **27**, 139-142.

Myrhaug, D., Dahle, E.A. & Slaatelid, O.H. 2000 Statistics of successive wave periods with application to rolling of ships. *International Shipbuilding Progress*, **47** (451), 253-266.

Namachchivaya, Sri, N. 1990 Stochastic bifurcation. *Applied Mathematics and Computation*, **30**, 37-95.

Nolan, V.J. & Namachchivaya, Sri, N. 1999 Almost sure stability of linear gyroscopic systems. *Journal of Sound and Vibration*, **227** (1), 105-130.

Namachchivaya, Sri, N. & Ramakrishnan, N 2003 Stochastic dynamics of parametrically excited two d.o.f. systems with symmetry. *Journal of Sound and Vibration*, **262**, 613-631.

Nayfeh, A.H. & Balachandran, B. 1995 Applied nonlinear dynamics. *Analytical, computational and experimental methods*. New York: Wiley.

Nayfeh, A.H. & Mook, D. 1979 *Nonlinear oscillations*. New York: Wiley.

Nayfeh, A.H., Mook, D. & Marshall, L.R. 1973 Nonlinear coupling of pitch and roll modes in ship motions. *Journal of Hydronautics*, **7** (4) 145-152.

Neves, M.A.S. 2002 On the excitation of combination modes associated with parametric resonance in waves. In *Proceedings of International Ship Stability Workshop*, Webb Institute.

Neves, M.A.S. & Rodriguez, C.A. 2004 Limits of stability of ships subjected to strong parametric excitation in longitudinal waves. In *Proceedings of 2nd International Maritime Conference on Design for Safety*, Sakai, Japan, October, 139-145.

Oh, I., Nayfeh, A. & Mook, D. 1992 Theoretical and experimental study of the nonlinearly coupled heave, pitch and roll motions of a ship in longitudinal waves. In *Proceedings of 9th Symposium on Naval Hydrodynamics*, Seoul, Korea, 93-111.

Paulling, J.R. & Rosenberg, R.M. 1959 On unstable ship motions resulting from nonlinear coupling. *Journal of Ship Research*, **3** (1), 36-46.

Ractliffe, A. 2002 Box stack forces underestimated. *Lloyd's List (Section: Insight and Opinion)*, June 25, London.

Roberts, J.B. 1982 Effect of parametric excitation on ship rolling motion in random waves. *Journal of Ship Research*, **26** (4), 246-253.

Roberts, J.B. & Spanos, P.D. 1986 Stochastic averaging: an approximate method of solving random vibration problems. *International Journal of Nonlinear Mechanics*, **21** (2), 111-134.

Roenbeck, R.G. 2003 Containership losses due to head-sea parametric rolling: implications for cargo insurers. In *Proceedings of International Union of Marine Insurance Companies Conference*, Sevilla, September 14-18.

Shin, Y.S., Belenky, V.L., Paulling, J.R., Weems, K.M., Lin, W.M. 2004 *Criteria for parametric rolling of large containerships in longitudinal seas.* SNAME Annual meeting, September 30 – October 1, Washington D.C.

Skalak, R. & Yarymovych, M.I. 1960 Subharmonic oscillations of a pendulum. *Journal of Applied Mechanics*, **27**, 159-164.

Soliman, M. & Thompson, J.M.T. 1992 Indeterminate sub-critical bifurcations in parametric resonance. In *Proceedings of the Royal Society of London, Series A*, **438**, 433-615.

Spyrou, K.J. 2000 Designing against parametric instability in following seas. *Ocean Engineering*, **27**, 625-653.

Spyrou K.J. 2000 On the parametric rolling of ships in a following sea under simultaneous periodic surging. *Philosophical Transactions of the Royal Society of London, Series A*, **358**, 1813-1834.

Spyrou K.J. 2004 *Criteria for parametric rolling.* To be presented at the 7th International Workshop on Ship Stability, Shanghai, November 1-3.

Stansell, P., Wolfram, J. & Linfoot, B. 2002 Statistics of wave groups measured in the northern North Sea: comparisons between time series and spectral predictions. *Applied Ocean Research*, **24**, 91-106.

Takaishi, Y., Watanabe, K. & Masuda, K. 2000 Probability to encounter high run of waves in the dangerous zone shown on the operational guidance IMO for following/quartering sea. *Contemporary Ideas on Ship Stability* (ed. D. Vassalos *et al.*), Oxford: Elsevier, ISBN 0-08-043652-8.

Tayfun, A. 1983 Effects of spectrum bandwidth on the distribution of wave heights and periods. *Ocean Engineering*, **10**, 107-118.

Taylor, J.H. & Narendra, K.S. 1969 Stability regions for the damped Mathieu equation. *SIAM Journal of Applied Mathematics*, **17** (2), 343-352.

Thompson, J.M.T. & Stewart, H.B. 2002 *Nonlinear dynamics and chaos, 2nd edition*, Chichester: Wiley, ISBN 0471876844.

Tinsley, D. 2003 DNV Project thinks about the box. *Lloyd's List (Section: Shipbuilding and Shiprepair)*. November 18, London.

Turyn, L. 1993 The damped Mathieu equation. *Quarterly of Applied Mathematics*, **LI** (2) 389-398.

Umeda, N., Hashimoto, H., Vassalos, D. Urano, S. & Okou, K. 2003 Nonlinear dynamics on parametric roll resonance with realistic numerical modeling. In *Proceedings of 8th International Conference, Stability of Ships and Ocean Vehicles*, Madrid 281-290.

Vinje, T. 1976 On stability of ships in irregular following sea. *Norwegian Maritime Research*, **2**, 15-19.

Oceanic Engineering International, Vol. 9, No. 1, 2005, pp. 28-34

Removal of Irregular Frequency Effect in the Computation of Wave-Body Interactions Using the Panel-Free Method

W. Qiu[1], H. Peng[2] and C.C. Hsiung[3]

[1] *Faculty of Engineering and Applied Science, Memorial University of Newfoundland, St. John's, Newfoundland, Canada A1B 3X5*
[2] *Oceanic Consulting Corporation, St. John, Newfoundland, Canada A1B 2X5*
[3] *Dalhousie University, Halifax, Nova Scotia, Canada B3J 1Z1*

e-mail: qiuw@engr.mun.ca

ABSTRACT

A panel-free method has been developed earlier to compute wave interactions with bodies in the frequency domain. Further development in this paper is to remove the effect of irregular frequencies by solving the modified desingularized integral equations. Additional Gaussian points are automatically distributed on the interior free surface. Robustness of the enhanced panel-free method is demonstrated by its applications to the radiation problems of a floating hemisphere, a vertically floating axisymmetric cylinder and a Wigley hull. Computed added-mass and damping coefficients are compared with analytical solutions and those by the panel-free method without the irregular-frequency removal.

Keywords: Frequency-domain analysis, panel-free method, NURBS, exact geometry, wave-body interaction, irregular frequencies

1. INTRODUCTION

A panel-free method has been developed by Qiu and Hsiung [2002] to remove the computational errors which occur in the conventional panel method. They first applied this method in the time-domain analysis. In their work, the desingularized integral equation in terms of source strength distribution was first developed by removing the singularity due to the Rankine term in the time-dependent Green function. The non-uniform rational B-splines (NURBS) were adopted to describe the exact body geometry mathematically. The integral equations were then globally discretized over the body surface by Gaussian quadratures. The assumption of a certain degree of source distribution, as in the conventional panel method, was not involved.

The panel-free method has been extended to compute the wave interactions with bodies in water of infinite depth and finite depth in the frequency domain [Qiu *et al.* 2003]. The accuracy of the method was demonstrated by its applications to the radiation and the diffraction problems of the three-dimensional bodies. This paper aims to remove the effects of irregular frequencies in the frequency-domain computations.

In the computation of wave-body interactions in the frequency domain, since the Green function satisfies the free surface conditions on the free surface outside and inside the body, the solutions of the boundary integral equations do not exist or are not unique at certain frequencies which are referred to as "irregular frequencies". The effects of irregular frequencies can be removed by distributing localized wave sources on the interior free surface or by modifying the integral equations.

Ogilvie and Shin [1977] placed a localized wave source on the interior free surface to remove the first irregular frequency for simple heaving bodies. Zhu [1994] distributed wave sources and their derivatives on the interior free surface to remove the irregular frequencies for practical three-dimensional problems. This method was, however, found to be sensitive to the body geometry, locations of singularities, and the wave frequency.

Hypersingular integral equations were also derived by Kleinman [1982] and Lee and Sclavounos [1989] to remove the irregular frequencies based on the work of Burton and Miller [1971]. Since the direct evaluation of the hypersingular over panels causes discretization error, the resulting discrete system is for a condition worse than that of the original integral equations, except in the vicinity of irregular frequencies. Subsequently, the convergence rate of the solution to the discretization is much slower than that of the original integral equations.

Ohmatsu [1975] removed the irregular frequencies by deriving modified integral equations in terms of source

strength and by imposing zero normal velocity on the interior free surface. Lee *et al.* [1996] further derived the modified boundary integral equations to remove the irregular frequencies for both the first-order and second-order boundary value problems. In their work, a Neumann condition has been imposed on the interior free surface to ensure the continuity of the normal velocity on the interior free surface and that outside the body.

In this paper, the method proposed by Ohmatsu [1975] was adopted to remove the irregular frequencies in the first-order solutions. In the enhanced panel-free method, modified non-singular integral equations were first developed. In addition to the distribution of Gaussian points over exact body surface, Gaussian points were automatically distributed on the interior free surface.

The modified non-singular integral equations are described in Section 2. The mathematical representation of the exact body surface and the interior free surface is presented in Section 3. The enhanced panel-free method was applied to the radiation problem of a hemisphere, a vertically floating cylinder and a Wigley hull. In Section 4, computed added mass and damping coefficients of these bodies by the enhanced panel-free method are compared with analytical solutions and those by the original panel-free method.

2. MATHEMATICAL FORMULATION

A Cartesian coordinate system o-*xyz* is employed to compute the wave interaction with a floating body at zero speed. The mean wetted surface is denoted by S_b. The *oxy* plane is on the plane with $z = 0$ which represents the undisturbed water surface. The *z*-axis is positive upward. Incident waves propagate at an angle β relative to the *x*-axis with a radial frequency ω The velocity potential at a field point $P(x, y, z)$ is assumed to be time harmonic and can be expressed by $\phi(P)e^{-i\omega t}$. The velocity potential satisfies the Laplace equation and the linearized free-surface boundary condition on $z = 0$. The velocity potential can be decomposed as

$$\phi(P) = \phi_R(P) + \phi_D(P) + \phi_I(P) \tag{1}$$

where ϕ_R, ϕ_D and ϕ_I are the velocity potentials due to radiated, diffracted, and incident waves, respectively. For a rigid body with six degrees of freedom, the radiation potential is expressed as

$$\phi_R(P) = -i\omega \sum_{k=1}^{6} \xi_k \phi_k \tag{2}$$

where ξ_k is the complex amplitude of the body motion in the k^{th} mode. Introducing $\phi_7 = \phi_D$, the radiation and the diffraction potentials can be computed from the desingularized integral equations in terms of source strength

$$\phi_k(P) = \int_{S_b} G_0(P,Q)\left[\sigma_k(Q) - \gamma(Q)\frac{\sigma_k(P)}{\gamma(P)}\right]dS + \phi_0\frac{\sigma_k(P)}{\gamma(P)} + \int_{S_b}\sigma_k(Q)G_F(P,Q)dS \tag{3}$$

where $k = 1,2,\ldots,7$, $Q(x', y', z')$ is the source point, and $\gamma(P)$ is the source distribution on S_b which makes the body surface an equipotential ϕ_0. The solution of ϕ_0 can be found in Qiu and Hsiung [2002]. In Equation (3), σ_k is the source strength which can be solved from

$$\frac{\partial\phi_k(P)}{\partial n_P} = -\sigma_k(P) + \int_{S_b}\left[\sigma_k(Q)\frac{\partial G_0(P,Q)}{\partial n_P} - \sigma_k(P)\frac{\partial G_0(P,Q)}{\partial n_Q}\right]dS + \int_{S_b}\frac{\partial G_F(P,Q)}{\partial n_P}\sigma_k(Q)dS \tag{4}$$

where

$$G_0(P,Q) = -\frac{1}{4\pi}\left(\frac{1}{r} + \frac{1}{r_1}\right) \tag{5}$$

$$r = \sqrt{(x-x')^2 + (y-y')^2 + (z-z')^2} \tag{6}$$

$$r_1 = \sqrt{(x-x')^2 + (y-y')^2 + (z+z')^2} \tag{7}$$

For infinite water depth,

$$G_F(P,Q) = -\frac{1}{2\pi}\int_0^\infty \frac{1}{\mu - K}e^{\mu(z+z')}J_0(\mu R')d\mu - i\frac{1}{2}Ke^{K(z+z')}J_0(KR') \tag{8}$$

with

$$R' = \sqrt{(x-x')^2 + (y-y')^2} \tag{9}$$

and $K = \omega^2 / g$, g is the gravitational acceleration, and J_0 is the Bessel function of the zeroth order.

The effects of irregular frequencies can be removed by developing a modified non-singular integral equation. Based on the work of Ohmatsu [1975], the desingularized integral equation (4) can be modified as

$$\frac{\partial\phi_k(P)}{\partial n_P} = -\sigma_k(P) + \int_{S_b}\left[\sigma_k(Q)\frac{\partial G_0(P,Q)}{\partial n_P} - \sigma_k(P)\frac{\partial G_0(P,Q)}{\partial n_Q}\right]dS + \int_{S_b}\frac{\partial G_F(P,Q)}{\partial n_P}\sigma_k(Q)dS + \int_{S_i}\frac{\partial G(P,Q)}{\partial n_P}\sigma_k(Q)dS \quad \text{for } P\in S_b \tag{10}$$

$$\frac{\partial\phi_k(P)}{\partial n_P} = \sigma_k(P) + \int_{S_b}\sigma_k(Q)\frac{\partial G(P,Q)}{\partial n_P}dS \quad \text{for } P\in S_i \tag{11}$$

where $G(P,Q) = G_0(P,Q) + G_F(P,Q)$ and S_i is the interior free surface. In equation (10), the body boundary conditions are identical to those used in the unmodified integral equation (4). The body boundary condition on the interior free surface is

$$\frac{\partial \phi_k(P)}{\partial n_P} = 0 \quad \text{for } P \in S_i \tag{12}$$

After the source strengths are solved from equations (10) and (11), the velocity potential on the body surface, S_b, can be computed by

$$\begin{aligned}\phi_k(P) = &\int_{S_b} G_0(P,Q)\left[\sigma_k(Q) - \gamma(Q)\frac{\sigma_k(P)}{\gamma(P)}\right]dS + \phi_0\frac{\sigma_k(P)}{\gamma(P)} \\ &+ \int_{S_b} \sigma_k(Q) G_F(P,Q)\,dS \\ &+ \int_{S_i} \sigma_k(Q) G(P,Q)\,dS \qquad \text{for } P \in S_b\end{aligned} \tag{13}$$

The desingularized integral equations, (10), (11) and (13), can be discretized over exact surfaces, S_b and S_i, using Gaussian quadratures with the Gaussian point as the collocation point.

3. GEOMETRY REPRESENTATION

Since the desingularized integral equations can be discretized over exact geometry with Gaussian quadratures, the next step is to accurately compute coordinates, normals and Jacobians of the Gaussian points. It can be achieved by describing the body geometry by mathematical representation. Non-uniform rational B-splines (NURBS) are adopted to describe the body surface in this work [Farin 1991].

It is assumed that N_p patches are used to describe a body surface. For example, for a ship with a flat transom, two patches, one for the main hull and one for the transom, may be used to describe the hull surface. Each patch can be represented by a NURBS surface. Let $\mathbf{P}(x(u,v), y(u,v), z(u,v))$ be a point on a NURBS surface, where x, y and z denote the Cartesian coordinates, and u and v are two parameters for the surface definition. On the NURBS surface, $\mathbf{P}(u,v)$ can be defined as

$$\mathbf{P}(u,v) = \frac{\sum_{i=0}^{n}\sum_{j=0}^{m} w_{ij}\mathbf{C}_{i,j}N_{i,p}(u)N_{j,q}(v)}{\sum_{i=0}^{n}\sum_{j=0}^{m} w_{ij}N_{i,p}(u)N_{j,q}(v)} \tag{14}$$

where w_{ij} are the weights; $\mathbf{C}_{i,j}$ form a network of control points; and $N_{i,p}(u)$ and $N_{j,q}(v)$ are the normalized B-spline basis functions of degrees p and q in the u- and v-directions, respectively; and n and m are the numbers of control points in the u- and v-directions. The normal vector at the point $\mathbf{P}(u,v)$ is written as

$$\mathbf{n}_P = \left(\frac{\partial \mathbf{P}(u,v)}{\partial u} \times \frac{\partial \mathbf{P}(u,v)}{\partial v}\right) \Big/ |J| \tag{15}$$

where the Jacobian $|J|$ is given by

$$|J| = \left|\frac{\partial \mathbf{P}(u,v)}{\partial u} \times \frac{\partial \mathbf{P}(u,v)}{\partial v}\right| \tag{16}$$

4. NUMERICAL RESULTS

The enhanced panel-free method with the irregular frequency removal, denoted by PFM-IRR, has been applied to the computation of hydrodynamic coefficients for a hemisphere, a vertically floating axisymmetric cylinder and a Wigley hull. The computed results are compared with those by the original panel-free method (PFM).

(a) Hemisphere

PFM-IRR was first applied to the radiation problem of a floating hemisphere with a radius $R = 5.0$ in water of infinite depth. The body surface of the hemisphere was represented by NURBS surfaces. In the NURBS representation, the hemisphere was described by four NURBS surfaces. Each NURBS surface is formed by a 4×4 control net and B-splines of degrees of 3 in the u- and v-directions. The coordinates of the control points and associated weights can be found in the paper of Qiu *et al.* [2004]. The number of Gaussian points over a quarter of the hemisphere is chosen as 8×8. The Gaussian points on the interior free surface S_i are automatically distributed according to the geometry of waterline. In order to investigate the effect of the number of Gaussian points on S_i on the solutions, 2×2 and 4×4 Gaussian points were used over a quarter of the entire interior free surface of the hemisphere. The computed surge added mass and damping coefficients by PFM and PFM-IRR are compared with the analytical solutions by Hulme [1983] in figure 1. The surge added mass and damping coefficients are nondimensionalized as $A_{11}/(\rho\nabla)$ and $B_{11}/(\rho\nabla\omega)$, respectively, where ∇ is the volume displacement. As we can see, the effects of irregular frequencies are removed from the results when 4×4 Gaussian points are used on the interior free surface. When only 2×2 Gaussian points are applied, the results by PFM-IRR are worse than those by PFM except in the vicinity of irregular frequencies. It indicates that sufficient Gaussian points should be used on the interior free surface.

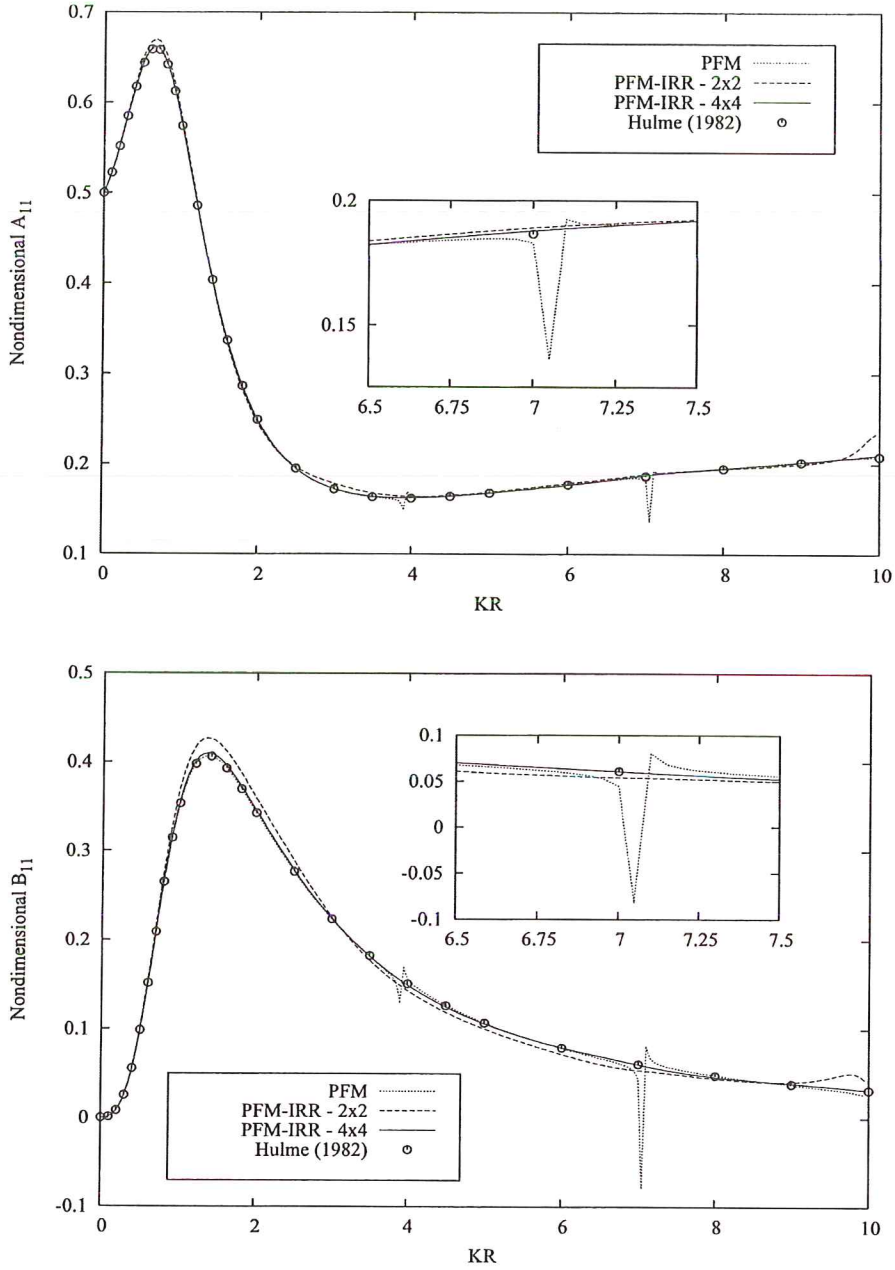

Figure 1. Surge added mass and damping coefficients for a hemisphere.

(b) Cylinder

Computations have been performed for the heave added mass and damping coefficients of a vertically floating cylinder in water of infinite depth. The ratio of draft (T) to radius (R) was set as 1/2. One quarter of the cylinder was represented by two NURBS surfaces, one for the bottom and one for the side wall. The NURBS control net and the surface are given in figure 2, where the dashed lines represent the control net and the solid meshes are the surface generated by the control net. The computed heave added mass and damping coefficients are nondimensionalized by $A_{33}/(\rho R^3)$ and $B_{33}/(\rho R^3\omega)$, respectively.

In Figure 3, the computed heave added mass and damping coefficients by PFM and PFM-IRR are compared with the benchmark results of Newman (1985), which were obtained by Fourier transformation of the impulse response functions from the time-domain analysis. In PFM and PFM-IRR, 6×8 and 12×6 Gaussian points were distributed on the bottom and side surfaces, respectively, i.e., the total number of Gaussian points is N=120 on one quarter of the cylinder. In PFM-IRR, 4×4 Gaussian points were applied on one quarter of the whole interior free surface. It is shown that effects of irregular frequencies are successfully removed by PFM-IRR.

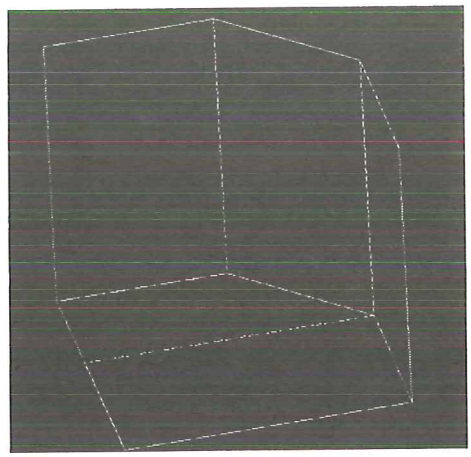

Figure 2. Surface and control net of a quarter of a vertically floating cylinder.

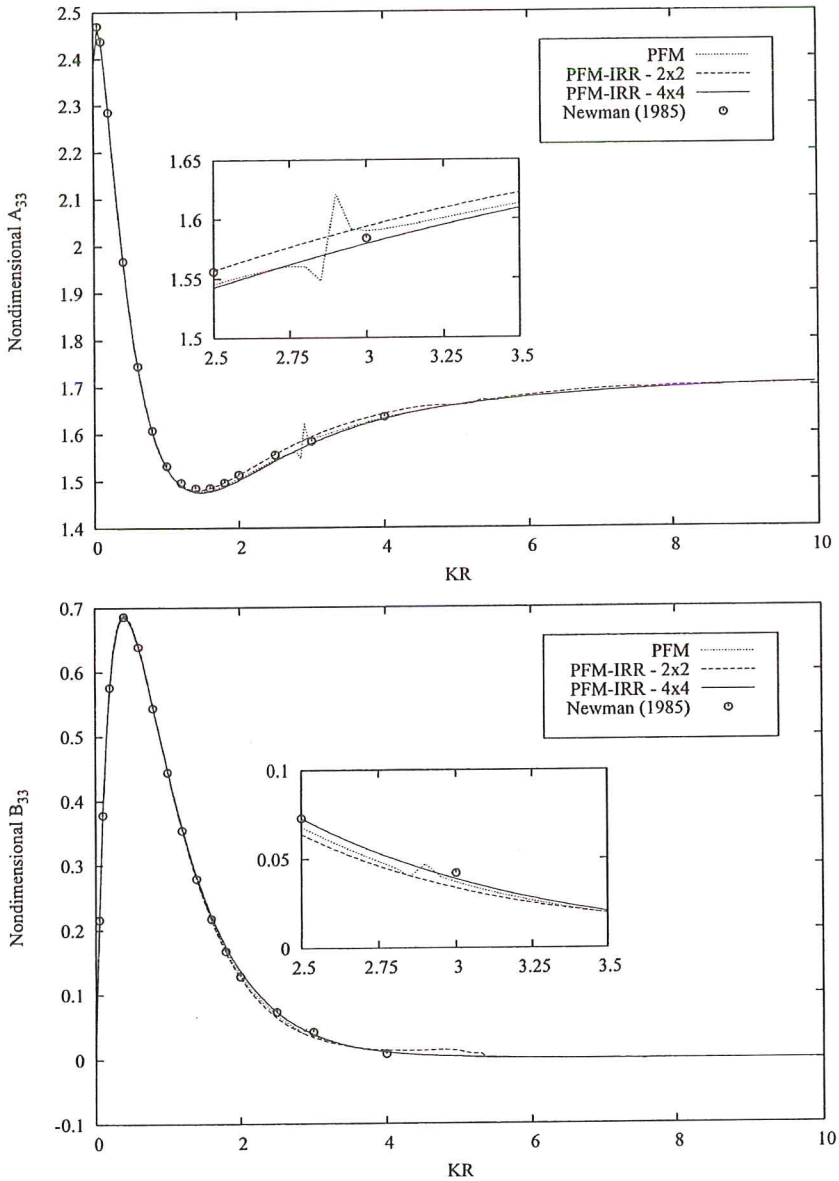

Figure 3. Heave added mass and damping coefficients for a vertically floating cylinder.

(c) Wigley Hull

Heave added mass and damping coefficients have been computed for a Wigley-hull ship at zero speed in water of infinite depth by PFM and PFM-IRR.

The hull geometry is defined by

$$\eta = (1-\zeta^2)(1-\xi^2)(1+0.2\xi^2) + \zeta^2(1-\zeta^8)(1-\xi^2)^4 \quad (17)$$

where the nondimensional variables are given by $\xi = 2x/L$, $\eta = 2y/B$ and $\zeta = z/T$, where L is the ship length, B is the beam, and T is the draft. The hull has $L/B = 10$, $L/T = 16$ and a block coefficient of 0.5606. NURBS representations were used for the computation. In the NURBS expression, the half Wigley hull was described by a 13×13 control net with degrees of 3 in both u- and v-directions. In the computation, 41×10 and 21×4 Gaussian points are distributed on half of the wetted surface and on half of the interior free surface, respectively. Figure 4 shows the distribution of Gaussian points on the hull surface and the interior free surface. In the figure, Gaussian points are denoted by '+'.

The results by PFM and PFM-IRR are compared in Figure 5. In the figure, the wave frequency is nondimensionalized as KB. The heave added mass and damping coefficients are nondimensionalized by $A_{33}/(\rho\nabla)$ and $B_{33}/(\rho\nabla)$, respectively. As shown in the figure, the irregular frequency effects are removed by the enhanced panel-free method.

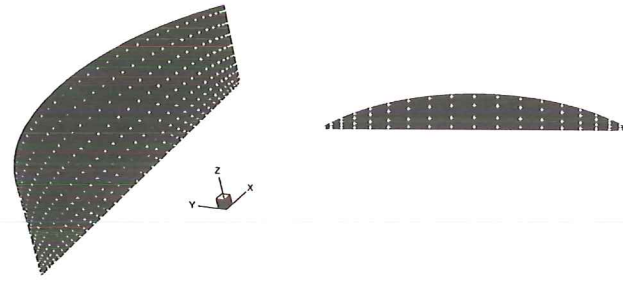

Figure 4. Gaussian points on the surface of a Wigley-hull ship and on the interior free surface.

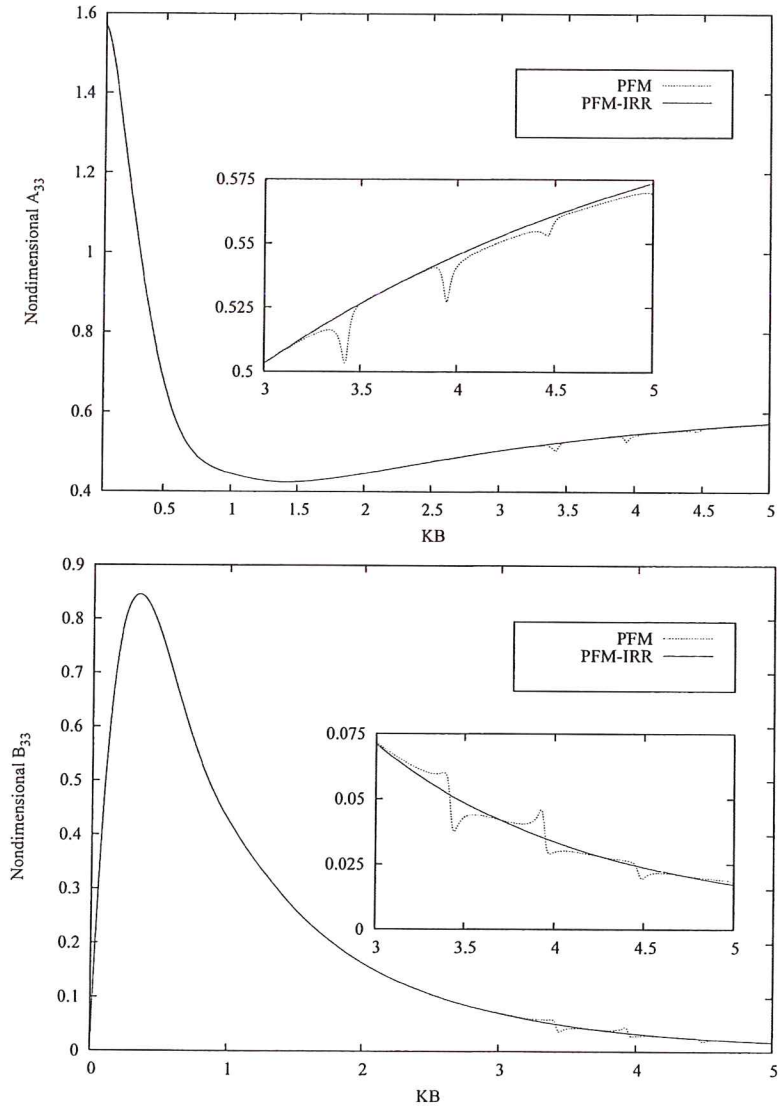

Figure 5. Heave added mass and damping coefficients for a Wigley-hull ship.

5. CONCLUSIONS

The panel-free method has been further developed for removing the irregular frequencies in the frequency domain. In the enhanced panel-free method, extended non-singular integral equations have been developed. Zero normal velocity conditions are applied on the interior free surface. The Gaussian points are automatically distributed on the interior free surface.

The robustness and accuracy of the enhanced panel-free method has been demonstrated by its applications to the radiation problem of a floating hemisphere, a vertically floating cylinder and a Wigley-hull ship in water of infinite depth.

ACKNOWLEDGEMENT

This work was supported by the Natural Sciences and Engineering Research Council of Canada.

REFERENCES

Burton, A.J. and Miller, G.F. 1971 The application of integral equation methods to the numerical solution of some exterior boundary-value problems. In *Proc. R. Soc. A.*, **323**, 201-220.

Farin, G.E. 1991 *NURBS for curve and surface design.* SIAM Activity Group on Geometric Design.

Hulme, A. 1982 The wave forces acting on a floating hemisphere undergoing forced periodic oscillations. *J. Fluid Mechanics*, **121**, 443-463.

Kleinman, R.E. 1982 On the mathematical theory of the motion of floating bodies – an update. *DTNSRDC-82/074.*

Lee, C.H., Newman, J.N. and Zhu, X. 1996 An extended boundary integral equation method for the removal of irregular frequency effects. *International Journal for Numerical Methods in Fluids*, **23**, 637-660.

Lee, C.H. and Sclavounos, P.D. 1989 Removing the irregular frequencies from integral equations in wave-body interactions. *J. Fluid Mechanics*, **207**, 393-418.

Newman, J.N. 1985 Transient axisymmetric motion of a floating cylinder. *J. Fluid Mechanics*, **157**, 17-33.

Ogilvie, T.F. and Shin, Y.S. 1977 Integral-equation solution for time-dependent free surface problems. *J. Society of Naval Architects of Japan*, **143**, 86-96.

Ohmatsu, S. 1975 On the irregular frequencies in the theory of oscillating bodies in a free surface. *Papers Ship Research Institute, No. 48.*

Qiu, W. and Hsiung, C.C. 2002 A panel-free method for time-domain analysis of radiation problem. *Ocean Engineering*, **29** (12) 1555-1567.

Qiu, W., Chuang, J.M. and Hsiung, C.C. 2004 Numerical solution of wave diffraction problem in the time domain with the panel-free method. *J. Offshore Mechanics and Arctic Engineering*, **126** (1) 1-8.

Qiu, W., Peng, H. and Chuang, J.M. 2003 Computation of wave-body interactions with the panel-free method and exact geometry. Accepted for publication *J. Offshore Mechanics and Arctic Engineering.*

Zhu, X., 1994 Irregular frequency removal from the boundary integral equation for the wave-body problem. *Graduate Thesis*, MIT, Cambridge, MA.

Oceanic Engineering International, Vol. 9, No. 1, 2005, pp. 35-41

Application of Artificial Cavitation for Reducing Ship Drag

Konstantin I. Matveev[1]

[1]*California Institute of Technology, 2264 B 35th St., Los Alamos, NM, 87544, USA*

e-mail: matveev@hydrofoils.org

ABSTRACT

Artificial cavitation, or ventilation, is a proven means for reducing hydrodynamic drag of surface ships and underwater projectiles. Among other ideas involving air assistance for marine vehicles, artificial cavitation is characterized by its high efficiency and its relatively simple practical implementation. The state-of-the-art Air Cavity Ships, which are surface vessels utilizing cavitating flows with negative cavitation numbers, are considered in this paper. Physical peculiarities of artificial cavitation, design procedures, and an example of the project under development are presented. The advantages of artificial cavitation, including a reduced environmental impact, make this technology attractive for the next generation of marine vessels.

1. INTRODUCTION

The Air Cavity Ship (ACS) has recently established itself as a new type of advanced marine vehicle. The ACS utilizes a special kind of cavitating flow that greatly improves the ship's hydrodynamic and economic characteristics. An air cavity beneath the vessel is formed by supplying gas to the specially profiled bottom recess, so that a steady air layer is formed that separates a significant part of the hull from contact with water as shown in figure 1. This results in a reduction of the ship's hydrodynamic resistance. At the present time, several classes of ACS are being mass-produced. An example is the ACS fast passenger ferry shown in figure 2 the specifications for which are available in Jane's High-Speed Marine Craft [1995-96].

Drag reduction achieved on full-scale ACSs is between 15% and 30%, while the power spent to support the air cavity is always less than 3% of the total propulsive power. Pressure in the air cavity usually exceeds the static pressure of incoming water flow by about 5% and this surplus pressure creates lift.

The air cavity is surrounded by solid hull sections that not only restrict air leakage from the cavity but also strongly affect cavity characteristics such as surplus pressure and the amount of air flow needed to maintain the cavity. These features distinguish the ACS from the common Surface Effect Ships (SES) where flexible skirts are applied in the bow and stern sections to keep compressed air inside the air cushion. Also, a SES is supported predominantly by the air cushion whereas, in case of an ACS, the wetted hull sections develop a lift component comparable to that produced by the surplus pressure in the cavity. A philosophical difference between the ACS and SES concepts is that the ACS goal is to lubricate wetted hull sections while the SES creates a volumetric air cushion. Air consumption on a SES is usually much greater than on an ACS. There are attempts to develop a skirtless SES [Burg & Johnson 1999; Tudem 2002] but the energy expense for the air supply is still quite high (10% - 20%) and applications are limited to only a narrow class of ship configurations.

Air lubrication by artificial cavitation is applicable not only to fast vessels but also to relatively slower ones such as tankers and cargo ships. In the case of slow vessels, a different configuration of the air cavity system is used. If the ship length is large and its speed is not sufficiently high, several cavitators must be employed because of the hydrodynamic stability limit on the cavity dimensions. A set of separate cavities can be generated on already existing vessels with a large-area flat bottom as shown in figure 3(a). A more efficient, specially designed displacement-type ACS can be built so that a large wave-like single cavity is formed in the cruising regime. This can be seen in figure 3(b). Several cavitators are also needed in this case to help form a single cavity, and to provide an effective drag reduction when a single cavity cannot be achieved (e.g. when sailing with a large trim or heel angle or in severe rough seas). While ships with suitable hull lines designed for a semi-displacement motion mode can also apply the artificial cavitation, the design objective in this case becomes the reduction of both wave and friction drag components.

Systematic research on artificial cavitation started at Krylov Shipbuilding Research Institute in the 1950s. These efforts resulted in approximately thirty development projects employing ACS concepts, and ships of 10 classes being built. The main specifications of several ACSs are given in table 1 [Sverchkov 2002a]. Most boats built are rather small, since the creation of large vessels with radical modifications requires a significant dedication from ship owners and investors, which is not yet the case for big ACS projects. However, worldwide attention to this concept has significantly increased in recent years [Matveev 2003a], since the ACS-type marine vehicles address the need for more economic and faster transoceanic transportation in both commercial and military applications.

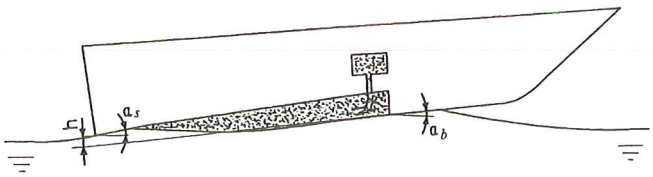

Figure 1. High-speed ship with air cavity.

Figure 2. Fast passenger ferry *Linda* equipped with an air cavity system.

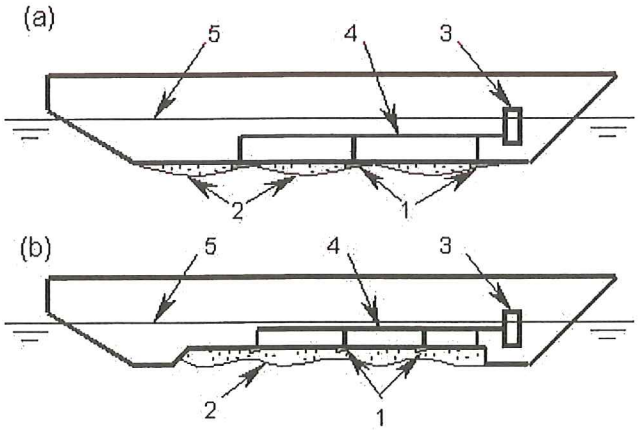

1: cavitators, 2: air cavities, 3: air blower, 4: gas pipeline, 5: waterline. Bottom recess height in (b) is shown not to scale.

Figure 3. Air cavity systems applied on displacement-type vessels.

	Saygak	Serna	Linda	Mercury
Number of ships built	> 40	5	14	4
Displacement (tons)	13.0	105	24.6	99.0
Length (m)	14.05	25.65	24.1	35.4
Beam (m)	3.5	5.85	4.6	8.3
Draft (m)	0.65	1.52	0.95	2.0
Power (KW)	735	4860	660	7340
Speed	40	32	38	52

Table 1. Specifications of serially built small and mid-size ACS.

2. PHYSICAL PROPERTIES OF ARTIFICIAL CAVITATION

In this section, some physical aspects of artificial cavitation important for understanding the methodology of designing an ACS are considered. A classical case [Butuzov 1967] of the flow around a wedge attached to the lower side of a horizontal wall is shown in figure 4. If the flow velocity is high enough, then a cavity filled with vapor or gases dissolved in the liquid is formed. However, the speeds typical for even modern large ships are not yet sufficient to naturally produce a large stable cavity. In order to separate a significant part of the wall from contact with water (with the purpose of reducing drag), it is necessary to supply a gas to the rear side of the wedge.

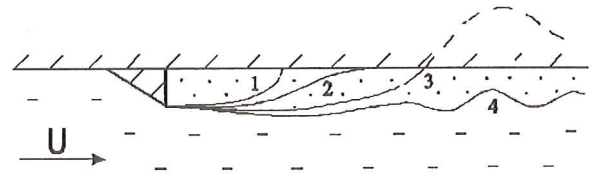

Figure 4. Various regimes of a ventilated flow behind a wedge under a horizontal wall.

The two most relevant non-dimensional combinations that characterize this type of flow are the cavitation and Froude numbers

$$\sigma = \frac{p_0 - p_c}{\rho U^2 / 2} \tag{1}$$

$$Fr = \frac{U}{\sqrt{gb}} \tag{2}$$

where p_0 is the pressure in the undisturbed incoming flow, p_c is the pressure inside the air cavity, ρ is the liquid density, U is

the incoming flow velocity, g is gravitational acceleration, and b is the characteristic dimension (length of the wedge).

Various regimes of cavitating flow are possible in the system considered (figure 4). In the case of cavity shape 1, a pulsating re-entrant jet is formed in the tail of the cavity, while the cavity boundary close to the wedge remains stable. This flow is similar to common supercavitation and ventilation with a positive cavitation number in the absence of a restricting wall [Knapp *et al.* 1970]. Cavity shape 2 is associated with a flow mode without a re-entrant jet, and the tail of the cavity attaches smoothly to the plate. In that case, the cavity-maintaining gas flow, as well as the cavitation drag, is theoretically equal to zero; the pressure inside the cavity exceeds that in the undisturbed flow, i.e. the cavitation number is negative [Butuzov 1967]. The peculiarity of shape 3 is that in theory the cavity pierces the plate at its aft end. Strong pulsations are usually observed all over the cavity during experiments similar to the over-ventilated flows with positive cavitation number [Silberman & Song 1961]. An unclosed cavity 4 is also possible at certain conditions. The last two regimes (3 and 4) are realized at high gas consumption, and therefore, are not favorable for practical drag reduction.

The flow mode characterized by cavity shape 2 is the most promising. It is found by calculations and verified in the tests that the cavity length L is proportional to the squared flow velocity U in this regime.

$$L \approx kU^2 \tag{3}$$

where coefficient k can be found experimentally or numerically by solving appropriate hydrodynamic equations. Usually, k is between 0.1 and 0.5. The length and velocity in equation (3) are given in meters and meters per second, respectively. Cavity geometrical characteristics and the cavitation number, corresponding to this most favorable flow mode, are called the limiting parameters and properly designed ACSs operate within this regime. In real situations, the complex hull geometry, flow non-uniformity, and nearby propulsors and control devices may significantly affect the cavitating flow characteristics, including the limiting regime [Matveev 2003b]. It was found that propulsors located very close to the cavity aft adversely affect the cavity performance, reducing its limiting length. These effects are sometimes observed on full-scale ships improperly designed, e.g. a case mentioned by Tudem [2002]. Interceptors or trim tabs, positioned behind the cavity, may produce positive effects on the cavity limiting characteristics.

3. DEVELOPMENT OF AIR CAVITY SHIPS

Artificial cavitation can be conveniently analyzed and adapted for applications on marine vehicles using a theory of the developed cavitating flows. During the early stages of ACS development, a two-dimensional linear model of ideal fluid was used [Butuzov 1967]. Later, this approach was extended to three dimensions including nonlinear effects [Butuzov 1988]. The outline of the 2D linear model and a discussion of its further extensions are given in the Appendix. Availability of the mathematical apparatus allows designers to develop an ACS in an effective manner, avoiding extremely tedious determination of the hull lines by purely experimental methods. However, a series of tests, following a numerical design, is always necessary since computational tools are not yet sufficiently accurate.

One of the first successful full-scale experiments applying artificial cavitation for drag reduction was a modification of a regular cargo ship of 5,300-ton displacement [Basin *et al.* 1969]. An air cavity system of the type shown in figure 3(a) was installed on that vessel. Drag reduction in operational regimes was 15% - 17%, while the power spent supplying air beneath the ship bottom was less than 3% of the propulsive power. The system appeared to be very reliable; even running aground did not produce any damage.

The first high-speed ACSs were built and tested at the Central Hydrofoil Design Bureau in the 1970s. For example, a 5-ton planing boat equipped with an air cavity system (a scheme shown in figure 1) demonstrated a 30% increase of the lift-drag ratio [Butuzov *et al.* 1981]. No special engine was required for a fan, which used power produced by a propulsive system. Some later developments did not use a fan at all – exhaust gases were supplied to the cavity.

A discussion of some other ACS developments, as well as dimensional analysis of fast ships with air lubrication, is described by Latorre [1997]. During the 1980s, more advanced experimental ACSs have been built and tested, including an experimental configuration shown in figure 3(b). These studies generated sufficient knowledge and experience for mass production of ACSs for military and civil applications (table 1). Specificity of the ACS resulted in establishing a new design methodology [Butuzov *et al.* 1999], which is somewhat different from the traditional procedure. In the case of the displacement ACS, developed from an existing conventional prototype vessel, the following five steps are accomplished at the design stage.

1. Pressure distribution over the ship hull is determined either experimentally (towing a ship model) or numerically (using tools of computational fluid dynamics).
2. Approximate calculation of the cavity system having parameters close to optimal (maximum cavity area at minimum gas consumption) is conducted.
3. A ship model is tested with further modifications of the cavity system aimed at optimizing ship performance under various conditions (cruising regime, full-load and ballast mode, maneuvering, and rough seas).
4. The hull-propulsor interaction is estimated, and a propulsor is selected and optimized followed by self-propelled model testing.
5. The results (resistance, trim, draft, cavity parameters, and air consumption) are scaled to a full-scale ship.

Since the bottom of an ACS is largely covered by an air layer, some amount of the air is constantly leaking from the cavity towards the stern. This may negatively affect the efficiency of the propulsor, which is usually designed to

operate in water flow only. Such an adverse phenomenon is even more pronounced during a pitching motion in rough seas. To counteract this problem, special deflectors are applied to protect conventional type propulsors. Supercavitating and surface propellers can tolerate air presence in the water flow, but disadvantages associated with these propulsors have to be overcome. The Ventilated Waterjet (VWJ), developed at Krylov Shipbuilding Research Institute [Ibragimova *et al.* 1995], has proved to be an excellent means to provide a thrust for an ACS and other ship types that encounter multi-phase incoming flow during operation. Air cavities, connected to the atmosphere, are formed on the suction sides of the blades of the VWJ rotor. The thrust is produced mostly by the pressure sides of the blades. Hence, this propulsor is not sensitive to the presence of air bubbles in the flow. The VWJ is characterized by a high efficiency (especially if drag caused by appendages is considered), and is currently applied on the serially-built ACSs.

There are only a few studies of the dynamics of an ACS in rough seas [Butuzov *et al.* 1981; Matveev 1999] but available data manifest the same or even enhanced seakeeping properties of the ACS in comparison with traditional ships of similar dimensions and in the same motion regimes. Compressible air in the cavity acts as a damper reducing vertical accelerations. Nevertheless, to achieve a smooth motion in rough seas, the high-speed sea-going ACS must have some kind of a control ride system similar to that applied to other fast ship types.

4. PROJECT EXAMPLE

In this section, an ACS designed for both ocean and river operation is described [Sverchkov 2002b]. The project development is presently being carried out at Krylov Shipbuilding Research Institute. Two types of air cavity arrangements are possible for vessels moving in a displacement mode, as was seen in figure 3. The second option, having a single wave-like cavity, can produce significantly better results. This type has been chosen for detailed study.

The sketch of the initial hull form is shown in figure 5. A 1:15 scale model was built for tests in a towing tank. Specifications of the full-scale ship and the model are given in table 2. According to the established procedure for development of an ACS, the original model was first tested without the air cavity system. Then, computations aimed at determining the optimal arrangement for application of artificial cavitation were completed. The outputs of the calculations are geometrical characteristics of the hull lines and appendages (cavitators) around and inside the region where the air cavity is to be positioned. Two variants of the air cavity system, differing in the form of the redan (step) in the beginning of the bottom recess, were selected for model testing (figure 6). The length of the recess in the first option was 53% of the waterline length while in the second option it reached 60%. The area of the recess was 35% and 38% of the total underwater hull surface area, respectively. The calculated air cavity systems were implemented on the model and towing tests were repeated. Visual observation of the flow around the model demonstrated that air escaping from the cavity did not appear in a propeller location and hence, neither special propulsors nor air-protective devices were needed for this vessel.

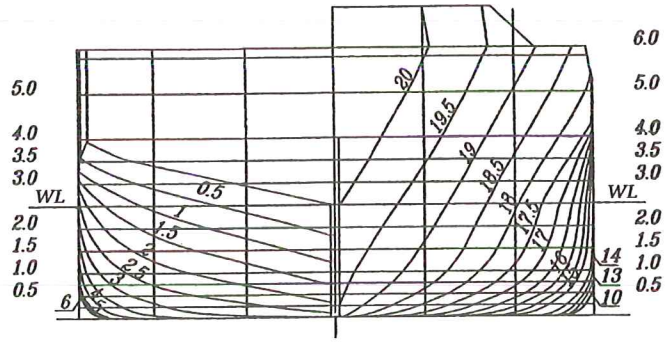

Figure 5. Initial hull form of the vessel model.

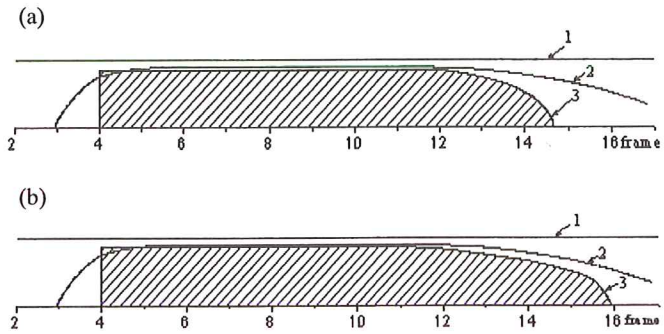

1: board line, 2: boundary of the flat portion of the bottom, 3: recess line. Recess area is shaded. Ship bow is on the right.

Figure 6. Bottom view on two variants of the recess for the air cavity.

		Ship	Model
Length overall	m	81.92	5.461
Waterline length	m	79.80	5.320
Beam	m	11.40	0.760
Draft	m	2.50	0.167
Displacement	m^3	1807	0.535
Block coefficient		0.795	
Waterline coefficient		0.891	
Middle section coefficient		0.992	
Speed		11 knots	1.46 m/s

Table 2. Geometrical and speed specifications of the ship/model tested.

The results for the towing resistance of the initial hull and two variants of the model with an air cavity system, as well as relative drag reduction obtained, are presented in figure 7. Significant improvement in hydrodynamic performance was

achieved when artificial cavitation was utilized. The model towed with speeds from 0.8 m/s to 1.6 m/s corresponds to a full-scale ship moving in the speed range from 6 to 12 knots. Since actual ships sometimes operate in non-optimal regimes, the model was also tested at different trim and heel angles, as well as at another load. The efficiency of the air cavity system did not decrease noticeably in these cases. To determine how a significant increase of the air supplied to the cavity may affect the ship performance, the airflow rate was increased by a factor of 10 relative to the flow rate sufficient for creating an air cavity with designed characteristics. This abnormally high air supply did not result in additional drag reduction, and led to rough cavity closure, air entrainment from board sides, and the appearance of air bubbles at the propeller location.

The results of this experiment scaled to a full-scale ship suggest that the vessel with the two air cavity arrangements under investigation would have its drag reduced by 17% and 21%, respectively, at the design speed of 11 knots and with the specifications given in table 2. The power needed for the air supply to maintain the air cavity, scaled to a full-size system, was found to be about 2% of the total propulsive power. Thus, an application of artificial cavitation produces a considerable enhancement of the ship performance without any adverse effects.

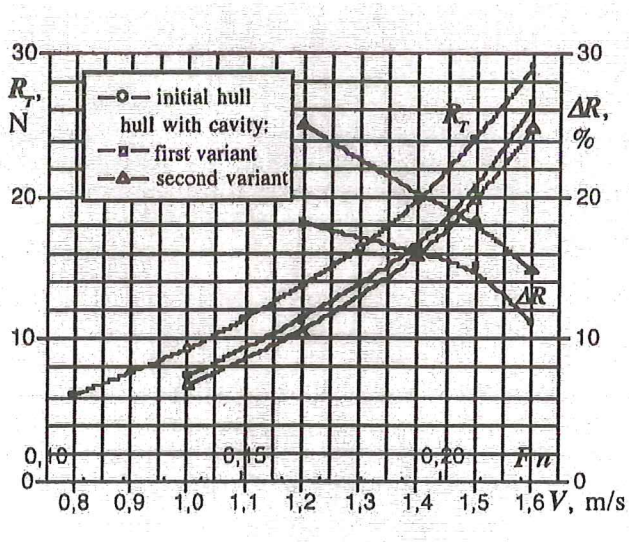

Figure 7. Towing resistance and resistance reduction of the model tested.

5. CONCLUDING REMARKS

Artificial cavitation is currently applied in practice to reduce hydrodynamic resistance of marine vehicles. Drag reduction reaches 15% - 30% on actual full-scale ships. The power needed to maintain the air cavity is within 3% of the total propulsive power. Maneuvering characteristics are not significantly affected by the presence of an air cavity, while seaworthiness of an ACS is better than that of analog vessels without an air cavity. Special attention has to be paid to a choice of propulsors, since they may operate in a flow which contains a small fraction of air escaping from the cavity. The ACS concept is truly energy-conserving and therefore, this technology has bright prospects for future marine transportation.

ACKNOWLEDGEMENTS

The author thanks David Gardner for help in preparing this paper.

REFERENCES

Basin, A., Butuzov, A., Ivanov, A., Olenin, Y., Petrov, V., Potapov, O., Ratner, E., Starobinsky, V. and Eller, A. 1969 Operational tests of a cargo ship 'XV VLKSM Congress' with air injection under a bottom. *River transport*, 52-53 (in Russian).

Burg, D. & Johnson, W. 1999 Air-assisted catamaran, the Seacoaster concept. In *Proceedings of the international conference on hydrodynamics of high speed craft*, London.

Butuzov, A. A. 1967 Artificial cavitation flow behind a slender wedge on the lower surface of a horizontal wall. *Fluid dynamics*, **3**, 56-58.

Butuzov, A. A. & Pakusina, T. V. 1970 Calculation of the planing surface with artificial cavitation. *Transactions of Krylov SRI*, **258**, 63-81 (in Russian).

Butuzov, A. A., Vasin, A. I., Drozdov, A. L., Ivanov, A. N., Kalyuzhny, V. G., Matveev, I. I. & Ruzanov, V. E. 1981 Full-scale trials of a boat with an air cavity. *Shipbuilding problems*, **28**, 45-51 (in Russian).

Butuzov, A. A. 1988 Spatial linearized problems on flow at the ship with artificial cavitation. *Shipbuilding problems, series ship design*, **8**, 1-18 (in Russian).

Butuzov, A., Sverchkov, A., Poustoshny, A. & Chalov, S. 1999 State of art in investigation and development for the ship on the artificial cavity. In *Proceedings of the international workshop on ship hydrodynamics*, China.

Eller, A.O. 1970 Determination of the parameters of the infinite air cavity system located on the lower side of the unbounded horizontal wall. *Transactions of Krylov SRI*, **258**, 54-62 (in Russian).

Ibragimova, T.B., Mavlyudov, M.A. & Roussetsky, A.A. 1995 Basic principles of propulsor efficiency comparisons. In *Proceedings of the 3rd international conference on fast sea transportation*, Hamburg.

Ivanov, A.N. 1980 *Hydrodynamics of developed cavitating flows*. Sudostroenie, Leningrad (in Russian).

Jane's High-Speed Marine Crafts, 1995-96.

Knapp, R. T., Daily, J. W. & Hammit, F. G. 1970 *Cavitation*. New York: McGraw-Hill.

Latorre, R. 1997 Ship hull drag reduction using bottom air injection. *Ocean engineering*, **24**, 161-175.

Matveev, K. I. 1999 Modeling of vertical plane motion of an air cavity ship. In *Proceedings of the 5th international conference on fast sea transportation*, Seattle.

Matveev, K. I. 2003a Air cavity ships are ready for a wider market. *Speed at sea*, **9**(1), 13-16.

Matveev, K. I. 2003b On the limiting parameters of artificial cavitation. *Ocean engineering*, **30**, 1179-1190.

Matveev, K. I. 2003c Two-dimensional modeling of the limiting air cavity system. In *Proceedings of the 41st aerospace sciences meeting & exhibit*, Reno, NV, USA. AIAA paper No. 2003-0624.

Sverchkov, A. V. 2002a A ship with air cavity and air-cushion catamaran. *Boats and yachts*, **179**, 46-50 (in Russian).

Sverchkov, A. V. 2002b Perspectives of artificial cavity application aimed at resistance reduction of ocean/river ships. In *Proceedings of the 3rd international shipbuilding conference*, St. Petersburg, Russia.

Silberman, E. & Song, S. 1961 Instability of ventilated cavities. *Journal of ship research*, **5**, 13-33.

Tudem, U. S. 2002 The challenge of introducing innovative air lifted vessels to the commercial market. In *Proceedings of the 18th fast ferry conference*, Nice, France.

APPENDIX

In this appendix, the basic theory of developed cavitating flows applied for design of an Air Cavity Ships is outlined. The simplest case is the two-dimensional cavitating flow behind a wedge on the lower side of the horizontal wall in the presence of gravity, as shown in figure 8 [Butuzov 1967]. The wall imitates the ship's bottom. The liquid is assumed to be ideal and incompressible; the flow is potential and steady. Pressure in the cavity, including its boundary, is uniform. A generalized Riabouchinsky scheme is applied, using a fictitious contour at the cavity tail. Bernoulli's equation at the cavity boundary streamline states

$$p_c = \frac{\rho U^2}{2} + p_0 - \frac{\rho u_c^2}{2} + \rho g y_c \qquad \text{(A1)}$$

where p_0 and U are the pressure and velocity, respectively in the undisturbed flow at $y = 0$ far from the air cavity, p_c and u_c are the pressure and velocity, respectively, at the cavity boundary streamline, g is gravitational acceleration, and y_c is the cavity boundary ordinate. When the cavity and the wedge are sufficiently thin, the problem can be linearized. Re-written in a non-dimensional form, using definitions of Froude and cavitation numbers from equations (1) and (2), equation (A1) gives

$$\frac{\sigma}{2} = -\frac{y_c}{Fr^2 b} + \frac{u_1}{U} \qquad \text{(A2)}$$

where b is the wedge length and u_1 is the horizontal velocity perturbation. In the linear theory, slender obstacles in the flow can be simulated by a distribution of sources with intensities proportional to the derivative of their boundary ordinate

$$q(x) = 2Uy' \qquad \text{(A3)}$$

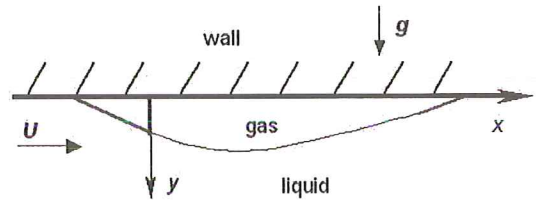

Figure A1. Scheme of a cavitating flow behind a wedge.

Velocity perturbation induced by the sources is computed by

$$u_1 = -\frac{1}{2\pi}\int_{-b}^{L}\frac{q(\xi)d\xi}{\xi - x} \qquad \text{(A4)}$$

where L is the total cavity length, including a fictitious contour at the end. A combination of equations (A2) through (A4) produces a final equation for the cavity shape y_c

$$\frac{y_c(x)}{Fr^2 b} + \frac{1}{\pi}\int_0^L \frac{y'_c(\xi)d\xi}{\xi - x} = -\frac{\sigma}{2} - \frac{1}{\pi}\int_{-b}^{0}\frac{\eta'(\xi)d\xi}{\xi - x} \qquad \text{(A5)}$$

where $\eta(x)$ is the known ordinate of the wedge surface. The resulting integral-differential equation (A5) is solved numerically. An additional equation is required to provide a closed contour comprising the air cavity and the wedge.

$$\int_{-b}^{0}\eta'(x)dx + \int_0^L y'_c(x)dx = 0 \qquad \text{(A6)}$$

The formulation outlined here allows for further straightforward extensions: multiple cavities formed under the ACS bottom [Eller 1970; Matveev 2003c], curved ship bottom profile, pressure gradient in the flow [Ivanov 1980; Matveev 2003c], free water surface before and after the ship hull [Butuzov & Pakusina 1970], and proximity of propulsors and control and lift devices to the air cavity [Matveev 2003b]. All of these factors can be accounted for by modifying the limits of integration and adding appropriate terms in equation (A5).

Linearized spatial problems aimed at determining the transverse flow effects and optimizing the hull lines of fast ACSs can be formulated and solved using the approach similar to that for the planar problem. Again, a distribution of hydrodynamic singularities is sought on the projections of the hull, cavity, and free water surface to the horizontal plane [Butuzov 1988]. Velocity perturbation depends now on two spatial coordinates. Appropriate matching conditions are imposed on the boundary between the air cavity and the hull surface.

The assumption of the air cavity thinness is not always satisfied. For example, the nonlinear problem arises for an

ACS moving in displacement and transitional regimes and having significant hull curvature. In this case, information on the flow and pressure distribution on the initial hull without air cavities is needed [Butuzov 1988]. Then, the linearization procedure for computing the flow with air cavities is accomplished with respect to the known initial flow. If there are several air cavities, they are computed starting from the upstream cavity.

Oceanic Engineering International, Vol. 9, No. 1, 2005, pp. 42-53

Scour due to Waves and Currents around Piles in Clay

M. Ram Babu[1], S. Narasimha Rao[2], and V. Sundar[2]

[1] *Department of Civil Eng., Vellore Institute of Technology, Vellore, TamilNadu, INDIA*
[2] *Department of Ocean Eng., Indian Institute of Technology Madras, Chennai, INDIA-600 036*

e-mail: snarasimharao@hotmail.com

ABSTRACT

The flow structure interaction in an ocean environment, for a pile placed in an erodible seabed where currents and waves are of prime concern, changes the bed elevation in the vicinity of the obstruction leading to scour. Although studies have been carried out on the scour around piles in cohesionless soils, only a few studies are carried out in cohesive soils and, in particular, on scour around structures due to the combined action of waves and currents. Hence, in the present investigation, the scour around piles induced by the combined action of waves and currents has been studied in a wave flume on model piles of diameter 50 mm, 90 mm and 110 mm embedded in cohesive soil bed. A special type of instrumentation was developed to measure the scour around the model pile. Based on the test results, an expression for the bed shear stress due to the combined action of waves and currents applicable for cohesive soils has been suggested.

Key words: Scour, piles, steady current, waves, silty clay.

1. INTRODUCTION

Many engineers all over the world have realized the importance of the studies of scour around foundations of offshore and coastal structures. Scour results from the disturbance to the ambient flow field caused by an obstruction to flow and is recognized as one of the important sources of damage for coastal structures. The key element in the scour process is the formation of vortices due to the interaction of velocity profile of the flow with the obstruction. In pile-supported structures, scour reduces the lateral support for the piles leading to an increase in bending moments. It is well accepted that many foundations of waterfront structures built in soils have suffered extensive damage due to scour. There are many under-consolidated marine clayey deposits located in several coastal areas all over the world and it is now realized that scouring can also be serious in soft under-consolidated clays. Therefore, it is important in the design of foundations of marine structures to consider the assessment of scour due to currents and waves and there is a need to predict, realistically, the maximum depth of the scour for the prevailing environmental conditions at the site.

Research on local scour has been extensive over the past few decades. The scour around the structure is directly related to the kinetics and dynamics of waves and the underwater current that significantly modifies the scour pattern [Armbrust 1982]. Some investigators [Clark & Novak 1982; Chow & Herbich 1978; Machemel & Abad 1975] have found that the combined action of waves and currents enhances the rate of scour. Kroezen *et al.* [1982] stated that the influence of waves on the scouring rate is of great importance when the steady state current alone is too weak to cause scour. Solutions developed for local scour around piles in cohesionless soils cannot be simply extended to cohesive soils (clayey soils). In clayey soils with particle sizes in the colloidal range (extremely fine), the influence of gravitational forces on such particles is less and in comparison, the surface inter-particle forces, viz., repulsive and attractive forces become more dominant and significantly influence the engineering behaviour. In the case of soft clays deposited with a lower degree of consolidation pressures and high moisture contents, inter-particle forces are less predominant and these conditions are favourable to scouring. Hence, an attempt has been made in the present investigation to study the scour around the piles embedded in soft marine clay under the combined action of waves and currents. It is proposed to suggest a methodology for predicting the ultimate scour depth around piles and an expression for the bed shear stress due to variations in the flow velocity and wave characteristics.

2. EXPERIMENTAL PROGRAMME

The present experimental investigation was carried out in a wave-current flume, 2 m wide, 1.7m deep and 30 m long. A similar flume set-up arrangement was earlier used by a few investigators [Herbich *et al.* 1984; Sumer *et al.* 1993; Briaud *et al.* 1999] for studies on scour around piles. This model set-up has been mainly used to study wave/current induced scour around model piles installed in the soil bed formed in the flume. The present investigation finds its importance in the study of stability analysis of pile foundations adopted to support seawater intake jetty structures and to provide foundation support for berthing structures. Also, the present work supports its application to several aqua-based industries and coastal power plants. The details of the flume and experimental set-up are presented in figure 1.

A plunger type wave generator with a variable gear system was used to generate regular waves at different wave heights and periods and a vertical turbine pump was used for the generation of water currents. The re-circulation of water from inlet and outlet arrangements of the false bottom provided current velocity at a constant discharge for a given water depth, d. In order to have a regulated water flow near the test section, an upstream steel ramp with a slope of 1 in 25 was provided. On the downstream end of the test section, another steel ramp followed by a soil trap was provided to prevent the entry of the soil particles into the current pump. The sloping beach end consisted of stone rubbles at 1 in 3.5 slope extending over a length of 6 m was provided at the downstream end to dissipate wave energy and to reduce wave reflections. The sizes and the materials for the model piles were chosen based on the considerations of (i) normal sizes of foundations adopted in the field, (ii) surface characteristics of field piers/piles, and (iii) rigidity of the foundation soil system. It has been shown by Sumer *et al.* [1993] that an hydrodynamically smooth surface can cause a good amount of scouring. PVC (Poly Vinyl Chloride) pipes are fairly smooth and hence, PVC pipe piles of diameters, D = 50 mm, 90 mm, and 110 mm were used as model piles in these studies. The model was placed at the centre of the test section and held rigidly in position by channel sections placed on the rails of the flume. A test section of fairly homogeneous and saturated silty clay bed of 300 mm thickness, 1.5m in length and 2m in width was formed in the centre region of the flume using the technique adopted by the earlier investigators [Narasimha Rao & Prasad 1993]. An enlarged section of this clay bed portion with an embedded model pile is shown in figure 1(c). As it is planned to test model sizes up to 110 mm diameter, it is considered to be sufficient to limit the thickness of the bed exposed to scour to 300 mm (nearly three times the diameter). Further, the radial distance over which there is the influence of scour is $6D$ along the flow direction and $4D$ in the perpendicular direction to flow [Carstens & Sharma 1975]. Considering these aspects, the dimensions of the cohesive soil bed formed is quite sufficient for the study. Because of the high moisture content used, there was no difficulty in forming a homogeneous soil bed. The undrained shear strength of the soil (c_u) was measured using an in-situ miniature vane shear apparatus. The index properties and grain size distribution of the soil as obtained from the tests as per relevant ASTM standards [ASTM D 4318-1984; D 422-63-1972] are

- Natural moisture content (n.m.c) - 32.94%.
- Liquid Limit (L.L) - 40 %.
- Plastic Limit (P.L) - 18 %.
- Plasticity Index (P.I) - 22%.

The soil consists of

- Clay fraction - 54%.
- Silt fraction - 37%.
- Sand fraction - 9%.

(a) Instrumentation - Scour Sensor

The rate of scour depth development can have an important influence on the ultimate scour depth. A suitable instrumentation was developed and used to monitor and record the progressive rate of scour development due to different combinations of currents and waves. Model piles of sufficient length were chosen and stainless steel wire probes of 2.0 mm diameter were embedded in the grooves (diametrically opposite) made on the outer periphery (length-wise) of the model. The portion of grooves with probe wires above the clayey bed was sealed with an insulating material to make them insensitive to other changes retaining the surface smoothness of the pile. The grooves with probe wires embedded into the clay bed were not filled with the insulating material. The details of this arrangement are shown in figure 2.

The scour sensor works on a principle of measuring the current flowing in a probe that consists of a pair of parallel stainless steel wires. The probes were energised with a high frequency square wave voltage to avoid polarisation effects at the wire surfaces. Probe wires were extended at the top of the model to the scour probe amplifier. Scour caused around the model removes the soil around the probe elements that, in turn, changes the current flow between the probe elements, sensed by an electronic circuit that provides an output voltage. The measurement by the scour probe amplifier at a particular instant gives output voltage proportional to the scour developed at that time. A set of calibrations was carried out before the commencement of each test and calibration charts were developed for obtaining a relationship between scour depth and voltage at any instant. The block diagram of instrumentation set-up for scour measurement is shown in figure 3.

At the start of each run, flow and wave characteristics were adjusted to the desired values. In another similar testing programme carried out in the same test flume with the soil bed formed using the same soil, the plots made between scour depth ratios and number of cycles, obeyed hyperbolic formulations and the analysis confirmed that 90% of the maximum scour depth had occurred for 11,000 wave cycles. This aspect is further elaborated upon in the next section. Hence, in this investigation also, the scour testing was continued for 11,000 wave cycles (of about 3 hours duration) for all tests so as to ensure that the rate of scour due to the combined action of waves and currents was decelerated to smaller values at the end of tests. The scour depth was

measured at four different locations (diametrically opposite) around the pile. The average of the four values was reported as 'scour depth', S_i developed at any instant, as the ratio of the standard deviation to the mean of the values at these four locations around the pile was less than 5%.

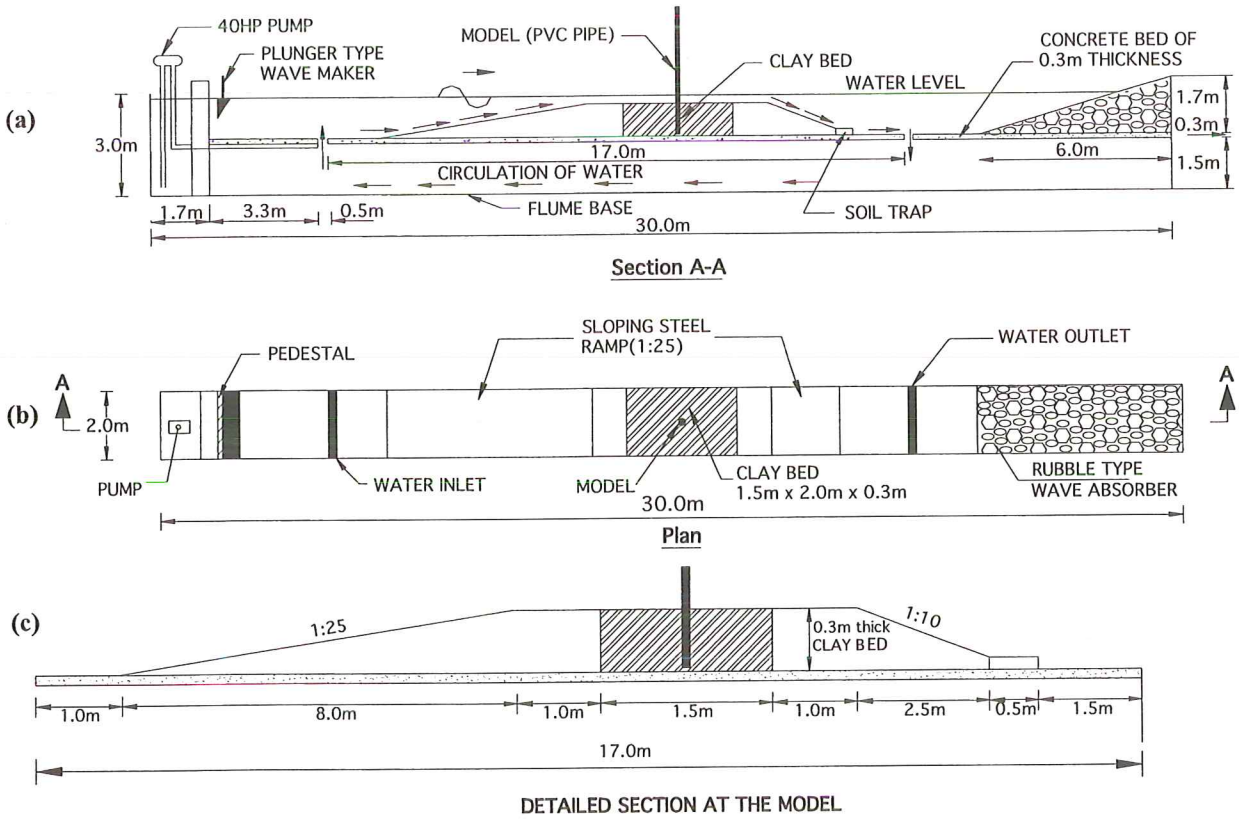

Figure 1. Schematic details of experimental set-up in wave-cum-current flume.

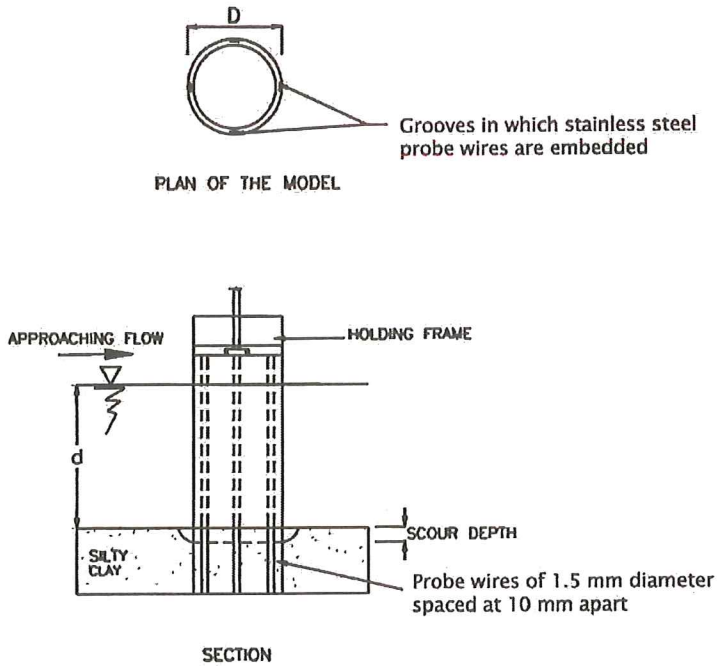

Figure 2. Details of the arrangement of a model with a holding frame.

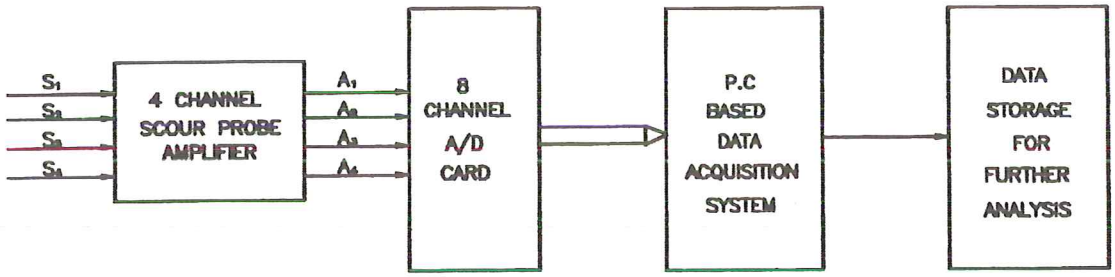

Figure 3. Block diagram of instrumentation set-up of scour measurement

3 ANALYSIS AND MODELLING

The different parameters adopted for the present investigation are given in table 1.

Selected Variables	Range of Model values	Employed Scale ratio	Prototype Magnitudes
Diameter(D), m	0.050 to 0.110	1:20	1 to 2.2 m
Water depth(d), m	0.30 to 0.60	1:20	6 to 12 m
Current Velocity(U), m/s	0.20 to 0.33	1:20	0.90 to 1.47 m/s
Wave Period(T), sec	1 to 2	1:20	4.5 to 9 sec
Wave Height(H), m	0.040 to 0.150	1:20	0.8 to 3 m.

Table 1 Scale ratios and the applicability range of model magnitudes to field considerations.

For a scale ratio of 1:20 used in this investigation and model parameters as given in table 1, the corresponding parameters for the prototype are worked out and presented in the same table. There are certain difficulties expressed by previous investigators in arriving at scaling effects [Sumer *et al.*, 1997]. With respect to soil grain size, it is difficult to adopt any modeling law. Hence, the soil that is deposited under the real field situations can be used to form the test bed in the laboratory model set-up. In clays, knowing the value of sensitivity (ratio of undisturbed strength to the remolded strength), the field conditions can be predicted for a particular soil. Normally, the sensitivity parameter is estimated from the in-situ strength tests carried out in the field and laboratory tests on remolded soil. For the soil used in this investigation, the sensitivity measured is 3.5. It should be ensured that the soil bed in the laboratory has been formed at almost the same field moisture content. To represent the field depositional conditions in clayey soils, the consistency index (I_C) parameter can be used. The consistency index, I_C is defined as the ratio of the liquid limit of the natural moisture content to the liquid limit of the plastic limit). To project the field strength, the measured strength in the laboratory can be multiplied by a factor equal to the sensitivity of the chosen soil deposit. Further, the extent of scour depends mainly on (i) the bottom water particle velocity (water-sediment interface) at the obstruction and (ii) the type of soil. Hence, the ultimate scour depth around a pile due to currents and waves, S_{ucw} is correlated with variables characterising the obstruction, soil and the flow parameters as given below.

$$S_{ucw} = f(D, d, H, T, U_{cw}, \nu, C_u, \tau_c, \tau_{cw}) \quad (1)$$

where H = wave height, T = time period, and U_{cw} = combined velocity due to waves and currents [Wang & Herbich 1983], and ν = kinematic viscosity of water, τ_c = maximum bottom shear stress due to currents in the absence of waves, τ_{cw} = maximum bottom shear stress due to waves and currents [Soulsby 1995].

The above variables involved in the problem can be combined to form dimensionless parameters as given below.

$$S_{ucw}/D = f(H/L, d/L, R_e, F_r, U_p, \psi) \quad (2)$$

where wave steepness is H/L; relative water depth is d/L, and L is wave length; Reynolds number, $R_e = U_{cw}.D/\nu$; Froude number, $F_r = U_{cw}/\sqrt{gd}$; Ursells parameter, $U_p = HL^2/d^3$; and the amplification factor (ψ) is τ_{cw}/τ_c. The justification for the choice of the dimensionless groups is discussed below.

- *Flow Froude number* (F_r) is the ratio of kinetic energy ($\rho U^2_{cw}/2$) to potential energy (ρgd) and is considered to be one of the major dynamic factors causing movement of soil particles in the scour process [Herbich *et al.* 1984].
- The importance of *model Reynolds number*(R_e) and its influence is felt in waterfront structures signified by characteristic dimension D [Carstens 1966; Chow & Herbich 1978]. It can be explained physically by the fact that scour formed due to the vortex system is a function of shape, size of the obstacle and viscosity of the fluid [Shen *et al.* 1969].
- *Ursells parameter* indicates the magnitude of wave energy transmitted to the sediment bed.

- *Amplification factor,* is a parameter in the study of movement of sediment beds. The lifting action of sediments from the soil bed is influenced by the wave steepness which determines the vertical amplitude of water particles

(a) Hyperbolic formulations for ultimate scour depth

In the literature, there is limited information concerning the required time to reach the ultimate scour depth. In clay, the time required to reach the ultimate scour depth in a model test can be many days [Yanmaz & Altinbilek 1991]. However, from a practical standpoint, it is very difficult to perform a wide range of experiments with such a long duration [Raudkivi 1986]. Since the scour depth obtained from a limited period of testing is not the ultimate scour depth, a data fitting formulation based on the hyberbolic law is suggested to extrapolate the measured data to arrive at the ultimate scour depth. Some of the geotechnical applications of this law are already demonstrated [Prasad & Narasimha Rao 1994].

The scour depth (S) can be expressed as function of time 't' as

$$S = t/(A + B\,t^2) \quad (3)$$

$$S_{ucw} = \lim_{t\to\infty} S = (1/B) \quad (4)$$

where 'A' and 'B' are constants that depend on soil and hydraulic conditions and the slope of the fit ($1/B$) between 't/S' and 't' gives the ultimate scour depth (S_{ucw}). To signify the application of hyperbolic formulation for estimating the ultimate scour depth, considering the field conditions, the scour depth versus time curve is generated for a bridge pier in clay and is presented in figure 4(a) [Briaud *et al.* 1999]. The transformed plot representing the variation of the ratio of time to the scour depth (t/S_i), with the time 't' shown in figure 4(b). For the considered range of field values given in figure 4(a), the estimated ultimate scour depth works out to be 2.803 m against the predicted value of 2.818 m from Hyperbolic law. These reported results of field observations carried out by Briaud *et al.* [1999] implicate the applicability of hyperbolic data fitting law.

The time development of scour depth for different model sizes at a particular velocity ratio (ratio of current velocity and celerity of wave, U/C) and wave steepness (H/L) is shown in figure 5. The actual duration of each of the experiments was 3 hours and the scour depth measured at the end of this period for pile size D = 110 mm at U/C = 0.196, H/L = 0.105 is 61.4mm (as shown in figure 5). This scour depth measured is not the ultimate scour depth for these conditions. To obtain the same, the variation of the ratio of time to the scour depth (t/S_i), with the time 't' for the three model sizes for the same experimental conditions are plotted, as shown in figure 6, and these results indicate straight line plots confirming the applicability of the hyperbolic law. By applying the above-mentioned hyperbolic formulations for the present experimental conditions, the ultimate scour depth (S_{ucw}) is predicted from the measured slope of the linear fits ($1/B$). For the test results (as shown in figure 5), the ultimate scour depth was found to be 72.46 mm. The intercept on the y-axis gives the initial rate of scour, $1/A$, which is equal to 0.050 mm/hr for this particular experiment. Therefore, as there is difficulty in continuing long duration tests, the use of an observational method that employs hyperbolic law for the estimation of ultimate scour depth is suggested. For the results obtained from the tests conducted for all the approach velocities, the validity of the hyperbolic law for the extrapolation of scour depths is confirmed. Ultimate scour depth values thus obtained by applying hyperbolic fitting law are used in the data analysis.

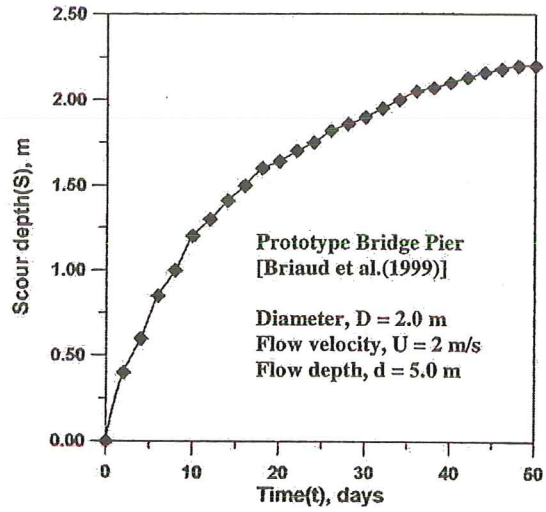

Figure 4(a). Example of scour depth versus time curve for full-scale pier prototype bridge pier.

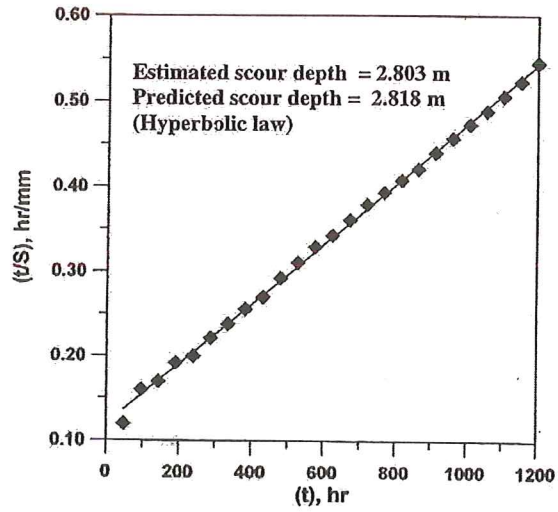

Figure 4(b). Application of hyperbolic formulation for prediction of ultimate scour depth - an illustration [Briaud *et al.* 1999].

Diameter, D = 2.0 m, flow velocity, U = 2 m/s, flow depth, d = 5.0 m, estimated scour depth = 2.803 m, predicted scour depth = 2.818 m, (Hyperbolic law)

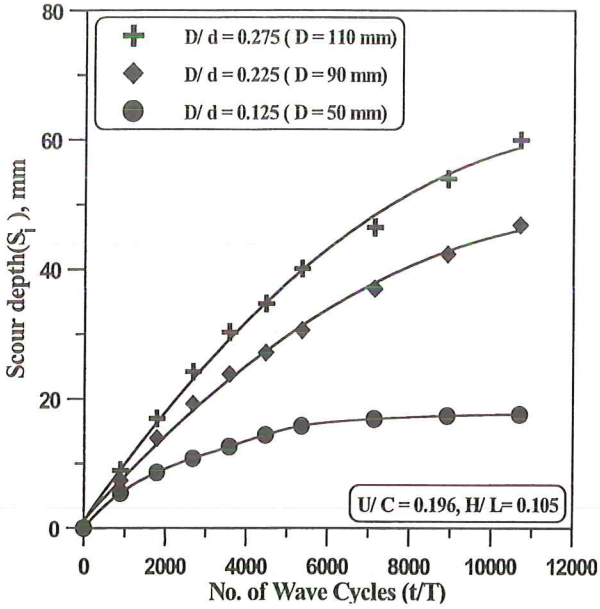

Figure 5. Time development of scour with wave cycles (influence of diameter).

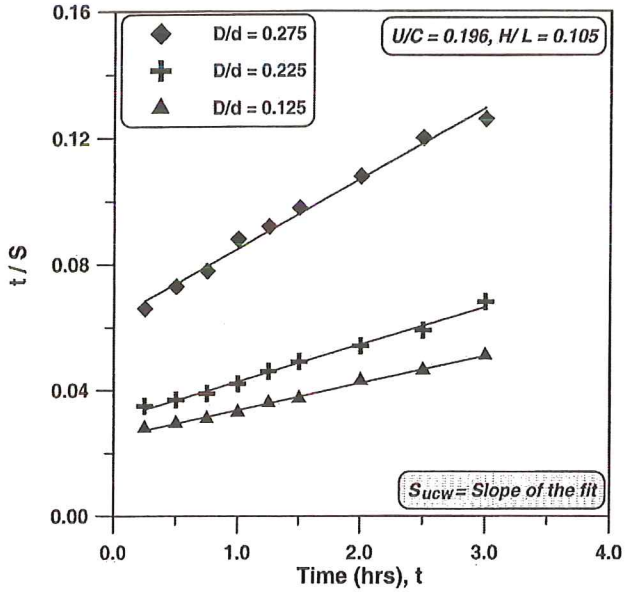

Figure 6. Prediction of ultimate scour depth using hyperbolic model (for data of figure 5).

4. RESULTS AND DISCUSSIONS

The characteristics of the waves and currents for three different water depths (corresponding to approach velocities of U = 0.289, 0.258 and 0.199 m/sec) adopted for the present experimental investigation are given in table 2. The model piles were subjected to wave cycles of constant amplitude and frequency and these were superimposed on steady state current for different combinations. The wavelength, wave height, and the velocity of the combined flow field due to currents and waves (U_{cw}) are evaluated with the measured current velocities and wave characteristics [Wang & Herbich 1983]. The scour development in the vicinity of the pile is continuously monitored through instrumentation employing a scour probe amplifier. All these tests were conducted on identical initial conditions of the soil bed, as the soil bed was formed at a soft consistency conforming to a consistency index of 0.32 where

$$\text{consistency index} = \frac{(\text{liquid limit - natural moisture content})}{(\text{liquid limit - plastic limit})} \quad (5)$$

Based on the scour depth values measured up to 11,000 wave cycles, the ultimate values of scour depths, S_{ucw} are predicted from the hyperbolic law formulations. These ultimate scour depths in non-dimensional form, S_{ucw}/D are worked out and presented in table 2.

It is inferred that the wave period and the wave height have a substantial influence on the scour depth. With an increase in wave height, there is an increase in the scour depth. The addition of wave field to the unidirectional current flow field expedites the rate of the scouring process, as there is an increased velocity due to waves and currents, and results in a greater scour. In order to highlight the salient features of 135 test runs made with different combinations of waves and currents on piles of three different sizes, a few typical results are considered. The influence of various flow associated parameters, viz., wave period, wave height, combined flow velocity due to currents and waves, bed shear stress on the ultimate scour depth have been studied.

(a) Influence of Model Size on the Time Development of Scour

The scour depths determined at different wave cycles for a water velocity at the obstruction, U = 0.289 m/s at a constant H/L of 0.105 and U/C of 0.196 for various sizes of obstruction (D = 50 mm, 90 mm, 110 mm) are already presented in figure 5. It may be noted that 'U' is the measured water velocity of the flow at the obstructed region of the test section (immediate vicinity of pile model). This plot brings out the effect of the pile sizes on the variation of scour depth with the number of wave cycles for a constant water depth, d = 400 mm. It may be noted that with a smaller diameter pile (D/d = 0.125), the increase in the rate of scour 'S_i' is quite gradual and reaches the steady value at a much lower number of cycles (5,500) compared to the one obtained for a larger pile (D/d = 0.275). For other values of D/d = 0.225 and 0.275, the tests have to be run for a greater number of wave cycles (about 11,000 wave cycles) to obtain steady state values of scour depth. These results demonstrate that with an increase in obstruction size, there is a proportionate increase in the scour depth. Scour depths and scour rates are significantly influenced by the size of the obstruction, keeping the wave and current characteristics constant. For projecting the percentage increase in scour depth with diameter for different U/C, the results obtained from the tests conducted using a pile of D = 50 mm are used for comparisons. For the set of results carried out with higher

current and long waves, it is observed that the ultimate scour depth increases by a factor of 2 when the diameter increases by a factor of 1.2. For a similar type of testing on cylindrical obstructions in sandy soils, the scour depth to diameter ratios of nearly 1.5 were reported [Breusers *et al.* 1977; Sumer 1992]. In comparison, scour depth to diameter ratios of 0.3 to 1.0 (depending on the flow velocity and the diameter of obstruction) are obtained in the present investigation of scour around pile foundations in cohesive soils.

Water depth, d = 400 mm						S_{ucw} / D			U = 0.289 m/sec	
T sec	L m	H mm	H/L	H/d	d/L	D=50 mm	D=90 mm	D=110 mm	U_w m/sec	U_{cw} m/sec
1.69	3.032	37	0.012	0.093	0.132	0.361	0.454	0.553	0.070	0.359
		51.30	0.017	0.128		0.435	0.529	0.604	0.096	0.385
		63.35	0.021	0.158		0.547	0.614	0.651	0.119	0.408
1.53	2.739	47.45	0.017	0.119	0.149	0.409	0.496	0.555	0.087	0.376
		65.51	0.024	0.164		0.520	0.621	0.682	0.120	0.409
		82.25	0.030	0.205		0.669	0.733	0.794	0.150	0.439
1.35	2.296	65.55	0.028	0.164	0.174	0.481	0.584	0.658	0.106	0.395
		85.85	0.037	0.214		0.623	0.712	0.791	0.150	0.439
		107.30	0.047	0.268		0.721	0.803	0.880	0.188	0.477
1.16	1.834	74.80	0.041	0.187	0.215	0.588	0.670	0.729	0.122	0.411
		102.75	0.056	0.257		0.730	0.790	0.850	0.168	0.457
		134.10	0.073	0.355		0.820	0.871	0.931	0.219	0.508
1.00	1.485	89.10	0.060	0.178	0.269	0.660	0.743	0.818	0.132	0.421
		121.65	0.081	0.243		0.839	0.880	0.950	0.180	0.469
		155.40	0.105	0.310		0.910	0.981	1.060	0.230	0.519
Water depth, d = 500 mm						S_{ucw} / D			U = 0.258 m/sec	
T sec	L m	H mm	H/L	H/d	d/L	D=50 mm	D=90 mm	D=110 mm	U_w m/sec	U_{cw} m/sec
1.69	3.032	37	0.012	0.074	0.165	0.312	0.368	0.406	0.057	0.315
		51.30	0.017	0.102		0.323	0.432	0.519	0.079	0.337
		63.35	0.021	0.127		0.391	0.504	0.586	0.097	0.355
1.53	2.739	47.45	0.017	0.095	0.186	0.346	0.424	0.473	0.071	0.329
		65.51	0.024	0.131		0.447	0.531	0.596	0.098	0.356
		82.25	0.030	0.164		0.517	0.596	0.677	0.123	0.381
1.35	2.296	65.55	0.028	0.131	0.218	0.423	0.497	0.549	0.087	0.345
		85.85	0.037	0.171		0.540	0.592	0.669	0.123	0.381
		107.30	0.047	0.215		0.630	0.691	0.770	0.154	0.412
1.16	1.834	74.80	0.041	0.149	0.269	0.537	0.586	0.625	0.100	0.358
		102.75	0.056	0.205		0.622	0.688	0.730	0.137	0.395
		134.10	0.073	0.268		0.712	0.760	0.830	0.179	0.437
1.00	1.485	89.10	0.060	0.178	0.337	0.606	0.645	0.710	0.108	0.366
		121.65	0.081	0.243		0.705	0.761	0.821	0.148	0.406
		155.40	0.105	0.310		0.802	0.871	0.950	0.189	0.447
Water depth, d = 600 mm						S_{ucw} / D			U = 0.199 m/sec	
T sec	L, m	H, mm	H/L	H/d	d/L	D=50 mm	D=90 mm	D=110 mm	U_w m/sec	U_{cw} m/sec
1.69	3.032	37	0.012	0.062	0.198	0.273	0.325	0.358	0.047	0.246
		51.30	0.017	0.085		0.303	0.377	0.432	0.065	0.264
		63.35	0.021	0.105		0.344	0.425	0.488	0.081	0.280
1.53	2.739	47.45	0.017	0.079	0.223	0.323	0.381	0.424	0.059	0.258
		65.51	0.024	0.109		0.372	0.453	0.508	0.081	0.280
		82.25	0.030	0.137		0.441	0.514	0.594	0.102	0.301
1.35	2.296	65.55	0.028	0.109	0.261	0.401	0.433	0.477	0.072	0.271
		85.85	0.037	0.143		0.470	0.522	0.561	0.102	0.301
		107.30	0.047	0.178		0.531	0.631	0.690	0.128	0.327
1.16	1.834	74.80	0.041	0.124	0.322	0.484	0.535	0.561	0.083	0.282
		102.75	0.056	0.171		0.556	0.591	0.661	0.115	0.314
		134.10	0.073	0.22		0.621	0.730	0.770	0.150	0.349
1.00	1.485	89.10	0.060	0.148	0.404	0.536	0.591	0.646	0.091	0.290
		121.65	0.081	0.202		0.628	0.700	0.760	0.124	0.323
		155.40	0.105	0.259		0.706	0.820	0.880	0.158	0.357

Table 2. Results of ultimate scour depth (S_{ucw}) due to combined action of currents and waves with various flow parameters.

(b) Relation of S_{ucw}/D with U_{cw}/C

Any increase in the current velocity in the wave field significantly increases the scour at obstructions [Herbich *et al.* 1984]. The increase in the water particle velocity in the immediate vicinity of the foundation along with the current velocity influences the scouring mechanism. A non-dimensional plot has been drawn between S_{ucw} /D with U_{cw}/C for the tests conducted and is shown in figure 7. The increasing trend in scouring is observed and this can be due to the increase in the magnitude of the vortex system with increasing U_{cw}/C and agrees with the observation made by Sumer [1997] in the case of cohesionless soils. Based on the regression analysis, the following expression is suggested for the functional relationship between U_{cw}/C and S_{ucw}/D. with $R^2 = 0.735$.

$$(S_{ucw}/D) = 0.092 + 2.45(U_{cw}/C) \quad (5)$$

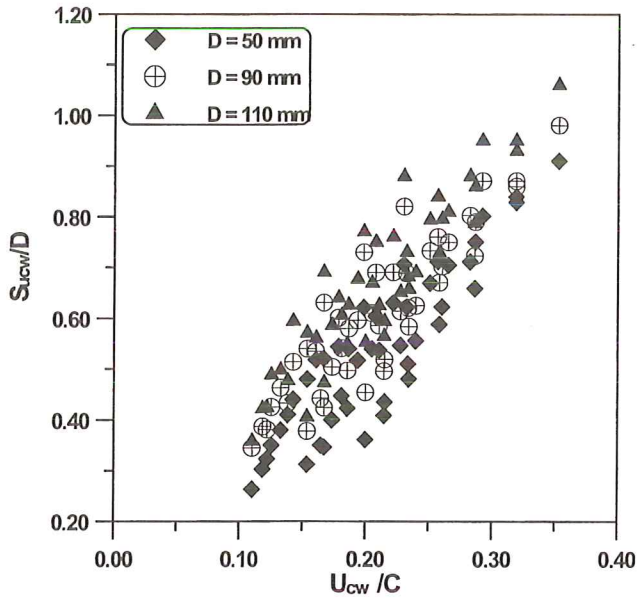

Figure 7. Relation of S_{ucw}/D with U_{cw}/C.

(c) Effect of Wave Steepness (H/L) and Relative Water Depth (d/L) on S_{ucw}

The influence of H/L on relative ultimate scour depth (S_{ucw}/D) for a constant relative water depth, d/L = 0.132 and relative velocity (U/C) of 0.16 for different pile sizes (D/d), is shown in figure 8. This plot indicates that for a given diameter, current velocity and relative depth, scour increases with wave steepness; the larger wave heights result in greater scour depths. The increase in H/L is associated with the increase in vertical and horizontal water particle velocities, and this results in an increase in the lifting up and dragging of sediment particles at the obstruction [Wang and Herbich 1983]. The scour depths obtained for all the test runs are plotted against wave steepness (H/L), as shown in figure 9, and an approximate expression can be suggested based on regression analysis. At a higher wave steepness, the strength of the shed vortices (coherent parcels of rotating fluid) may be sufficient to cause significant scour depth [Sleath 1991]. It is suggested that the below equation can be used to estimate scour depth in the range of wave steepness, $0.012 < H/L < 0.10$. This needs further confirmation from data obtained for similar types of testing for a wide range of cohesive soils.

$$S_{ucw}/D = 2.283(H/L)^{0.421} \quad (6)$$

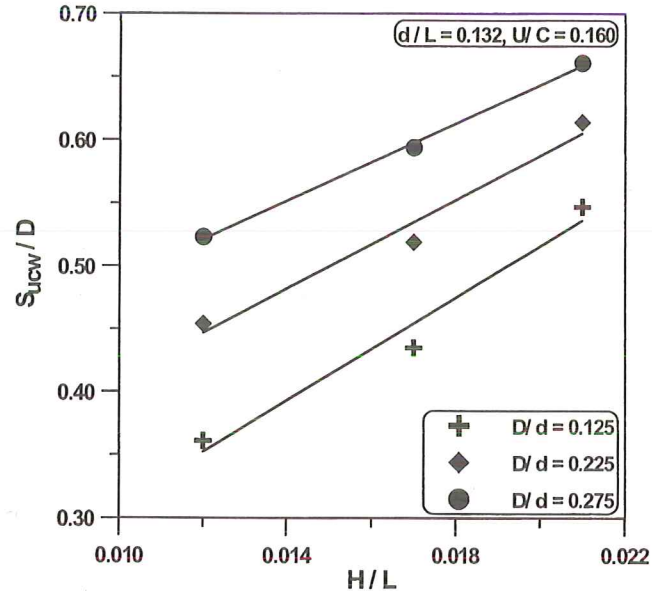

Figure 8. Effect of wave steepness (H/L) on S_{ucw}/D.

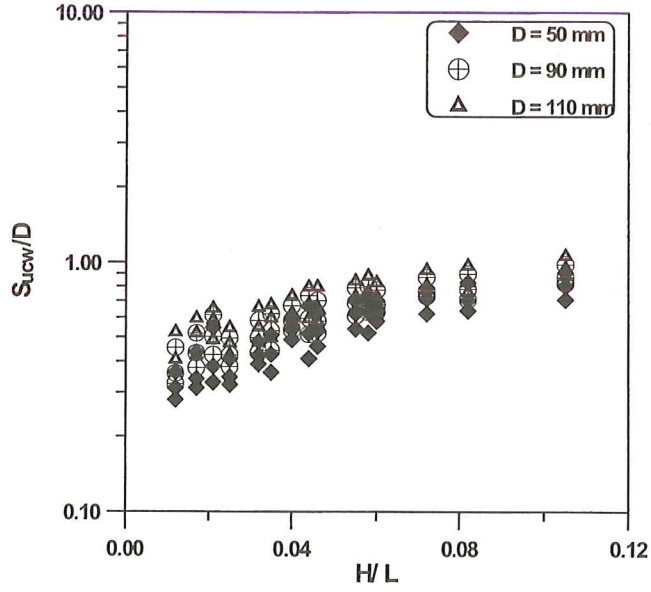

Figure 9. S_{ucw}/D as a function of wave steepness.

The influence of relative water depth (d/L) on ultimate scour depth, S_{ucw}/D is brought out in figure 10. It is observed that with an increase in d/L, there is a reduction in ultimate scour depth for a given wave steepness and diameter of obstruction. For smaller values of d/L, an increase in the velocity gradient is expected which possibly results in higher shear stress at the bed and consequently a greater scour.

(d) Effect of Reynolds Number on S_{ucw}

An effort has been made to relate the scour depth to Reynolds number (R_e), as the parameter includes pile size and dynamic factors of wave and current. The product of combined velocity, U_{cw} and the diameter of obstruction signify the inertial component in the expression of Reynolds number and determine the magnitude of scour depth. Figure 11 shows the relationship between normalized scour depth (S_{ucw}/D) and the Reynolds number for a particular current velocity (U = 0.289 m/sec) for all the model sizes tested. There is an increase in the ultimate scour depth with an increase in Reynolds number ($12000 < R_e < 57000$). These results reveal that the rate of change of scour is larger for a smaller diameter of obstruction, as the strength of the vortex is dependent on the size of obstruction. The common field conditions involve Reynolds numbers much greater than those achieved in the laboratory. Hence, an extrapolation is usually necessary by considering the scale effects.

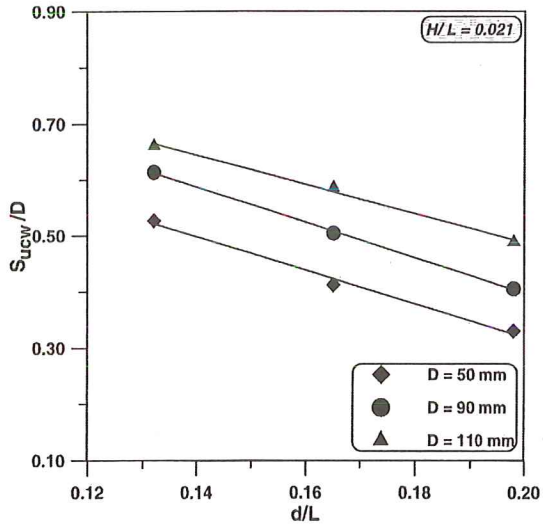

Figure 10. Effect of relative water depth (d/L) on S_{ucw}/D

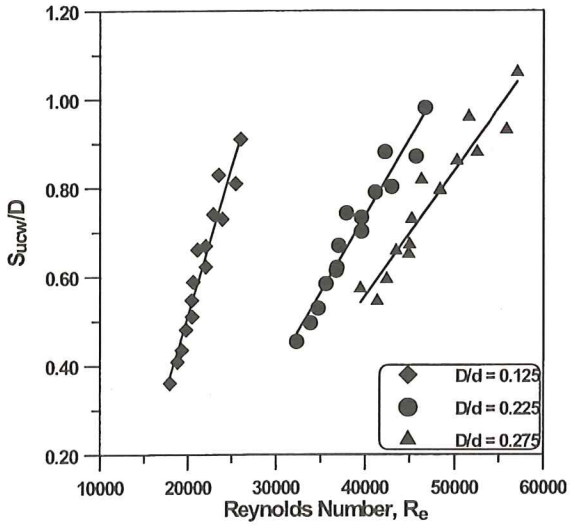

Figure 11. S_{ucw}/D as a function of Reynolds Number

(e) Relationship between S_{ucw}/D and combined dimensionless parameter (β_{cw})

Some of the variables that include pile size and dynamic factors of current and wave are grouped into the following flow parameters like flow Froude number, model Reynolds number, wave steepness, and Ursell parameter. These parameters are combined as a single non-dimensional parameter, namely, β_{cw} which can be taken as a composite relationship. The justification for choosing the above parameters has already been discussed in the previous sections. To express the ultimate scour depth in terms of the combined non-dimensional parameter (β_{cw}), the following relationship has been considered.

$$S_{ucw} = f(\beta_{cw}) \tag{7}$$

where the combined dimensionless parameter

$$\beta_{cw} = (H/L).(F_r).(U_p).(R_e) = (U^2H^2DL)/\sqrt{g^{0.5}d^{3.5}} \tag{8}$$

Figure 12 brings out the variation of S_{ucw}/D with β_{cw}. Based on the regression analysis, the following relationship is obtained with $R^2 = 0.732$.

$$S_{ucw}/D = 0.172\ (\beta_{cw})^{0.192} \tag{9}$$

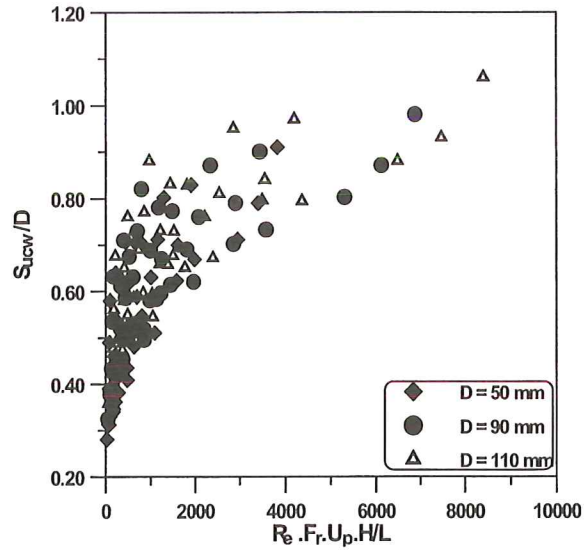

Figure 12. Relationship between combined dimensionless parameter (β_{cw}) and S_{ucw}/D.

It may be noted that Wang and Herbich [1983] reported a similar relationship for scour around a pile due to combined wave and current action in cohesionless soils. From the results presented in figure 12, it is seen that there is a good amount of scatter and this may be because of a large variation in the consistency index, I_c. Hence, these results are further re-plotted, corresponding to the different values of I_c (characterizing soft to medium stiff cohesive soil by varying I_c from 0.32 to 0.60 as found in the field), and these are presented in figures 13(a) to 13(c). Based on the test results, a set of

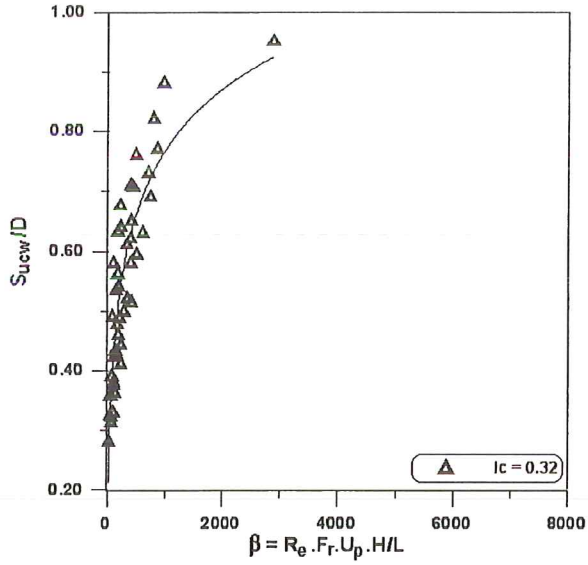

(a)

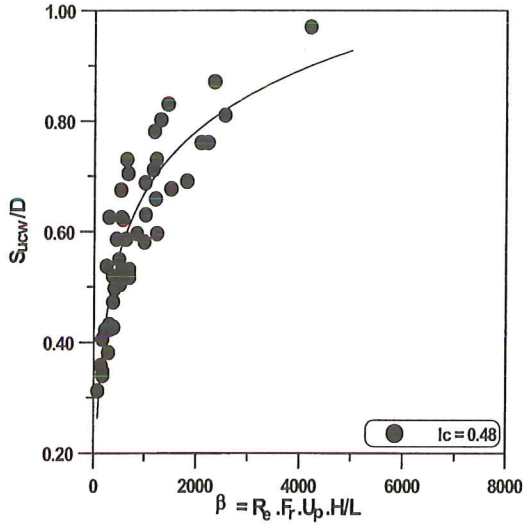

(b)

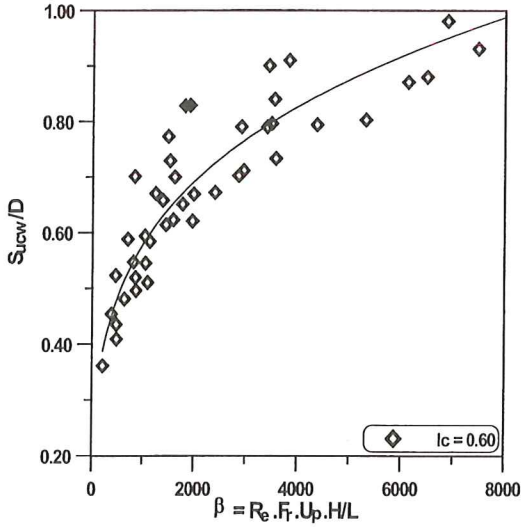

(c)

Figure 13. Variation of combined dimensionless parameter (β_{cw}) with S_{ucw}/D for different consistency indices.

equations are given below for scour depth with the various flow parameters as obtained from test beds formed at different consistency indices.

$$S_{ucw}/D = 0.128(\beta_{cw})^{0.263} \quad (\text{for } I_c = 0.32) \tag{10}$$

$$S_{ucw}/D = 0.106(\beta_{cw})^{0.264} \quad (\text{for } I_c = 0.48) \tag{11}$$

$$S_{ucw}/D = 0.111(\beta_{cw})^{0.240} \quad (\text{for } I_c = 0.60) \tag{12}$$

This set of equations (10) to (12) can be used for cohesive soils for the range of β_{cw} up to a value of 8000 for the appropriate range of I_c values.

(f) Bed Shear Stress and its Amplification due to Combined Action of Waves and Currents

The scour process is highly dependent on the shear stress developed by the flowing water at the soil-water interface. One of the purposes of the study is to investigate the bed shear stress induced around a vertical pile by the flowing water. In the present study, the magnitude of maximum bottom shear stress, τ_{cw} for wave-current combination is estimated by taking the vector addition of τ_m (mean shear stress) and τ_w (wave related bed shear stress) as shown in figure 14 [Soulsby 1995]. The above expression accounts for the non-linearities introduced when waves and currents interact and has been calibrated against laboratory and field data.

$$\tau_{cw} = \sqrt{\left\{\left[\tau_m + \tau_w \cos(\phi)\right]^2 + \left[\tau_w \sin(\phi)\right]^2\right\}} \tag{13}$$

where

$$\tau_m = \tau_c\{[1 + 1.2\,[\tau_w/(\tau_c - \tau_w)]^{3.2}\} \tag{14}$$

Further, current and wave related bed shear stresses are given by

$$\tau_c = \rho(U_{*c})^2 \tag{15}$$

$$\tau_w = \rho(U_{*w})^2 \tag{16}$$

Due to the action of the waves superimposed over current, You Zai-Jin [1995] suggested that there is an increase in bottom shear velocity. The increase in current bottom shear velocity, U_{*c} in the presence of waves is given by

$$U_{*c} = U_* + m(A\omega) \tag{17}$$

The critical velocity for currents (U_*) in the absence of waves is determined based on the measured velocity profiles and '$A\omega$' is the near-bed wave orbital velocity amplitude and is estimated by linear wave theory as $(\pi H)/[T \sin h(kd)]$, where 'k' is the wave number ($2\pi/L$). After analyzing incipient motion for a wide spectrum of grain sizes, You Zai-Jin [1995] concluded that the constant of proportionality 'm' = 0.026 in the above equation is dependent on near-bed wave orbital velocity amplitude ($A\omega$) and is practically independent of bed roughness. It is to be noted that there can be variations in the

strength depending on the type of soil and drainage conditions (controlled by the hydraulic conductivity of the soil) used during testing. Considering all these limitations, it is suggested that the above equation can be used for cohesive soils as a first approximation. The shear velocity (critical) due to waves is given by the following expression by You Zai-Jin [1994].

$$U_{*_w} = \sqrt{0.5 f_w (a\omega)} \qquad (18)$$

where f_w, the friction factor due to waves equals $0.108(a/z_o)$, where z_o is the hydraulic roughness length related to the soil type. Based on the experiments on erosion of cohesive sediments by Mitchener *et al.* [1996], the value of $z_o = 0.2$ mm is reported for the silty clay soil and the same is used in the present study. The angle between the wave and current shear stresses is ϕ. In the present study, as the waves are superimposed on currents in the same direction, $\phi = 0^o$.

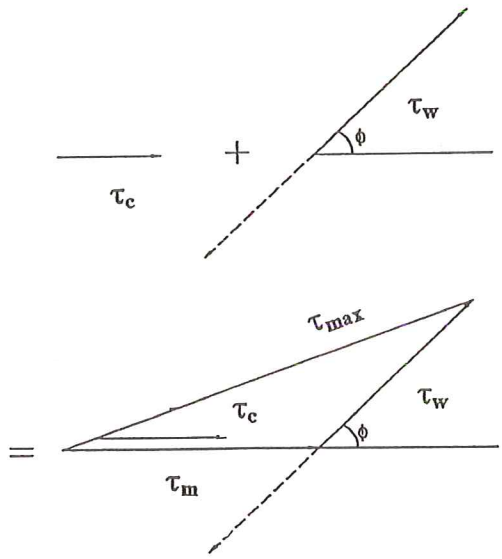

Figure 14. Definition of shear stress vectors due to combined action of waves and currents.

(g) Amplification Factor

The amplification in the bed shear stress due to the combined action of currents and waves in comparison with currents alone is given by $\psi = \tau_{cw}/\tau_c$ in which τ_{cw} is the bed shear stress $[(\tau_{cw} = \rho(U_{*cw})^2]$ and τ_c is shear stress due to currents imposed by the water on the soil when scour is initiated and is obtained from the undisturbed velocity profiles over the depth. Initiation of scour is identified as the water becomes turbid. It has been observed during the experiments that scour near edges perpendicular to the flow is larger and that could be due to the increase of bed shear stress near the edge of the pile (due to vortices). The results presented in figure 15 bring out the variation in amplification in bed shear stress due to the combined action of waves and currents for all the model sizes. The acceleration in flow due to increased velocity at the obstruction generates an increase in the bottom shear stress. The corresponding amplification factor in shear stress is observed depending on the model size as shown in the above figure. Based on the test results of the present study, the maximum amplification in bottom shear stresses by a factor of 2.4 is observed. According to Sumer *et al.* [1997], the amplification in the bed shear stress can be mainly due to (i) the contraction of streamlines near the side edges of the pile and (ii) the vortex formed in front of/behind the pile. Finally, it may be noted that the amplification factor presented in figure 15 can be useful with regard to its application in the design of scour protection around piles, if τ_{cw} and τ_c are known. Based on the regression analysis of the test results, the following expression is suggested for the amplification factor variation with ultimate scour depth. The range of applicability of this equation is $1.2 < \psi < 2.4$.

$$S_{ucw}/D = 0.538\ (\psi) + (-0.258) \qquad (19)$$

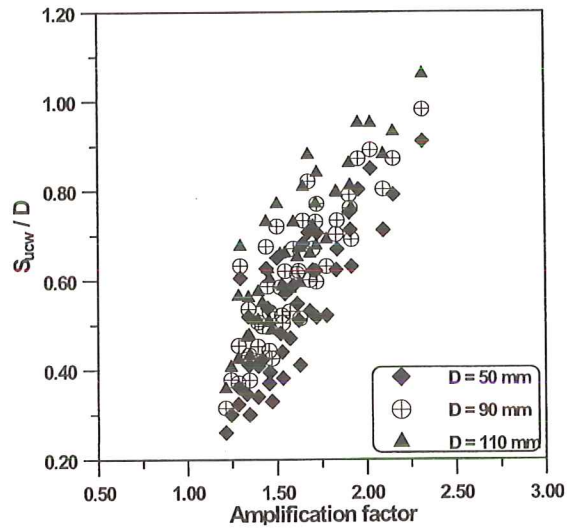

Figure 15. S_{ucw}/D as a function of amplification factor.

5. CONCLUSIONS

From the testing carried out in a special flume in which regular waves are superimposed over currents in the same direction, it has been found that both wave height and wave period have a significant influence on the ultimate scour depth formed around piles embedded in clay soil. Scour depths are found to increase substantially in comparison to conditions under currents alone by as much as 80%.

Scour is very much increased when incident wave steepness has increased. An increase in relative water depth (d/L) reduces the scour. Ultimate scour depth increases with an increase in Reynolds number for the range of tested conditions.

A set of empirical relations for scour at different values of consistency indices, I_c are presented in terms of a non-dimensional parameter (β_{cw}) containing flow parameters (wave steepness, Froude number, Reynolds number and Ursell parameter) and soil strength characteristics (consistency

index).

A simplified expression for the determination of bed shear stress for the combined action of currents and waves is proposed for cohesive soils. For the tested conditions, the bed shear stress around a pile increases by a factor of up to 2.4 in comparison with bed stress induced under a steady state current alone.

Due to the complex nature of the physico-chemical forces involved in cohesive sediments, a simple empirical analysis may not be adequate for the predictions for scour depths over a complete range of cohesive soils. At best, the results from this study can be applicable to a similar type of cohesive soil tested under suitable simulated conditions. However, these results can be further confirmed from the data obtained from similar types of testing over a wide range of cohesive soil deposits.

REFERENCES

Armbrust, S.L. 1982 Scour about a cylindrical pile due to steady and oscillatory motion. *M.S. Thesis*, Texas A&M University, College Station, Texas (as reported by Herbich *et al.* [1984]).

ASTM D 422-62 1972 Standard method for particle size analysis of soils. *Annual book of ASTM standards*, **04:08**, 83-92.

ASTM D 4318 1984 Standard test method for field vane shear test in cohesive soils. *Annual book of ASTM standards*, **04:08**, 308-310.

ASTM D 4318 1984 Standard test method for liquid limit, plastic limit and plasticity index of soils. *Annual book of ASTM standards*, **04:08**, 579-589.

Breusers, H.N.C., Nicollet, G., & Shen, H.W. 1977 Local scour around cylindrical piers *J. hydraulics research*, **15** (3), 211-252.

Briaud, J.L., Ting, F.F., Chen, H.C., Gudavalli, R., Perugu, S., & Wei, G. 1999 SRICOS: Prediction of scour rate in cohesive soils at bridge piers. *J. geotechnical and geoenvironmental engineering*, ASCE, Reston, Virginia, USA., **125** (4), 237–246.

Carstens, M.R. 1966 Similarity laws for localised scour. In *Proc. Am.soc. civil engrs, J. hydraul. div,* **92** (3), 13-36.

Carstens, T. & Sharma, H.R. 1975 Local scour around large obstructions. In *Proc. 16th IAHR Congress,* Salpaulo, **2**, 251-262.

Chow, W.Y. & Herbich, J.B. 1978 Scour around a group of piles. In *Proc. offshore technology conference*, Houston, Texas, Paper No. 3308.

Clark, A. & Novak, P. 1982 Local erosion at vertical piles by waves and currents. *J. sea bed mechanics*, 233-249.

Herbich, J.B., Schiller, R.E., Watanabe, R.K. & Dunlap, W.A. 1984 *Seafloor scour: design guidelines for ocean-founded structures* New York: Marcel Dekker and Basel.

Kroezen, M., Vellinga, P., Linderberg, J. & Burger, A.M. 1982 Geotechnical and hydraulic aspects with regard to sea bed and slope stability. *Delft hydraulics laboratory publication 272*, Delft.

Machemel, J.L. & Abad, G. 1975 Scour around marine foundations in *Proc. offshore technology conference*, Houston, Texas, OTC 2313, 691-702.

Mitchener, H.J., Torfs, H., & Whitehouse, R.J.S. 1996 Erosion of mud/sand mixtures *Coastal engg,* **29**, 1-25. (Erratum, 30 [1997] 319).

Narasimha Rao, S. & Prasad, YVSN 1993 Estimation of uplift capacity of helical anchors in clays *J. geotechnical engineering,* Feb.93, ASCE, **119** (2), 352-357.

Prasad, Y.V.S.N. and Narasimha Rao, S. 1994 Pullout behaviour of model piles and helical pile anchors subjected to lateral cyclic loading. *Canadian geotechnical journal*, **31**, 110-119.

Raudkivi, A.J. 1986 Functional trends of scour at bridge piers. *J. hydraulic engineering,* ASCE, **112** (1), 1-13.

Shen, H.W., Schneider, V.R., & Karaki, S. 1969 Local scour around bridge piers. *J. hydraulics division,* ASCE, **95** (6), 1919-1938.

Sleath, J.D. 1991 Velocities and shear stresses in wave-current flows. *J. geophysical research,* **96**, 15237-15244.

Soulsby, R.L. 1995 Bed shear-stresses due to combined waves and currents. Section 4.5 in *Advances in coastal morphodynamics*, (eds. Stive, M.J.F. *et al*), Delft: Delft Hydraulics.

Sumer, B.M., Christiansen, N. & Fredsoe, J. 1992 Scour around vertical pile in waves. In Proc. Am. soc. civ. engrs, *J. waterway, port, coastal, and ocean eng.,* **118** (1), 15-31.

Sumer, B.M., Christiansen, N & Fredsoe, J. 1993 Influence of cross section on wave scour around piles, *J. waterway, port, coastal and ocean eng.* In *Proc. am. soc. civ. engrs*, **119** (5), 477 – 495.

Sumer, B.M., Christiansen, N. & Fredsoe, J. 1997 The horseshoe vortex and vortex shedding around a vertical wall-mounted cylinder exposed to waves.

Wang, R.K. & Herbich, J.B. 1983 Combined current and wave produced scour around a single pile. Texas Engineering, Experiment Station, *Report No.COE 269*, Texas, A&M University, Texas (as reported by Herbich *et al.* [1984]).

Yanmaz, A.M. & Altinbilek, H.D. 1991 Study of time-dependent local scour around bridge piers. *J. hydraulic engg*, **117** (10), 1247-1268.

You Zai-Jin 1994 A simple model for current-velocity profiles in combined wave-current flows *J. coastal engg.*, **23**, 289-304.

You Zai-Jin 1995 Increase of current bottom shear stress due to waves - technical note. *J. coastal engg.,* **26**, 291-295.